Technical Report

TR-99-19

Effects of ice melting and redox front migration in fractured rocks of low permeability

Jordi Guimerà, Lara Duro, Salvador Jordana, Jordi Bruno
QuantiSci, SL, Barcelona, Spain

September 1999

Svensk Kärnbränslehantering AB
Swedish Nuclear Fuel
and Waste Management Co
Box 5864
SE-102 40 Stockholm Sweden
Tel 08-459 84 00
+46 8 459 84 00
Fax 08-661 57 19
+46 8 661 57 19

Effects of ice melting and redox front migration in fractured rocks of low permeability

Jordi Guimerà, Lara Duro, Salvador Jordana, Jordi Bruno
QuantiSci, SL, Barcelona, Spain

September 1999

Abstract

The geochemical stability of a KBS-3 type repository could be adversely affected by oxygenated water inflow during glaciation-deglaciation periods. We have assessed on a quantitative basis the extent and depth of such an oxidising front. This has been done by using limited regional groundwater flow schemes in combination with heterogeneous geochemical models.

We consider that the consumption of oxidants under the soil cover will be governed by the reactions between groundwater and redox buffering minerals. The ability of the media to buffer an oxidant intrusion will be dominated by the presence of iron(II) bearing minerals such as chlorite, biotite and pyrite.

We approach the problem under two perspectives:

1) the equilibrium approach, where groundwater reaches equilibrium with Fe(II) containing minerals) and

2) the kinetic approach, where the interaction between oxidants and the minerals is governed by kinetic rate laws.

The results show that, while the equilibrium approach is applicable to groundwater systems with sufficiently long residence times. The kinetically controlled reactive transport gives more accurate results, provided that characteristic reaction times are longer than groundwater residence time.

Multicomponent reactive transport results show that despite the input of meltwaters from glacial origin, the ground-water system remains anoxic after periods of thousands of years for most of the scenarios and conceptual models considered. The redox state is governed by the presence of iron(II) in the system. We have performed a sensitivity analysis of the effects of varying the groundwater flow velocity, the available reactive surface and the presence of different Fe(II) minerals. The majority of the simulations indicate that the resulting geochemical composition of the system would not jeopardise the geochemical stability of the spent fuel, at repository depths. Consequently, the intrusion of melting ice water does not pose any threat to the chemical stability of the repository system at the depths considered in the SKB concept.

Contents

		Page
Executive summary		9
1	**Introduction**	17
1.1	Objectives and scope	17
1.1.1	Uncertainties related to the hydrogeological system	17
1.1.2	Uncertainties related to water from melting ice	18
1.1.3	Uncertainties related to the geochemical model	18
1.2	Calculation approach	18
1.3	Structure of this document	18
2	**Conceptual model**	19
2.1	Geological constrains	19
2.2	Oxygen content in the ice sheets and melting water	20
2.3	Hydrogeological constrains	21
2.4	Geochemistry of the System	23
2.4.1	Soil	26
2.4.2	Oxidised Zone	26
2.4.3	Reduced Zone	26
3	**Preliminary calculations**	31
3.1	Stationary-state approach	31
3.2	Equilibrium approach	35
3.2.1	Fractured media	36
3.2.2	Host rock	41
3.3	Equilibrium vs. Kinetics	45
3.3.1	Fractured media	45
3.3.2	Host rock	46
4	**Numerical model**	47
4.1	Background on modelling of reactive transport	47
4.2	The ARASE code	48
4.3	Definition of the problem	49
4.3.1	Chemistry	49
4.3.2	Structure of the 1D models	52
4.3.3	Structure of the 2D models	55
4.4	Results	58
4.4.1	1D cases	58
4.4.2	2D cases	67
4.5	Summary of the calculations and mass balance analysis	74
4.5.1	Definition of the flow field distribution	75
4.5.2	Oxidants mass balance	76
4.5.3	Implications for safety assessment	76
5	**Conclusions**	81
References		83

List of figures

		Page
Figure 2.1	Conceptual model scheme	24
Figure 2.2	Comparison between measured and calculated pe values	25
Figure 2.3	Saturation index of several minerals in the Äspö groundwaters	27
Figure 2.4	Saturation index of annite, phlogopite, biotite and pyrite	29
Figure 3.1	Velocity of migration of the redox front through fractures	34
Figure 3.2	Scheme of the system considered in the equilibrium approach	35
Figure 3.3	Cumulative moles of calcite dissolved as a function of time	37
Figure 3.4	Precipitation of Fe(OH)3(s) as a function of time	38
Figure 3.5	Evolution of the chlorite and the Fe(OH)3(s) content with time and depth	39
Figure 3.6	Evolution of pe in the system	39
Figure 3.7	Mineralogical changes in the system as oxygen is added	40
Figure 3.8	Comparison between the moles of pyrite present in the system	43
Figure 4.1	Weathering rate of chlorite as a function of pH	51
Figure 4.2	Sensitivity analysis of the arrival time and magnitude of the redox front	53
Figure 4.3	Comparison of different dispersion coefficients	54
Figure 4.4	Distribution of material zones, grid used and number of flow boundaries	56
Figure 4.5	Groundwater flow at regional scale (several km)	57
Figure 4.6	Comparison of the evolution of the pe for different cases	60
Figure 4.7	Fe(II) variation in the systems	61
Figure 4.8	Sulphate evolution for different systems	62
Figure 4.9	Summary of the runs of the system not buffered by calcite (I)	63
Figure 4.10	Summary of the runs of the system not buffered by calcite (II)	64
Figure 4.11	Case B2. Time and space evolution of the system	65
Figure 4.12	Results achieved with the EXCHANGE code	66
Figure 4.13	pe and pH values at repository altitude control points	67
Figure 4.14	pe and pH values at repository altitude control points	68
Figure 4.15	Evolution of the Fe(II) species for runs 5 and 7	69
Figure 4.16	Chloride concentration at run 10	70
Figure 4.17	Evolution of pe and pH assuming slow groundwater flow	71
Figure 4.18	Evolution of the dominant specie of Fe(II) assuming slow flow	71
Figure 4.19	pe profiles at different simulation times	72
Figure 4.20	pe and pH evolution at different depths of the domain	73
Figure 4.21	Evolution of the RDC of the system	74
Figure 4.22	Moles of O2 reaching the repository depth per unit area	77
Figure 4.23	Moles of Fe III $_{(aq)}$ reaching repository depth per unit area	78
Figure 4.24	Stability diagram of uranium species and evolution trends of groundwater	79

List of tables

		Page
Table 2.1	Mean annual composition of snow pits in South Central Greenland	21
Table 2.2	Initial values of fundamental parameters for numerical simulations	23
Table 2.3	Composition of the Äspö groundwater (Banwart, 1995)	28
Table 3.1	Parameters used to evaluate the velocity of migration of the redox front	33
Table 3.2	Velocities of migration of the redox front	33
Table 4.1	Thermodynamic and kinetic equations of the geochemical system	50
Table 4.2	Thermodynamic equations of the geochemical system not buffered	52
Table 4.3	Compositions of groundwater used in the models	54
Table 4.4	Parameters used in 2D simulations	57
Table 4.5	Flow boundary conditions used in the 2D models	58
Table 4.6	Summary of the 1D cases analysed	59
Table 4.7	Flow distribution. Units in m and years	75
Table 4.8	Number of moles of oxidants after 1000 years	76

Executive summary

The Swedish concept of deep spent fuel disposal is based on deep geological disposal in granitic bedrock under geochemically reducing conditions. Therefore, one of the potential scenarios explored concerns the inflow of oxidising groundwaters to critical depths. This could adversely affect the ability of engineered and natural barriers to limit radionuclide releases from the disposal system to acceptable levels.

A recent safety assessment exercise (SITE 94) considers that a sequence of glaciation-de-glaciation periods could induce the presence of deep oxidising water, thus jeopardising the chemical conditions for the stability of the repository. In this context, studies performed in the Fennoscandian shield indicate the presence of isotopically light water, of glacial origin within major fracture zones at depths down to 400 m (Outokumpu case, Blomqvist et al., 1992; Glynn et al., 1997).

The general objective of the present work is to quantitatively asses the depth and extent of penetration of an oxidising front due to the infiltration of melt water after a deglaciation period. The calculations we will perform will be based on a number of assumptions and simplifications, due to the complexity of the problem and the uncertainties associated with some critical parameters and conditions. These assumptions are discussed in the following paragraphs.

Water infiltration due to deglaciation will last for approximately 5000 years (Björck and Svensson, 1992). The next major glaciation is expected to occur in about 60000 to 75000 years. The melting rate can be extrapolated from present measurements that indicate some 50 l/m^2/year (Boulton et al., 1995 in Svensson, 1996). It is not clear, however, how long this infiltration rate will last and which are the expected fluctuations of such a rate.

The data concerning oxygen content in ice sheets and in ice melting water has to be taken from research projects in polar areas -Antarctica and Greenland- and other glacial areas. Most of the data from polar programmes concerns the stable isotopic composition of ice, information on oxygen and major components contents in melt water is less abundant.

The reductive capacity of the geochemical system (RDC) is considered to be given by Fe(II) containing minerals in both fractures and the bedrock. The main mineral phases to be considered are: pyrite, biotite and chlorite and their thermodynamic evolution in contact with groundwater is rather well established. However, the knowledge about their kinetic alteration is far more limited and some assumptions have to be taken in order to perform the reactive transport calculations.

The problem is envisaged under two approximations. First, the equilibrium approach. Whenever the residence time of groundwater lasts longer than the characteristic reaction time (groundwater velocity is slow enough, v <3 m/y) water-rock interactions are assumed to be governed by thermodynamic controls. In this case, the geochemical evolution of the system is assessed by using the PHREEQC code with the Hatches database (Cross and Ewart, 1989). The system is physically viewed as a column of granite or fracture filling material divided into a series of compartments with changing water composition. The melting water enters through the top end and changes its composition subsequently by reaching equilibrium with the key minerals.

For faster groundwater velocities (v>3 m/y) as equilibrium cannot be assumed for the main water-rock interactions, we have performed reactive transport simulations to couple groundwater flow and the kinetically controlled geochemical system. The reactive transport system is then by means of the ARASE code (Grindrod et al., 1994).

Conceptual model

The geology of the study area consists of fractured rocks of low permeability. On top of these, advance and retrieval of ice sheets takes place. The depth of the repository is estimated to be 500 m below surface. The host rock is divided into two regions which are geochemically different:

- an upper one, where redox conditions are likely to be oxidising, extending down to about 100 m below surface. The reducing capacity of the top soil due to the presence of organic matter and microbial activity is not taken into account.

- a lower one of approximately 400 m thick with reducing chemical conditions and which reaches the repository zone.

Changes in the hydraulic boundary conditions due to the advance and retrieval of ice sheets and transient hydromechanic states due to the pressure exerted by the ice load are not considered in this study.

The deglaciation period is assumed to last in the order of thousands of years and the time expected to have a maximum enhanced infiltration due to ice melting lies between 1000-2000 years of a total period of some 5000 years. Such conditions have already been used by Svensson (1996) in the flow analysis during advance and retrieval of ice sheets. A critical issue for the topic assessed in this work is the oxygen content in ice. Estimations made by Ahonen and Vieno (1994) conclude that the dissolved oxygen in the melt water is 1.4 mM (about 45 mg/l). In terms of redox conditions, water with such a high oxygen content would have a pe = 11 to 13.

We start by envisaging the system as 1D. This is quite a simplification, but has some obvious computational advantages and not much information is lost, provided the basic rules for groundwater flow and geochemical evolution are maintained. In order to achieve this, we combine groundwater velocity and travel distances to simulate the advance of the redox front in a realistic way. We reproduce the effects of dilution due to hydrodynamic dispersion, although this is not expected to exert much control on the redox front. The effect of matrix diffusion is not taken into account.

The infiltrating water is considered to be in equilibrium with the oxidising bedrock; consequently, reactive transport simulations are carried out in the reducing zone, where the evolution of the redox front is presumed to display more variability. Thus, flow and transport parameters will be pertinent for such depths, which will be considered either as fracture with the corresponding filling materials or as massive bedrock.

In order to increase the physical representativeness of the calculations, the problem has also been approached in 2D. In this case, the flow field has been varied to reproduce the most likely real flow schemes with the limitations of multicomponent reactive transport codes. However, different material zones simulating fractures, host rock and reducing and oxidising conditions have been included.

It is now well established that in deep granitic groundwaters the redox state is mainly governed by electron transfer reactions between Fe(II) and Fe(III) in aqueous species and mineral phases. Therefore, the largest reductive capacity of such systems will be

given by the iron(II) content. The occurrence of iron(II) in nature is dominated by minerals such as Fe(II) sulphides, carbonates (siderite) and clay minerals. The ability of Fe(II) containing clays to act as oxidant sinks has been pointed out by several authors. White and Yee, (1985) propose an structural oxidation of Fe(II) expressed by the following process:

Fe(II) silicate = Fe(III) silicate

That is, Fe(II) is oxidised without being released to the aqueous phase.

Also homogeneous Fe(II) oxidation has been reported, in which Fe(II) is released in the form of Fe^{2+} from the clay and it is subsequently oxidised to Fe(III) in solution.

At pH > 4, the oxidation of Fe(II) is fast and leads to the precipitation of amorphous Fe(III) solid phases, mainly "$Fe(OH)_3.nH_2O$". The half life for this oxidation process at pH = 8 is on the order of 500 s. This implies that oxidation of iron(II) occurs immediately on release from the minerals and for this reason the redox state of most natural waters can be explained in terms of an equilibrium $Fe^{2+} \Leftrightarrow Fe(OH)_3(s)$. In the case of an unlimited and readily available source, all the oxidants could be instantaneously reduced, but if the availability of iron(II) is not infinite or if the rate at which iron(II) is available is lower than the rate at which it is oxidised, then the factor limiting the oxidant consumption will be the rate of release of iron(II) to solution, in other words, the rate of dissolution of Fe(II)-bearing minerals, such as clays.

A good evidence of the role that the ferrous iron released from the weathering of silicates on the redox state of aqueous solutions plays is exemplified by the laboratory experiments reported by Malmström et al. (1995) on the dissolution of Fe(II)-bearing biotite. The results highlight the role of Fe(II) present in minerals as one of the important oxidant sink of a deep groundwater system.

From 100 m to 500 m depth, where the repository is presumably located, the medium is reducing. Therefore, this will be the zone with a larger capacity to retard the migration of an oxidising front. The reducing capacity of the media (RDC) will be given by the presence of reductants, mainly ferrous iron (Banwart and Gustafsson, 1991). The major reservoirs of iron(II) are aqueous Fe(II) and Fe(II) contained in minerals, mainly pyrite, biotite and chlorite.

The mineralogy of this reducing zone can be regarded as different depending on whether we focus on water flowing mainly through fractures or through the host-rock.

Chlorite was identified as the main Fe(II)-bearing mineral in the fracture fillings of Äspö. In fact, chlorite represents a 35% of the fracture coating in this zone, with an average content of 20% wt. in FeO (Banwart et al., 1992). With this information it is possible to estimate an stoichiometry of 1.5 moles of Fe per mole of chlorite. Chlorite can be regarded as a solid solution whose end-members are daphnite ($Fe_5Al_2Si_3O_{10}(OH)_8$) the ferrous end-member, and clinochlore ($Mg_5Al_2Si_3O_{10}(OH)_8$) the magnesian end-member. We have assumed that it behaves ideally and, according to the calculated stoichiometry, the following solubility constant has been used:

$$\text{Chlorite14A } (Fe_{1.5}Mg_{3.5}Al_2Si_3O_{10}(OH)_8) + 16H^+ = 1.5Fe^{+2} + 3.5Mg^{+2} + 2Al^{+3} + 3H_4SiO_4 + 6H_2O$$

with logK = 59.9

Biotite can be regarded as a solid solution whose end members are annite ($KFe_3AlSi_3O_{10}(OH)_2$) and phlogopite ($KMg_3AlSi_3O_{10}(OH)_2$). We have considered an ideal solid solution of these two end members to generate the biotite phase:

Biotite ($KMg_2AlFeSi_3O_{10}(OH)_2$) + $10H^+ = K^+ + 2Mg^{+2} + Al^{+3} + Fe^{+2} + 3H_4SiO_4$

with logK = 35.88

Preliminary calculations

In a first approximation, we have applied the stationary-state approach (Licthner, 1988) to the problem in order to compare the results obtained with the rest of approaches. The equilibrium problem has been solved by using the geochemical code PHREEQC (Parkhust, 1995). Several cases have been set-up in order to test and compare the ability of the different compartments to buffer the intrusion of oxidative deglaciation water always by assuming water-rock equilibrium.

In the stationary state approach, it is assumed that the oxygen introduced into the system due to the advective inflow of oxygenated water will be reduced as soon as it contacts the minerals able to use it. Therefore, this is a quasi-equilibrium approach. According to this theory, the time needed to deplete all the RDC of the system will be given by the velocity of oxygen inflow. One of the limitations associated with the use of the stationary-state is the underlying assumption of immediate total oxygen consumption as it contacts the Fe(II) containing minerals.

In this respect, a way of improving the calculations is to consider that although the reactions occurring between oxygen and minerals are instantaneous, the extent of oxygen consumption is limited by thermodynamics. The PHREEQC code has been used to perform the calculations. The system is chemically envisaged as two compartments: oxidised and reduced zone. The following water-rock interaction reactions and initial water compositions are considered in each one of the zones:

Oxidised zone

Initial groundwater: Shallow groundwater reported in Banwart (1995)

Mineral equilibria:

$Calcite = Ca^{2+} + CO_3^{2-}$	log Kso = -8.48
$Fe(OH)_3(s) + 3H^+ = Fe^{+3} + 3\ H_2O$	log Kso = 4.89

Reduced zone

Initial groundwater: Native Äspö groundwater

Mineral equilibria:

$Calcite = Ca^{2+} + CO_3^{2-}$	log Kso = -8.48
$Fe(OH)_3(s) + 3\ H^+ = Fe^{3+} + 3\ H_2O$	log Kso = 4.89
$SiO_2(s) + 2\ H_2O = H_4SiO_4$	log Kso = -3.98
$Kaolinite + 6\ H^+ = 2\ Al^{3+} + 2\ H_4SiO_4 + H_2O$	log Kso = 7.43

A.- Fractured media

Chlorite oxidation: we assume that as the Fe(II) of chlorite is oxidised and $Fe(OH)_3(am)$ is being produced. In order to minimise chemical changes in the system, the precipitation of clinochlore, the magnesian end member of chlorite, has been allowed (Deer et al., 1992, p. 334). In this way the system behaves as if only the structural iron of chlorite is released to the system and equilibrated with $Fe(OH)_3(s)$ due to the initial constraints introduced in the problem.

B.- Host rock

Equilibrium with pyrite

$$FeS_2 + 2H^+ + 2e^- = Fe^{+2} + 2HS^- \qquad \log Kso = -16.23$$

Equilibrium with biotite

$$\text{Biotite } (KMg_2AlFeSi_3O_{10}(OH)_2) + 10H^+ = K^+ + 2Mg^{+2} + Al^{+3} + Fe^{+2} + 3H_4SiO_4$$

with log Kso = 35.88

In this case, both, pyrite and biotite are able to accept oxidants and to precipitate in the form of $Fe(OH)_3(am)$.

The oxic intrusion is buffered by the dissolution of chlorite in the fractured medium. The pH evolves from 7.7 to 8.3 and the initial pe (-2) slightly increases due to the equilibration of the system with chlorite (final pe = -1.07). The dissolution of chlorite gives arise to a precipitation of $Fe(OH)_3(s)$. If the oxic intrusion is buffered by biotite and pyrite (host rock), then the chemistry of the system is efficiently buffered to a pH of 8.27; pe, -4.37; $Ca_{tot}\,6.00\cdot10^{-4}$; $Fe_{tot}\,8.03\cdot10^{-5}$; $HCO_3^-\,1.07\cdot10^{-3}$. The redox buffering exerted by biotite is negligible if pyrite is present in the system.

The equilibrium approach can be regarded as a useful way of understanding the system, although it presents some limitations with regards to the aplicability of the results obtained:

a) The water replacement is complete, i.e., the water initially contained in cell 1 passes to cell 2 and so on. Therefore, the approach will be more valid as the size of the cells becomes small enough to represent the true equilibrium situation. This problem could be solved by increasing the number of cells but this renders the calculation time out of reach.

b) The evolving groundwater is assumed to equilibrate with the minerals present in the system. This assumption is only valid when the characteristic reaction times of the critical water/rock interactions are shorter than groundwater residence times of. This approach can be valid when dealing with fast kinetics heterogeneous processes, such as calcite or $Fe(OH)_3(s)$ dissolution/precipitation of,.However, it can lead to important misinterpretations when considering weathering reactions of aluminosilicates (such as chlorite and biotite) or sulphides (e.g. pyrite) due to sluggish kinetics of these processes at low temperature/low pO_2 conditions.

Multicomponent reactive transport model

The analysis of the oxidising front migration due to melt water infiltration has been performed by means of the ARASE code (Grindrod et al., 1994) which permits multicomponent reactive transport simulation. The problem has been analysed using both 1D and 2D geometry. On one hand, 1D calculations provide a simple and efficient description of the most relevant processes. The disadvantage of the 1D approach is that the regional flow patterns are better reproduced in 2D, although they still present some limitations.

In order to make the calculations manageable, the kinetic equations of the minerals contributing to the RDC of the system (chlorite, biotite and pyrite) has been reduced to a function of Fe (II) release which is either dependent on pH in the case of the silicates or on the oxygen content in the case of pyrite. In this way, the number of equilibrium equations has been reduced to a maximum of 20.

Concerning the hydrogeological parameters and the water composition they have been kept as close as possible to values derived from field measurements (Rhén et al., 1997) or to expected values during glaciation periods (Boulton and de Marsily, 1997).

Some 30 cases were analysed in 1D by combining hydrodynamical parameters (basically, groundwater velocity), type of mineral and its reactive surface. The results from these calculations indicate that the oxidising front arrival time to repository depth is mainly controlled by the groundwater velocity and that the magnitude of the redox front, the resulting pe value- depends on the reactive surface area of the mineral considered. Despite the relevance of the arrival time of the oxidising front, we observe that the effect of groundwater velocity on the final pe value is important when the kinetics of the redox reaction is not limited by the saturation with respect to the dissolving mineral. In this case, differences of one unit pe are achieved depending on groundwater velocity. When the reaction rate is limited by the saturation state of the reacting mineral, then the calculated pe values are exactly the same, independently of the assumed groundwater velocity.

All the cases analysed independently of the chemical and/or hydrogeological condition- indicated that dissolved oxygen contents below 10^{-20} mole/l are obtained in relatively short reaction times. This observation has some critical implications concerning the reactive oxidants of the system. As a result of these calculations we can assume that the main reactive oxidants will not be those entering with the recharge water, but those released as a result of the water rock-interactions.

The effect of the advance of the oxidising front can be analysed in terms of RDC variation. Differences in aqueous $Fe^{+2,}$ which is the dominant aqueous species contributing to the RDC, are usually small (-6.75×10^{-5} mole/l). The dissolution of chlorite becomes zero, far from the oxidant boundary, after 100 years the system is calculated to be in equilibrium or slightly oversaturated with respect to chlorite.

Six cases were analysed by using a 2D geometry, according to different flow field configurations. The main differences with respect to 1D configurations arisen from the degree of groundwater renewal at repository depth, as a considerable part of water flows by the top oxidising zone in some of the cases.

In terms of performance assessment, the most conservative simulations showed variations of the RDC comparable to those produced in 1D. The calculated pe values switched from no variation or it increased to pe values in the range 4-5. This is the result

of the RDC either not being depleted or being decreased by of 4 orders of magnitude. This latter case is only achieved when downward flow of melt water is considered along a highly transmissive fracture (groundwater velocity around 10^{-5} m/s, which by no means reflects "low permeability"), which directly intercepts the repository zone.

Implications for performance assessment

The calculations and discussions from previous sections show that the inflow of oxidising fronts within a glaciation time span is possible. We have computed the amount of oxidants in the system in order to asses whether their presence could disturb the geochemical stability of the repository system. At this point we should recall that the simulations presented in this report do not reflect the presence of the engineered barriers in the near-field. Hence, the calculations evaluating the amount of oxidants present at repository depths should be understood as an indicator of the redox conditions at the geosphere near-field interface.

Under these premises, when the geochemical conditions at this interface are compared with the stability diagrams of some relevant components of the HRLW geochemistry, only in the case of assuming flow through fast fractures indicates a potential threat if for the spent fuel system.

Conclusions

We have performed a thorough quantitative analysis of the potential advance of an oxic front as a result of ice-melt water infiltration in a granitic environment. The analysis has been done by using the relevant geological, hydrogeological and geochemical conditions of the Fennoscandian Shield, with particular emphasis in the local conditions of the Äspö underground laboratory.

Several conceptual hydrogeochemical models have been produced based on varying hydraulic conditions, geologic domain and availability of oxygen reducing minerals to flowing groundwater. This have been used in a variety of reactive transport approaches: steady state, and thermodynamic vs kinetic control.

The results of the analysis indicate that during a glaciation cycle, the redox conditions at the repository would only be disturbed in the immediate vicinity of a highly transmissive fracture. A thorough site characterisation and the use of engineered barriers will prevent such disturbance to progress to the spent fuel and consequently the oxic front migration as a result of ice melting poses no danger whatsoever to the geochemical stability of the SKB repository.

1 Introduction

The Swedish concept of deep geologic disposal of nuclear spent fuel is based on geologic environments under reducing conditions. Therefore, the inflow of oxidising groundwaters to critical depths could adversely affect the ability of engineered and natural barriers to limit radioelement releases from the disposal system to acceptable levels. A recent safety assessment exercise (SKI SITE 94) considers that a sequence of glaciation-de-glaciation periods could induce the presence of deep oxidising water, thus jeopardising the chemical conditions for the stability of the repository. Arthur (1996) has produced scoping calculations making use of field data from the Äspö hard-rock laboratory by means of an analytical code, and concludes that such possibility is plausible if not very likely. In this context, studies performed in the Fennoscandian shield indicate the presence of isotopically light water, of glacial origin within major fracture zones at depths down to 400 m (Outokumpu case, Blomqvist et al., 1992; Glynn et al., 1997). Although there are overwhelming geological evidences to support the hypothesis that the overall redox state of the Earth's crust has remained essentially constant (Holland, 1984 among others), some local oscillations in the sulphur, iron and oxygen cycles may have some implications for the geochemical stability of deep underground repositories.

1.1 Objectives and scope

The general objective of the present work is to quantitatively asses the penetration of an oxidising front due to the infiltration of de-glaciation water. We will proceed with a number of assumptions and simplifications, due to the complexity of the problem and the uncertainties associated to some critical parameters and conditions. These are outlined below and extensively discussed in Chapter 2.

1.1.1 Uncertainties related to the boundary conditions of the hydrogeological system

Water infiltration due to de-glaciation will last for approximately 5000 years (Björck and Svensson, 1992). The next major glaciation is expected to occur in about 60000 to 75000 years. The melting rate can be extrapolated from present measurements that indicate some 50 mm/year (Boulton et al., 1995 in Svensson, 1996), however, it is not clear how long it will last and which are the expected fluctuations of such a rate. Boundary conditions of groundwater flow will also vary with time due to elastic crustal rebound induced by the ice load and to fluctuations on the sea level. Elastic rebound will also affect the hydraulic properties since they are dependent on the geo-mechanical properties, that is, they vary according to the stress field and regime. It is likely that such changes are already taking place, since transient effects tend to last very long in low permeability media and could be assessed by means of coupled hydro-mechanical approaches.

1.1.2 Uncertainties related to the oxygen content of the water from melting ice and, to a much lesser extend, to the groundwater composition

Our knowledge about the variation of groundwater composition with depth is quite firm, due to the multiple site characterisation programmes. However, the data concerning oxygen content in ice sheets and in ice melting water has to be taken from research projects in polar areas -Antarctica and Greenland- and other glacial areas. Most of the data from polar programmes concerns the stable isotopic composition of ice, while information on oxygen and major components contents in melt water is less abundant.

1.1.3 Uncertainties related to the geochemical model and to the reducing capacity of the system (RDC) which will exert control on the redox front advance

The occurrence and content of certain iron containing minerals, such as pyrite, biotite or chlorite is well characterised. There are some studies concerning the thermodynamic evolution of these minerals in contact with groundwater. However our knowledge about their kinetic alteration is far more limited and some assumptions have to be done in order to perform the reactive transport calculations. These will be thoroughly discussed in Chapter 2.

1.2 Calculation approach

Whenever the residence time of groundwater is sufficiently long and groundwater velocity slow enough water-rock interactions are assumed to be governed by thermodynamic controls. In this case, the geochemical evolution of the system is assessed by using the PhreeqC code with the Hatches database (refs). The system is viewed as a column of granite or fracture filling material divided into a series of compartments with changing water composition. The melting waters enters through the top end and changes its composition after reaching equilibrium with the key minerals.

For faster groundwater velocities, as equilibrium cannot be assumed for the main water-rock interactions, we have performed reactive transport simulations to couple groundwater flow and the kinetically controlled geochemical system. The reactions are assessed by means of the ARASE code (Grindrod et al., 1994). Chapter 3 shows that under the current conceptual model the threshold for adopting one of the approaches is a groundwater velocity value of v = 0.03 m/year.

1.3 Structure of this document

Chapter 2 describes the conceptual model. The uncertainties of the source term, geological constrains, hydraulic parameters and geochemistry of the system are discussed in this chapter. In Chapter 3 we present the results of equilibrium and kinetic scoping calculations and we compare them with the results from previous authors. As a result, a series of sensible parameters are produced, which will be tested in the reactive transport simulations. Chapter 4 describes the most relevant results obtained by means of numerical models of reactive transport, followed by a discussion and comparison. Finally, we end with some relevant conclusions for the geochemical performance of the HLNW repository under these conditions.

2 Conceptual model

The geological, hydrogeological and hydrogeochemical constrains are presented and the associated uncertainties discussed. Preliminary calculations assuming equilibrium are compared with the results from previous authors. We end up with a set of parameters which are used as input in the numerical model described in chapter 4.

2.1 Geological constrains

The geology of the study area consists of fractured rocks of low permeability in top of which, advance and retrieval of ice sheets takes place. The depth of the repository is estimated to be 500 m below surface. A zone of "top soil" of tens of metres thick is located between the bottom of the ice sheet and the top of the rock mass - glacial moraines-. The host rock is divided into two regions which are geochemically different: an upper one, where redox conditions are likely to be oxidising, extending down to 100 m below surface, and a lower one of 400 m thick which reaches the repository top. Groundwater redox conditions are reducing in this latter zone, in accordance with the data from the Äspö site and other site characterisation programmes.

The ice load exerts a confining pressure on top of the rock mass equivalent to its thickness -1 to 2 km. Accumulation and melting of ice causes the pressure to build-up and decrease. Effects on the rock mass can be outlined as changes in hydraulic properties due to changes in the stress field. To a lesser extent, crustal rebound (Peltier, 1985) will induce uplift in the rock mass, which in turn, will change the position of the coast line, the discharge zone of most of the melt water. Additionally, the position of the coast line will change due to freezing of the sea (Björck and Svensson, 1992) as we will later discuss. Laboratory experiments on core samples showed that hydraulic conductivity (expressed as $Q/\Delta h$, being Q the injection rate and Δh the pressure change) decreases three orders of magnitude by increasing the confining pressure up to 20 MPa (Tsang and Witherspoon, 1985). According to these values, the pressure build up due to an ice sheet of 1-2 km thick, would range between 10-20 MPa. However changes observed in underground excavations (Martínez-Landa et al., 1997) point to a less dramatic influence than in laboratory conditions, the changes being of the same order of magnitude. For this study, the change of the hydraulic conductivity induced by this process will not be relevant

Changes in the boundary conditions due to the rebound and shift of the coast line are difficult to predict. Björck and Svensson (1992) report a range of 10 to 100 m of sea level change due to past glaciations in the Fennoscandian shield. Whenever a hydrogeological domain covers an area which includes discharge to the sea, the boundary conditions should adjust to this event. There is some experience in treating time-dependent conditions due to ice sheet advance and retrieval and its effect on the salinity distribution in depth (Svensson, 1996). In fact, they are not the same problem; but it is likely that both cause changes in groundwater flow regime which reach repository depths.

The duration of enhanced infiltration due to ice melting will be influenced by atmospheric conditions, which causes ice to accumulate or melt. Björck and Svensson (1992) forecast the likely duration and extension of ice sheets in Scandinavia. Their prediction relies on marine records, past climate and Milankovitch's orbital parameters.

During the next 23000 years, it expected that a maximum glacial period will be reached in about 5000 y. From 23000 to 45000 y, glaciation will be limited to the mountains, and no ice sheet formation is expected in coastal areas. From 45000 to 75000 y, another major glaciation will occur, the top taking place at about 63000 y. After 75000 y, it is expected that general de-glaciation will take place. Summarising, deglaciation periods will last on the order of thousands of years and the time expected to have a maximum enhanced infiltration due to ice melting lays between 1000-2000 years of a total period of some 5000 years. Such conditions have already been used by Svensson (1996) in the flow analysis during advance and retrieval of ice sheets.

2.2 Oxygen content in the ice sheets and melting water

Groundwater reaching the repository is envisaged to have originated as melted ice which infiltrates and flows downwards. Hence, it is important to assess the composition of the melted ice since it constitutes the source of oxidants which eventually, could jeopardise the geochemical stability of the repository. Following we discuss the composition of the melt water, with special emphasis in the O_2 content; the resulting composition after equilibration with soil and host rock with oxidising groundwater is further described in section 2.4.

Ice composition in polar glaciers has long been studied since they record climatic changes at global scale (Weertman, 1968; Broecker and Dong., 1970, among others). CO_2 content in air bubbles and $\delta^{18}O$ are indicatives of global temperature and its variations. There is some experience at measuring gas content at ice cores and interpreting their past climatic implications. Particularly, Stauffer et al. (1985) studied long term variations of CO_2 at air extracted from Greenland ice samples. Measurements made extend to other air gases, such as N_2, O_2 and Ar. The percentage of molecular oxygen found in such samples never differed more than 10% from atmosphere at 0ºC and ranged from 21 to 30%. Craig et al. (1992) measured around a 32% of oxygen in super saturated water lakes below ice sheets, in agreement with the former.

Gas content in ice is controlled by molecular capture in gas inclusions. In perpetual snow areas, where seasonal melting can be neglected, gas inclusions are formed by a "dry sintering" process (Raynaud and Laben, 1979; Ahonen and Vieno, 1994). As long as snow accumulates, vertical stress causes re-crystallisation of snow into "firn", where pore space is still at atmospheric pressure. As long as "firn" becomes ice -by increasing pressure- pore space losses connectivity and air bubbles are formed. The amount of void space decreases with increasing pressure and consequently with depth. Total gas content may be as low as 4 $cm^3/100$ g ice or even close to zero at the glacier basement, as reported by Herron and Langway (1979) down to 2163 m at Byrd Station, Antarctica. Estimations based upon such figure would give rise to an oxygen content of the melt ice of 0.5 to 5 ppm, which is rather low compared to the O_2 content at equilibrium with atmosphere at 0ºC (about 15 ppm). However, gas is maintained at a pressure equivalent to the ice thickness at the bottom of the glacier. There are some evidences that high pressures are effectively maintained, such as blow-ups occurred during borehole drilling (Fountain, 1994), but no direct measurements have been found. In short, an equivalent pressure of 1 km of ice (P≅100 atm), would give rise to an oxygen content of 50 to 500 ppm assuming the previous figures. The lower boundary agrees with independent estimations made by Ahonen and Vieno (1994). Their study concludes that in similar conditions the dissolved oxygen in the melt water is 1.4 mM (about 45 mg/l). In terms of redox conditions, water with such a high oxygen content would have a pe = 11 to 13.

We assume that this is the oxygen content of the water that mixes and interacts with the existing groundwater and that the mineralogy of the rock mass will act as a barrier of this oxidising front. However, only a minor part of the melted ice will percolate down to the repository, some of the reasons being explained below.

Melting at the basement of the glaciers takes place following a rather heterogeneous pattern (Boulton and de Marsily, 1997). It usually gives rise to preferential flow paths (tunnels) which are or may be at atmospheric pressure (Schouez an Lorraine, 1991). Hydraulics of drill holes in the South Cascade glacier (Washington st., USA) also evidence such patterns (Fountain, 1994), and generally, sub-glacial water pressures are close to local ice overburden pressures. The existence of a high permeability zone (log K = -4 to -5 m/s) between the ice overburden and the host rock (glacial moraine) is inferred by permeability measurements. The piezometric surface shows that the debris layer would be drained by preferential flow paths which are close to atmospheric pressure. Experimental evidences from Antarctica (Bindschadler et al., 1998) also seem to point to this figure. Such high permeability layer acts as a hydraulic drainage and chances are that degasification -and in turn, oxygen volatilisation- may occur.

Finally, as regards melt water composition, measurements done in Greenland (Yang et al., 1996) show that it is extremely diluted. Such data is not crucial for the development of the project but, for the sake of completeness, Table 3.1 shows an example of composition of snow pits.

Table 2-1. Mean annual composition of snow pits in South Central Greenland (in ppb, after Young et al., 1996).

Cl^-	NO_3^-	SO_4^{2-}	Na^+	K^+	Mg^{2+}	Ca^{2+}
16.2	6	78.1	5.7	0.9	1.5	10.5

2.3 Hydrogeological constrains

Hydrogeology of low permeability fractured media has progressed during last decades thanks to research conducted by site characterisation programmes for isolating radioactive and toxic wastes. A common feature of the study sites is the large variability of hydraulic conductivity of a given rock volume. Heterogeneity exerts control over variability of hydraulic conductivity and heterogeneity is in turn caused by geological features - say fractures. Actually, fractures can be viewed as an extreme case of heterogeneity.

Values from study sites reported in literature show that variability of hydraulic conductivity is high compared to, for instance, porosity or fracture aperture available for solute transport. Guimerà and Carrera (1997) show that while K ranges over ten orders of magnitude, porosity varies less than six in fractured media. Such difference also applies for other geological material suchs as sandstones, clays or limestones.

Since the objective of this report is focusd in a sensitivity analysis of a redox front advance, rather than in producing accurate hydrogeologic models of a given site, we select a range of parameter values to produce a meaningful sensitivity analysis. For that, we rely on previous data measured at the Äspö hard rock laboratory (Rhén et al., 1997, among others) and used in previous numerical models (Svensson, 1996).

As described in section 2.1, geological constrains affecting hydrogeology are complex. For the sake of simplicity, and due to their limited relevance for the actual problem most of them have been skipped. However, the geometry of the flow field will be fully 3D as already described by Svensson (1997). Also, the residence time and the dynamics of the water -rock interactions will rule the redox front position and value with respect to the repository. In this context, Tóth and Sheng (1996), inspecting the influence of the location of the repository within a given flow system, concluded that the closer to the regional discharges, the faster the arrival of the nuclide releases to the biosphere; but as long as the repository is kept far away from the recharge zones, evolution of groundwater after infiltration prevents oxidising conditions to threaten the chemical stability of the repository.

We start by envisaging the system as 1D. This is quite a simplification, but has some obvious computational advantages and no much information is lost, provided the basic rules for groundwater flow and geochemical evolution are maintained. For that, we combine groundwater velocity and travel distances to simulate the advance of the redox front in a realistic way. We reproduce the effects of dilution due to hydrodynamical dispersion, although it is not expected that it exerts much control on the redox front. The effect of matrix diffusion is not taken into account.

The system is viewed as a column of two different materials: an upper part of oxidising conditions and a lower one which is reducing (Figure 2.1). The reducing capacity of the top soil due to the presence of organic matter and microbial activity is not taken into account although it may be relevant (Banwart et al., 1992, 1995). The infiltrating water is considered to be in equilibrium with the oxidising bedrock; consequently, simulations are carried out in the reducing zone, where the evolution of the redox front is presumed to display more variability. Thus, flow and transport parameters will be pertinent for such depths, which will be considered either as fracture with the corresponding filling materials or as a host rock. Table 2.2 shows the set of parameters chosen for the numerical simulations.

The problem is also approached in 2D and the flow field is varied so as to reproduce the most likely real flow. In spite of the limitations of the multicomponent reactive transport codes, different material zones simulating fractures, host rock and reducing and oxidising conditions have been included.

According to the figures presented in Table 2.2, some of the resulting groundwater velocities are fast for the medium considered (10^{-5} to 10^{-7} m/s). When present, they are expected to happen in reduced portions of the domain, that is, parts of the most conductive fractures. By no means, such velocities (10^{-5} m/s) are expected to happen over a domain of 400 m, which is the one of the 1D models. However, we analyse their effect to keep our study in the safe side of the problem. In other words, the results of our calculations will be highly pessimistic (conservative).

Table 2-2. Initial values of fundamental parameters for numerical simulations in 1D

Parameter	Fracture filling	Host rock
Porosity ϕ (-)	10^{-2}	10^{-3}
Hydraulic conductivity K (m/s)	10^{-7}	10^{-9}
Hydraulic gradient ∇h (-)	1, 10^{-1}, 10^{-2}	
Dispersion D (m^2/s)*	10^{-7}	
Surface area S_A (m^2/m^3)	10, 1, 10^{-1}, 10^{-2}, 10^{-3}	
Minerals	Chlorite, 35% clinochlore (in equilibrium)	Pyrite, biotite

α_L varied from 1 to 10 m

2.4 Geochemistry of the system

As already stated in the Introduction, the chemical stability of the repository will be mainly affected by the redox conditions of deep percolating groundwater. Therefore, in order to assess the consequences associated to the infiltration of glacial meltwater it is of crucial importance to evaluate the main redox processes which will control the progression of the oxidising front associated to the enhanced infiltration

It is well accepted that in granitic groundwaters the redox state is governed by electron transfer between Fe(II) and Fe(III) aqueous and mineral species. Therefore, the largest reductive capacity of such systems will be given by the iron(II) content.

The occurrence of iron(II) in nature is dominated by minerals such as Fe(II) sulphides, carbonates (siderite) and clay minerals. In places where Fe(II) sulphides are the dominant minerals, the uptake of oxidants will probably increase the acidity of water due to the oxidation of sulphide to SO_4^{2-}, besides the precipitation of Fe(III). The stoichiometry of the oxidation of sulphide clearly illustrates that acidity increase:

$$S^{2-} + 4\ H_2O = SO_4^{2-} + 8\ H^+ + 8\ e^- \qquad [2.1]$$

As a consequence, an increase in the sulphate concentration of groundwater will be observed.

An example of this increase in the sulphate content of groundwater after an oxic disturbance can be seen in the redox experiment performed in Äspö. In this case, the increase of sulphate was attributed to microbially mediated oxidation of sulphide, i.e., it was a process mainly produced in the soil layer.

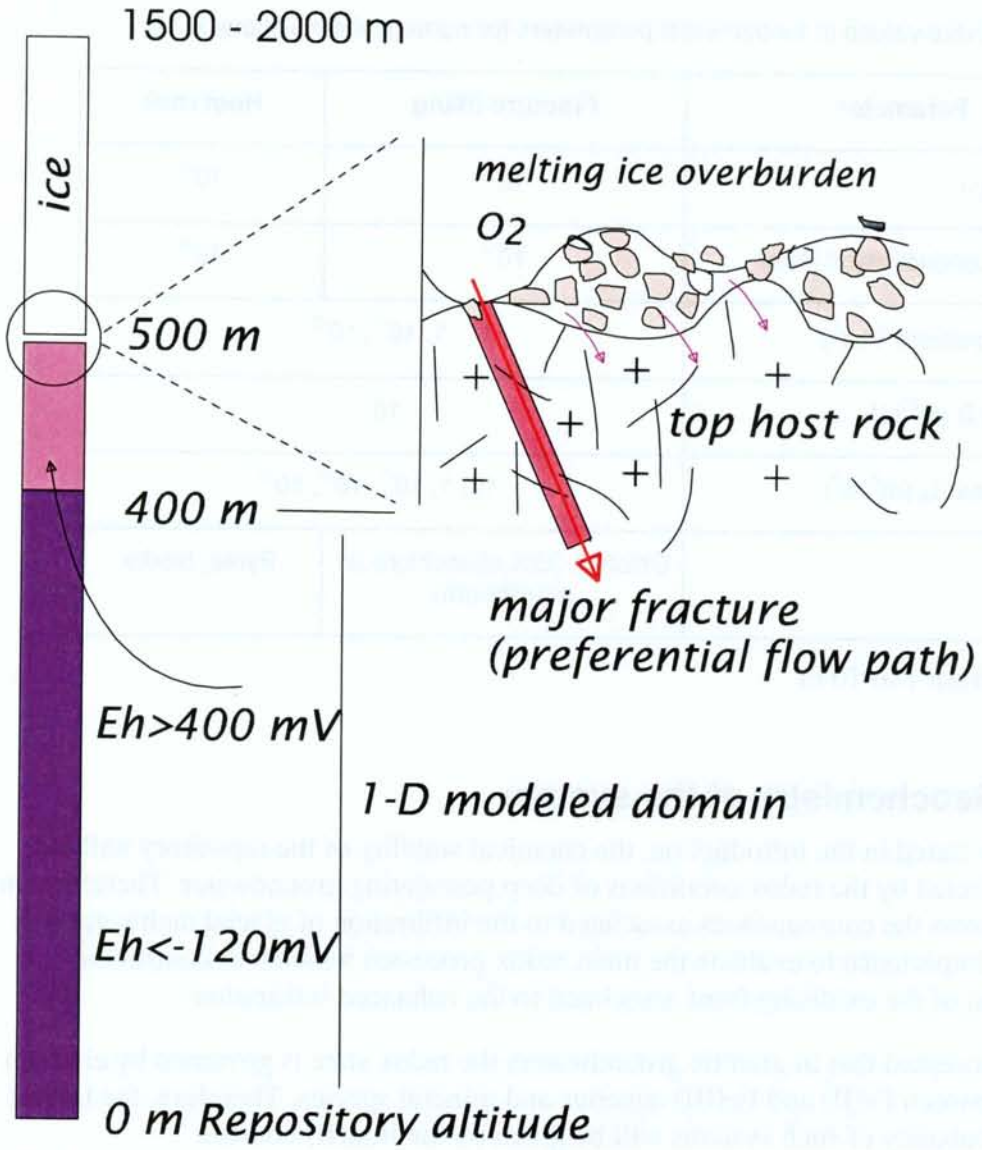

Figure 2-1. *Conceptual model scheme. The ice overburden is viewed as pressure exerted on top of the modeled domain (prescribed head). Ice melts and infiltrates through the top host rock, where redox conditions are oxidant (Eh > 400 mV). Thus, groundwater flows downwards through the modeled domain whose initial redox state is reducing (Eh < -120 mV). Initial groundwater composition for both fracture and host rock are assumed to be the same.*

The ability of Fe(II) containing clays to act as oxidant sinks has been pointed out b several authors. White and Yee, (1985) propose a structural oxidation of Fe(II) expressed by the following process:

$$\text{Fe(II) silicate} = \text{Fe(III) silicate} \qquad [2.2]$$

That is, Fe(II) is oxidised without being released to the aqueous phase.

Also homogeneous Fe(II) oxidation has been reported, in which Fe(II) is released in the form of Fe^{2+} from the clay and it is subsequently oxidised to Fe(III) in solution.

At pH > 4, the oxidation of Fe(II) is fast and leads to the precipitation of amorphous Fe(III) solid phases, mainly "$Fe(OH)_3.nH_2O$". The half life for this oxidation process at pH = 8 is on the order of 500 s. This implies the immediate oxidation of iron(II) as soon

as it is released from the minerals and for this reason, the redox state of most natural waters can be explained in terms of an equilibrium $Fe^{2+} \Leftrightarrow Fe(OH)_3(s)$.

Therefore, if the limiting factor for the oxidant uptake is the oxidation of iron, low Eh should be measured in groundwater, providing enough dissolved Fe(II) in solution so as to consume all the oxidant species entering the system. Nevertheless, this is not always the case and it is in those scenarios when the Fe(II) source plays an important role. In the case of existing an unlimited and readily available source, all the oxidants could be instantaneously reduced, but if the availability of iron(II) is not infinite or if the rate at which iron(II) is available is lower than the rate at which it is oxidised, then the factor limiting the oxidant consumption will be the rate of release of iron(II) to solution, in other words, the rate of weathering of Fe(II)-bearing minerals, such as clays.

A good evidence of the role that the ferrous iron released from the weathering of clays on the redox state of aqueous solutions plays is exemplified by the laboratory experiments reported by Malmström et al. (1995) on the dissolution of Fe(II)-bearing biotite. The dissolution of biotite is studied in 0.5 M $NaClO_4$ solutions under batch and continuous flow experiments. The authors report that at acidic pH´s, biotite dissolved congruently, and the redox potential of the system is fairly well described by an equilibrium between aqueous Fe^{2+} and amorphous $Fe(OH)_3(s)$, as can be seen in Figure 2.2:

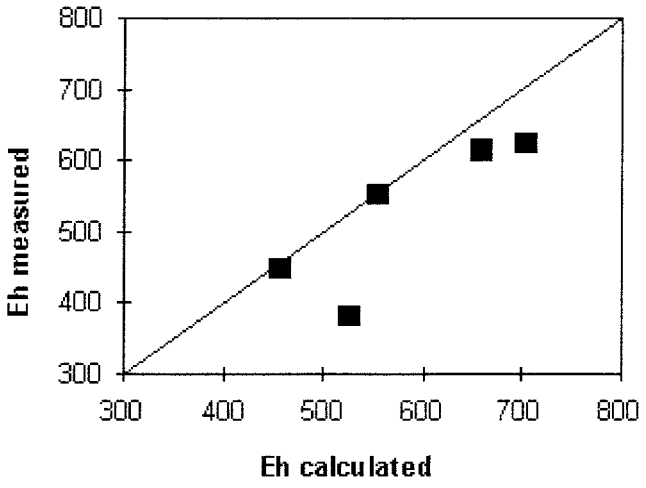

Figure 2-2. *Comparison between measured and calculated Eh (values in mV) by assuming $Fe^{2+}/Fe(OH)_3(s)$ equilibrium in acid solution.*

At neutral to basic pH this test on the redox potential of the system cannot be done due to the low reproducibility of the redox measurements. However, the iron concentrations in solution can be well described by equilibrium with $Fe(OH)_3(s)$, as reported by Malmström et al (1995).

These results highlight the role of Fe(II) present in clay minerals as one of the important oxidant sink of a deep groundwater system.

In order to set the conceptual model of the potential oxidant sinks in our system, we have separated the media into the following compartments: soil; near-surface oxidised zone and deep reduced zone (approx. 400 m depth)

The mineralogy of each of these compartments is of great importance to understand the changes in the composition of the inflowing water due to water-rock interaction and,

therefore, will be decisive to estimate which will be the role of every compartment in buffering the intrusion of oxidising water. We have focused on the mineralogical and geochemical data from Äspö in order to define the hypothetical fractured granitic system treated in this study. A short description of the mineralogy and of the processes considered in each one of the compartments is presented:

2.4.1 Soil

The effect of soils in buffering the oxic disturbance caused by an intrusion of oxygenated water has been clearly illustrated by the results of the redox experiment (REX) performed in Äspö.

The results obtained in the mentioned project indicated a substantial increase in the sulphate and in the alkalinity of the inflowing water while the value of pH was kept more or less constant. This can be only achieved by an increase in the partial CO_2 pressure in the media. One of the possible hypotheses given in order to explain these results was the occurrence of microbially mediated processes, mainly carbon respiration coupled to iron reduction, i.e., it was proposed that the iron(III) fracture minerals were acting as oxidants:

$$8\ Fe(OH)_3(s) + FeS(s) + 16\ H^+ = 9\ Fe^{2+} + SO_4^{2-} + 20\ H_2O \qquad [2.3]$$

$$4\ Fe(OH)_3(s) + CH_2O + 8H+ = 4\ Fe^{2+} + CO_2 + 11\ H_2O \qquad [2.4]$$

Despite the importance that can have these processes in the case studied in Äspö, we have neglected their influence in our analysis due to the fact that it is not clear how long will take in the permafrost to regenerate microbial activity. It is not clear, either, at which rate this processes will occur and, therefore, any attempt to use a rate of reaction could result in an overestimation of the actual reducing capacity of the system.

2.4.2 Oxidised Zone

The melt water will flow through an oxidised zone of approximately 100 m. depth close to the surface before entering the reduced zone. In the case of Äspö this area is manifested by the presence of iron(III) oxyhydroxides and the absence of pyrite. We should assume that no oxidant scavenging is produced in this zone, as the reducing capacity of the system is already depleted. In general this zone is thinner than used here.

2.4.3 Reduced Zone

From 100 m to 500 m depth, where the repository is presumably located, the media is reducing. Therefore, this will be the zone with a larger capacity to retard the migration of an oxidising front. The reducing capacity of the media (RDC) will be given by the presence of reductants, mainly ferrous iron (Banwart and Gustafsson, 1991). The major reservoirs of iron(II) are aqueous Fe(II) and Fe(II) contained in minerals, mainly pyrite, biotite and chlorite.

The conceptual models envisages two different domains according to the mineralogy and hydrodynalmical properties: conductive fractures and fractured host rock.

Chlorite was identified as the main Fe(II)-bearing mineral in the fracture fillings of Äspö. In fact, chlorite represents a 35% of the fracture coating in this zone, with an average content of 20% wt. in FeO (Banwart et al., 1992). With this information it is possible to estimate an stoichiometry of 1.5 moles of Fe per mole of chlorite. Chlorite can be regarded as a solid solution whose end-members are Daphnite ($Fe_5Al_2Si_3O_{10}(OH)_8$) the ferrous end-member, and Clinochlore ($Mg_5Al_2Si_3O_{10}(OH)_8$) the magnesian end-member.

We have assumed that it behaves ideally and, according to the calculated stoichiometry, the following solubility constant has been introduced in our database:

$$\text{Chlorite14A } (Fe_{1.5}Mg_{3.5}Al_2Si_3O_{10}(OH)_8) + 16H^+ = \\ = 1.5Fe^{+2} + 3.5Mg^{+2} + 2Al^{+3} + 3H_4SiO_4 + 6H_2O \qquad [2.5]$$

with log Kso = 59.9

Chlorite accounts for a 2.5-11.5% of the mineral content of the bulk rock, and its presence in the fresh bulk-rock is lower: 0.3% wt, mainly due to the lower extent of chloritization of biotite (present in the host rock in a 10% wt.). The composition of the Äspö groundwater present in the reduced zone is summarised in the Table 2.3.

Figure 2-3. shows the saturation state of this groundwater with respect to those minerals presenting a saturation index between +0.6 and -0.6 is shown.

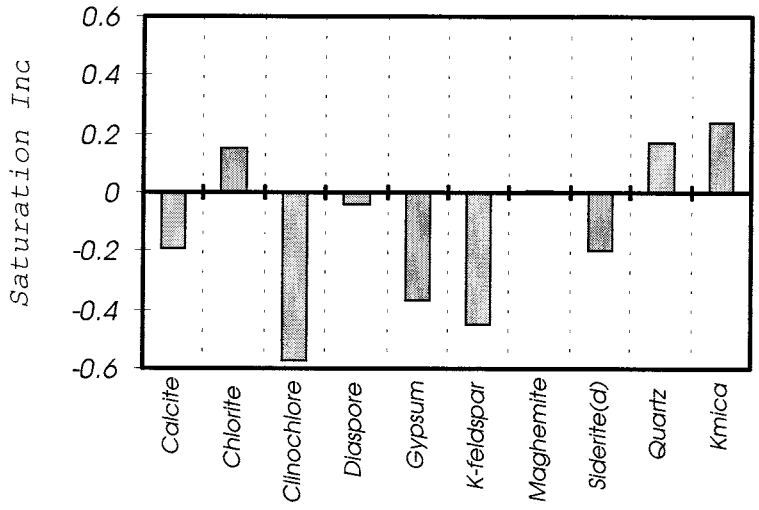

Figure 2-3. *Saturation index of several minerals in the Äspö groundwaters sampled in the reduced zone.*

Table 2-3. Composition of the Äspö groundwater (Banwart, 1995)

Parameters	values
pH	7.7
pe	-2
units	**mmol/kgw**
Ca	42.1
Na	91.3
Mg	1.73
K	0.205
Fe	0.033
Si	0.146
Cl	181
S	5.83
C(+4)	0.164
Al	0.00001

From this plot, we can observe that the assumption of equilibrium with quartz and calcite is reasonable. Also equilibrium with maghemite (an iron(III) oxide) and siderite seems to be reproduced in the system. Finally, the assumption of equilibrium with chlorite and clinochlore is likely to occur in these groundwaters.

These analyses gives important clues to simulate the evolution of the system under equilibrium assumption.

Besides chlorite and biotite, pyrite is another potential oxidant sink, which is present in the fresh host-rock in a 0.1% wt.

According to the analysis reported in Banwart et al. (1992) biotite contains 1 mole or iron per mole of mineral. As in the case of chlorite, biotite can be regarded as a solid solution whose end members are Annite ($KFe_3AlSi_3O_{10}(OH)_2$) and Phlogopite ($KMg_3AlSi_3O_{10}(OH)_2$). We have considered an ideal solid solution of these two end members to generate the biotite phase included in our database:

$$\text{Biotite } (KMg_2AlFeSi_3O_{10}(OH)_2) + 10H^+ = K^+ + 2Mg^{+2} + Al^{+3} + Fe^{+2} + 3H_4SiO_4 \qquad [2.6]$$

with log Kso = 35.88

According to our database, though, the Äspö groundwater sampled in the reduced zone is highly undersaturated with respect to phlogopite and pyrite, and it is supersaturated with respect to annite (see Figure 2.4).

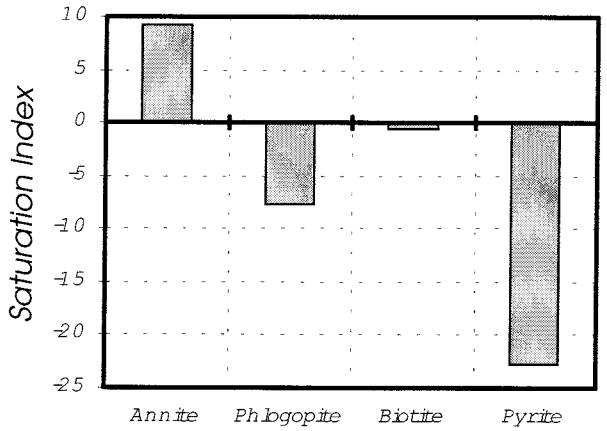

Figure 2-4. *Saturation index of annite, phlogopite, biotite and pyrite in the Äspö groundwaters.*

This analyses shows that these minerals (in particular pyrite) are not likely to be the ones controlling the redox state of the Äspö system. Nevertheless, the hypothetic redox control exerted by biotite and pyrite will be calculated for the sake of comparison.

One of the parameters with a larger associated uncertainty in this study is the groundwater velocity. When the groundwater velocity results in water residence times larger than the kinetics of the water reactions taking place in the system, we can assume that a equilibrium is reached In this case, we can treat the system as a set of successive equilibrium states. On the contrary when the groundwater velocity results in water residence times which are shorter than the time required to reach equilibrium in the key water rock interactions, then the kinetic control of the system has to be considered. (see Bruno, 1997 for a detailed discussion of these concepts).

Accordingly, the thermodynamic and kinetic control cases have to be approached differently in our calculations.

First of all we have applied the stationary-state approach (Licthner, 1988) to the system in order to compare the results obtained in the rest of approaches we use with the stationary-state model, used by other authors to evaluate the velocity of migration of the redox front (Arthur, 1996).

The equilibrium problem has been approached by using the geochemical code PHREEQC (Parkhust, 1995). Several cases have been set-up in order to test and compare the ability of the different compartments to buffer the intrusion of oxidative de-glaciation water. Always by assuming water-rock equilibrium.

On the other hand, the dynamic (or non-equilibrium) problem has been approached by using the computer code ARASE (see Chapter 4).

3 Preliminary calculations

3.1 Stationary-state approach

The stationary-state approach assumes a series of subsequent stationary states of the system and it has been used by other authors when evaluating the migration velocity of a redox front (Lichtner, 1988; Arthur, 1996).

As discussed, the reductive capacity of the system, i.e., the ability of the system to consume oxidants will be mainly given by its content in iron(II), either in aqueous or in solid phases. In general, as we have seen during the former analyses, the main species containing iron(II) in our system are: pyrite, biotite and chlorite and, therefore, the reducing capacity of this system will be given by the following expression:

$$RDC = n_{biotite}\, \nu_{biotite} + n_{chlorite}\, \nu_{chlorite} + n_{pyrite}\ \nu_{pirite} \qquad [3.1]$$

where n_i stands for the moles of iron containing mineral i per rock volume and ν_i stands for the stoichiometric factor of oxygen in the process of oxidation of the mineral i. As an example, in the reaction of oxidation of pyrite:

$$FeS_2(s) + 15/4\ O_2 + 7/2\ H_2O = Fe(OH)_3(s) + 2\ SO_4^{2-} + 4\ H^+$$

the value of $\nu_{pirite} = 15/4$

Therefore we can evaluate the initial reductive capacity of the fracture fillings and of the host rock as:

$$RDC = \rho \sum_{\substack{i=pyrite,\\ chlorite\\ biotite}} f_i \frac{w_i \cdot \nu_i}{M_i} \text{ (moles of } O_2/dm^3 \text{ of media)} \qquad [3.2]$$

where

f_i = fraction of mineral available for water-rock interaction (-)

w_i = mass of mineral i/mass of geological medium (-)

ρ = density of the fracture filling material or of the host rock

ν_i = stoichiometric factor of oxygen in the process of oxidation of the mineral. (This value will equal the number of moles of iron times ¼ moles of O_2 needed to oxidise each mole of iron for biotite and chlorite, and will be equal to 15/4 in the case of pyrite, due to the oxidation of sulphate).

M_i = molecular weigth of mineral i

(in consistent units)

In the stationary state approach, it is assumed that the oxygen introduced into the system due to the advective inflow of oxygenated water will be reduced as soon as it contacts

the minerals able to use it. In a way, this is a quasi-equilibrium approach. According to this theory, the time needed to deplete all the RDC of the system will be given by the velocity of oxygen inflow.

Let us assume a compartment of our system of dimensions 1 $dm^2 \times 1\ dm^3$ of material. Oxygen will not flow through the compartment until all the RDC of the system has been depleted and, therefore, the time necessary for oxygen to advance a distance of 1 dm will be equal to the time needed for the depletion of the RDC previously calculated plus the time needed for water to travel that distance.

The velocity at which oxygen is introduced in the system is: $v \times [O_2]_o$, where v is the Darcy velocity and $[O_2]_0$ is the concentration of oxygen in the inflowing water. Therefore, the time needed for oxygen to deplete all the RDC in one dm^3 of depth will be:

$$t_d = \rho \frac{\sum_{\substack{i=\text{pyrite,}\\ \text{chlorite}\\ \text{biotite}}} f_i \frac{w_i \cdot \nu_i}{M_i}}{v \cdot [O_2]_0} \qquad [3.3]$$

and therefore, the velocity of the redox front will be:

$$v_{RF} = \frac{v}{\phi \cdot \left(1 + \frac{\rho \sum_{\substack{i=\text{pyrite,}\\ \text{chlorite}\\ \text{biotite}}} f_i \frac{w_i \cdot \nu_i}{M_i}}{[O_2]_0 \cdot \phi}\right)} \qquad [3.4]$$

where ϕ stands for the porosity of the media and the rest of parameters have been already defined.

Table 3.1 summarises the values of the parameters used in equations [3.3] and [3.4] in order to estimate the velocity of migration of the redox front for both fractures and host-rock media.

Table 3-1. Values of the parameters used to evaluate the velocity of migration of the redox front according to equation 3.4

	v	ϕ	ρ	$[O_2]_0$	i	f_i	w_i	N_i	M_i
	dm/y	(-)	g/dm^3	mol/dm^3			g_i/g medium	$MolO_2/mol_i$	g_i/mol_i
Fractures	31;310;3100	0.01	1600	$2.6 \cdot 10^{-4}$	chlorite	0.01;0.1;1	0.35	3/8	604
Host-rock	3.1;31;310	0.001	2700	$2.6 \cdot 10^{-4}$	biotite	0;0.1;1	0.1	3/8	462
					pyrite	0;0.1;1	0.001	15/4	120

By substituting the values from Table 3.2 in equation [3.4] to evaluate the migration velocity of the redox front, one obtains values very similar to those obtained by Arthur (1996), that used the stationary state approach in a very similar system. Table 3.2 illustrates an example of front penetration.

Table 3-2. Migration velocities of the redox front and time needed to reach the repository depth calculated by substituting the values shown in Table 3.1. into equation 3.4

	v (dm/y)	f_i	v_{RF} (dm/y)	t (years)
Fractures	310	chlorite: 1 biotite: 1 pyrite: 1	0.19 0.03	$2.12 \cdot 10^4$ $1.48 \cdot 10^5$
Host-rock	31	biotite: 1 pyrite: 0 biotite: 0 pyrite: 1	0.037 0.097	$1.07 \cdot 10^5$ $4.12 \cdot 10^4$

As expected, the results obtained are very similar to the ones obtained by Arthur (1996), because of the application of the same approach to a very similar system. The differences in the results are mainly due to the difference in the Darcy velocities and the porosity and mineral abundance values.

Table 3.2 shows that the redox front migrates faster through fractures as a consequence of the fastest Darcy velocity. On the other hand we can see that biotite exerts a more efficient effect on the migration of the redox front in the host-rock than pyrite, mainly due to the lower abundance of pyrite in the medium.

In general, the results obtained show that the Darcy velocity and the fraction of mineral available for water-rock interaction exert an inverse effect on the velocity of migration of the redox front, i.e., the larger the amount of mineral and/or the lower the Darcy velocity, the slower the redox front migration. This effect can be observed in Figure 3.1.

One of the limitations associated to the use of the stationary-state approach in the way we have applied it in the former analysis is the underlying assumption of immediate total oxygen consumption, that is, we are assuming that oxygen is completely reduced in the medium as it contacts the minerals.

A way of improving the calculations is to consider that the reactions occurring between oxygen and minerals are instantaneous, as in the stationary-state approach but that the extent of oxygen consumption is limited by the equilibrium state. The following example illustrates this difference.

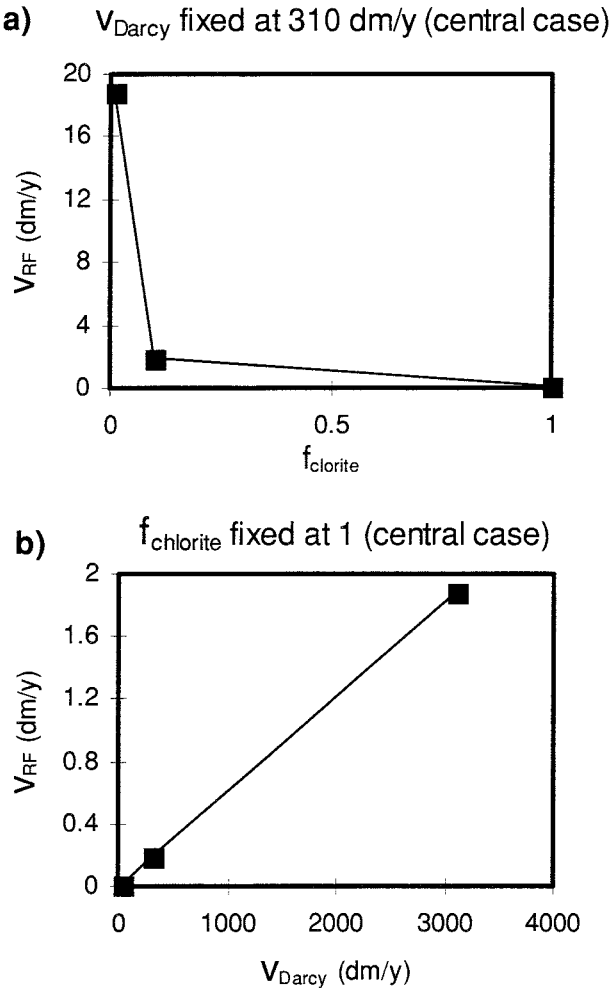

Figure 3-1. *Velocity of migration of the redox front through fractures.a)Effect of the value of the Darcy velocity; b) Effect of the fraction of chlorite available for water-rock interaction (f_i).*

In the stationary state approach, we are assuming that if 10^{-4} moles of oxygen enter the system (by considering a system of $1dm^3$ of water) and react with pyrite, the reaction taking place in the system will be:

$$FeS_2(s) + 15/4\ O_2 + 7/2\ H_2O \Rightarrow Fe(OH)_3(s) + 2\ SO_4^{2-} + 4\ H^+ \qquad [3.5]$$

and, therefore the amount of pyrite exhausted in the system after the intrusion of 10^{-4} moles of oxygen will be: $10^{-4} \cdot 4/15 = 2.67 \cdot 10^{-5}$ moles.

On the contrary, if we use an equilibrium approach, we have to consider the equilibrium constant of the former reaction, log K = 222.34, which depends on the pH and the sulphate content of the water, and which forces the system to leave an amount of

oxygen in the system enough as to ensure the equilibrium state, that is, different from zero.

For this reason, we have used an equilibrium approach by using the PHREEQC code. The methodology and the results obtained are presented in the following section.

3.2 Equilibrium approach

The PHREEQC code simulates pure advective transport where the chemical interactions of the system are considered always to reach equilibrium. The transport is simulated by consecutive replacement of the pore water contained in one cell. Each cell is assumed to contain one liter of pore water. We have defined different cells in our system. Each cell can be equal or different to the previous one. In pore water replacement, the water initially filling cell 1 is transported to cell 2, the water initially filling cell 2 is transported to cell 3 and so on. In this way, it is possible to translate the number of water replacements to time if we know the velocity of the groundwater.

In principle, and due to the facts explained above, we have neglected the influence of microbially mediated processes occurring in the top soil layer. Therefore, we have defined in our system 25 different cells. Cells 1 to 5 are assumed to represent the near-surface oxidised zone (zone B), extended up to 100 m depth. Cells 6 to 25 are 2 m long each and represent zone C, i.e., the reduced one. Figure 3.2 illustrates the system.

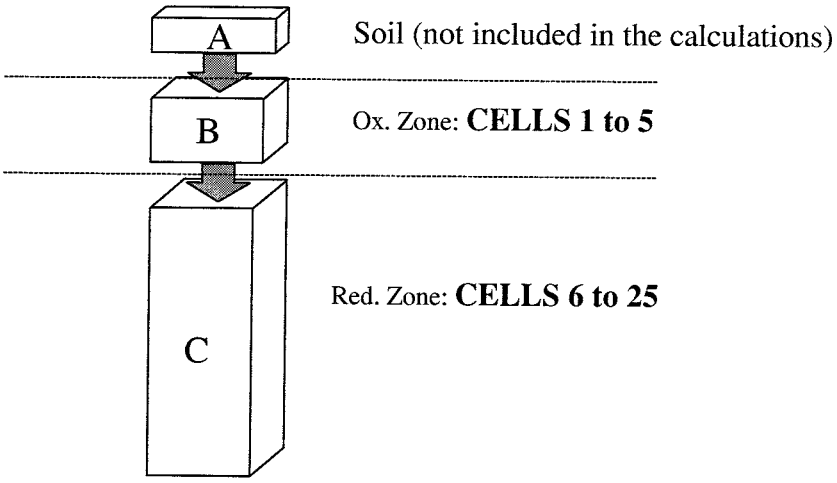

Figure 3-2. *Scheme of the system considered in the equilibrium approach.*

The following water-rock interaction reactions and initial water compositions are considered in each one of the compartments:

Compartment A: Soil

Compartment B: Oxidised zone

Initial groundwater: Shallow groundwater reported in Banwart (1995)

Mineral equilibria:

$Calcite = Ca^{2+} + CO_3^{2-}$ log Kso = -8.48

$Fe(OH)_3(s) + 3H^+ = Fe^{+3} + 3\ H_2O$ log Kso = 4.89

Compartment C: Reduced zone

Initial groundwater: Native Äspö groundwater

Mineral equilibria:

$Calcite = Ca^{2+} + CO_3^{2-}$ log Kso = -8.48

$Fe(OH)_3(s) + 3\ H^+ = Fe^{3+} + 3\ H_2O$ log Kso = 4.89

$SiO_2(s) + 2\ H_2O = H_4SiO_4$ log Kso = -3.98

$Kaolinite + 6\ H^+ = 2\ Al^{3+} + 2\ H_4SiO_4 + H_2O$ log Kso = 7.43

The main geochemical process considered in fractures is chlorite oxidation. We assume that chlorite oxidises and that, as oxidation product produces $Fe(OH)_3(am)$. In order to keep controlled the chemistry of the system, the precipitation of clinochlore, the magnesian end member in the composition of chlorite, has been allowed. Therefore, the system behaves as if the structural iron of chlorite is being released to the system and equilibrated with $Fe(OH)_3(s)$ due to the initial mineral constraints introduced in the problem.

Geochemical processes in host rock are:

Equilibrium with pyrite

$FeS_2 + 2H^+ + 2e^- = Fe^{+2} + 2HS^-$ log Kso = -16.23

Equilibrium with biotite according to [2.6].

In this case, both minerals, pyrite and biotite are able to accept oxidants and to precipitate in the form of $Fe(OH)_3(am)$.

3.2.1 Fractured media

Chlorite has been introduced as the main oxidant acceptor in the reduced zone, where the porosity is 0.01 and groundwater velocity is 31 m/y. We consider that all the chlorite present in the fracture filling is available for reaction, which means a content of 35% wt. of chlorite, as shown in Table 3.1.

Following, we present the results indicating the evolution of the chemistry in each one of the compartments:

Oxidised zone

The intrusion of oxic de-glaciation water (pe = 12) causes calcite and ferric oxyhydroxide dissolution, resulting in an slight increase of the alkalinity and the pH is kept constant at a value of 8.2. The redox potential becomes oxidising, with a value of pe = 12.9. Figure 3.3 shows the moles of calcite dissolved as a function of time in this compartment. According to the calculations, the rate of dissolution of this mineral is of $7.58 \cdot 10^{-4}$ moles per liter per year (by assuming a groundwater velocity of 31 m/year).

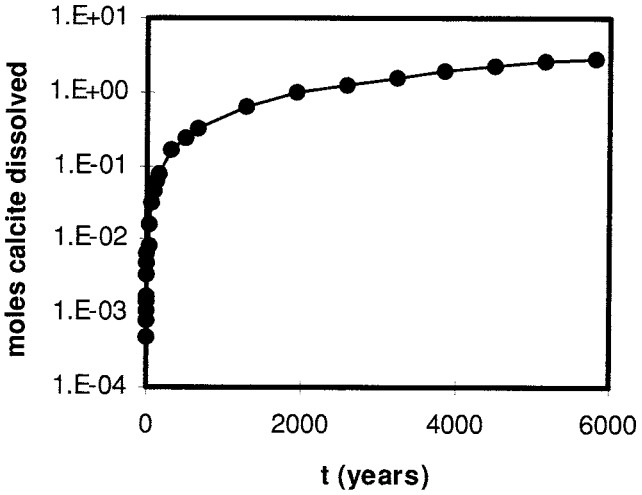

Figure 3-3. Cumulative moles of calcite dissolved in compartment B as a function of time.

The chemistry of the system is buffered to the following values in the oxidised zone:

pH	pe	Ca_{tot}	Fe_{tot}	HCO_3^-
8.29	12.29	$4.91 \cdot 10^{-4}$	$2.63 \cdot 10^{-8}$	$9.44 \cdot 10^{-4}$

Reduced zone

The oxic intrusion is buffered by the dissolution of chlorite. The pH evolves from 7.7 to 8.3 and the initial pe (-2) slightly increases due to the equilibration of the system with chlorite (final pe = -1.07). The dissolution of chlorite gives rise to a precipitation of $Fe(OH)_3(s)$, as it can be observed from Figure 3.4. The water, once equilibrated with chlorite in first cell of the compartment, passes to the next cell and so on. This implies that chlorite in the subsequent cell does not dissolve until it has been exhausted in the former cell, i.e., until there is not enough chlorite in the former cell as to equilibrate with groundwater.

This evolution can be followed with time and with depth, as shown in Figure 3.5. In this figure, depths down to 100 m correspond to the oxidised zone, where the initial chlorite content is 0 and the initial $Fe(OH)_3(s)$ content is 10, in order to have an infinite pool of $Fe(OH)_3(s)$ available. On the contrary, in the reduced zone, i.e., at depths from 100 m to 500 m, the initial chlorite content is given by the abundance of the mineral in the fracture fillings (18.4 moles in this case) and the initial $Fe(OH)_3(s)$ content is assumed

to be zero. Thus we can ensure that all the iron(III) hydroxide precipitated is a result of the oxidation of chlorite. A natural consequence of the assumptions outlined above is that the profile of precipitation of $Fe(OH)_3(s)$ in the reduced zone matches the profile of dissolution of chlorite in the same zone.

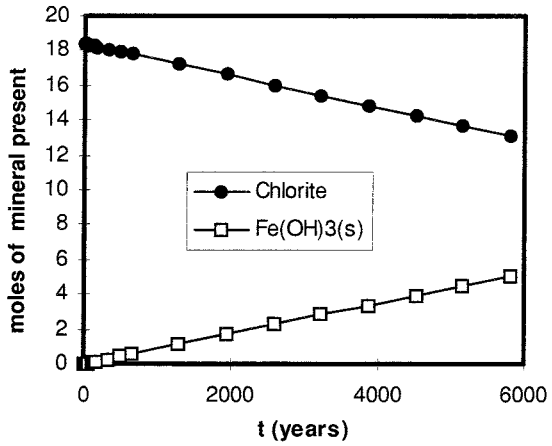

Figure 3-4. *Precipitation of $Fe(OH)_3(s)$ as a function of time in the first cell of the reduced zon. Chlorite does not exhaust during the time span studied here.*

The redox front is effectively retarded in this case, as can be observed in Figure 3.6., where the pe value is shown as a function of depth for different time steps.

The chemistry of the system is buffered to the following values in the reduced zone:

pH	pe	Ca_{tot}	Fe_{tot}	HCO_3^-
8.34	-1.07	$4.53 \cdot 10^{-4}$	$9.78 \cdot 10^{-7}$	$9.05 \cdot 10^{-4}$

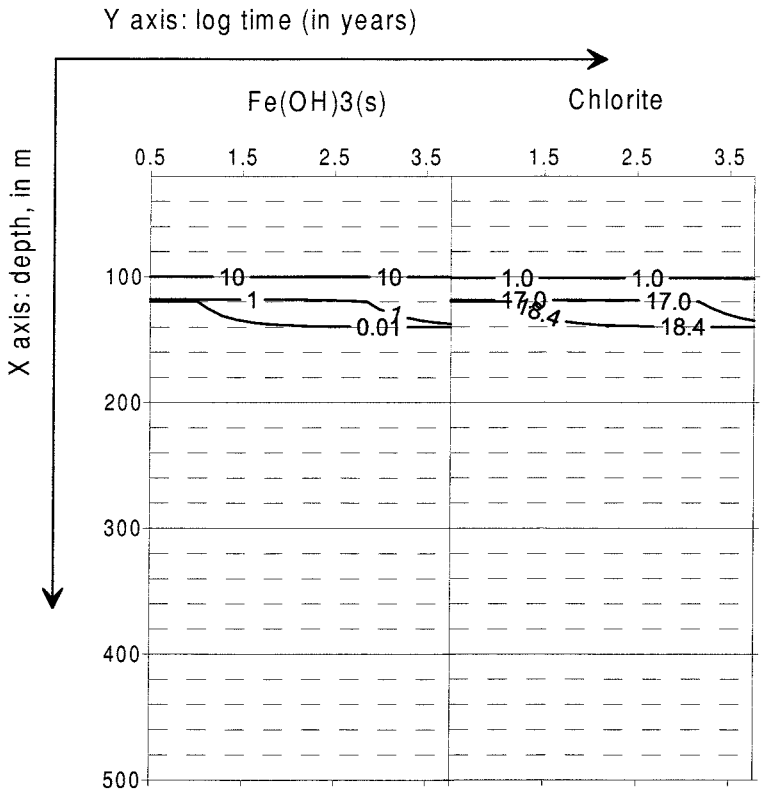

Figure 3-5. *Evolution of the chlorite and the $Fe(OH)_3(s)$ content with time and depth.*

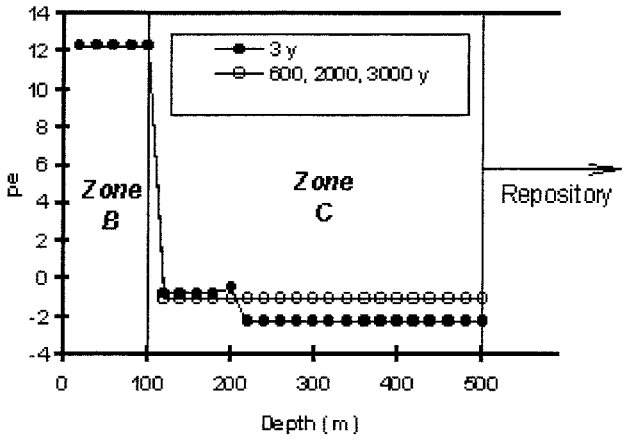

Figure 3-6. *Evolution of pe in the system. The first 100 m correspond to the oxidised zone.*

In order to illustrate which is the general effect of an oxic intrusion in a system where chlorite is the main oxidant acceptor, we have plotted in figure 3.7. the moles of chlorite dissolved and the moles of the different minerals precipitated as oxygen is being added to the system.

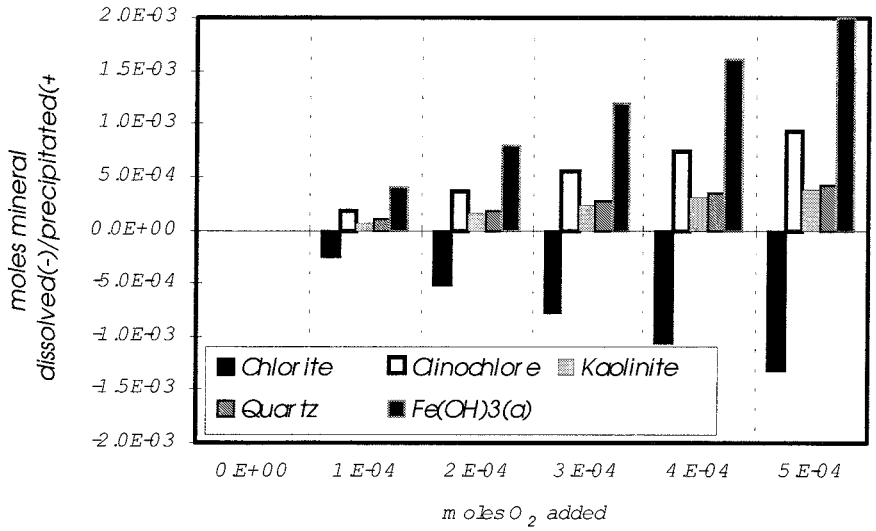

Figure 3-7. *Mineralogical changes in the system as oxygen is added.(Chlorite always dissolves, negative; Fe(OH)3(a) always precipitates, positive).*

From the previous figure, we can calculated the ratio of the transformation Chlorite → Fe(OH)3(a) to be 1.5, expected due to the stoichiometry of iron in chlorite (1.5). In the same way, we can estimate the ratio of the transformation Chlorite → Clinochlore as 0.7, given by the ratio of Mg^{2+} in both minerals (3.5 versus 5). From this analyses, it seems clear that the redox couple considered to buffer the redox potential at mildly reducing values and retarding the migration of the oxidant intrusion is Chlorite/$Fe(OH)_3$(s).

The exhaustion of chlorite has an important effect on the migration of the redox front. Once the main oxidant acceptor, chlorite in the case studied here, is exhausted, the redox front will migrate at the groundwater velocity.

From the results, it is possible to calculate the velocity of chlorite dissolution: $9.05 \cdot 10^{-4}$ moles of chlorite per liter per year. By taking into account the initial chlorite content in each cell, we can see that chlorite will be exhausted in $2.03 \cdot 10^{4}$ years in one cell, i.e., the redox front will advance 20 meters in this time and, therefore, the velocity of migration of the redox front is calculated to be: $9.86 \cdot 10^{-4}$ meters per year through the reduced zone. This implies that the time needed to reach the repository depth will be: 3.2 years through the oxidized zone B + $4.05 \cdot 10^{5}$ years through the reduced zone C ~ 0.4 million years if the main groundwater flow occurs through this type of fractures.

By comparing the values of the redox front velocity and the time estimated to reach the repository depth obtained in the equilibrium approach with those values obtained by using the stationary-state approach we can see that under equilibrium assumption, the redox front is more effectively retarded due to the fact that the dissolution of the mineral is slower than when assuming total oxygen consumption, as is the case of the stationary-state approach. The exact values are as follows:

	v_{RF} (m/y)	t (y)
Stationary-State*	1.9×10^{-2}	2.12×10^{4}
Equilibrium	9.9×10^{-4}	4×10^{5}

*values taken from Table 3.2.

3.2.2 Host rock

In these calculations we consider that the groundwater flux occurs through a homogeneous porous medium of granite. Compartment B is exactly the same as in the previous case.

In order to proceed as in the stationary-state model, we have tested three different assumptions in this case corresponding to the ones shown in Table 3.2:

Case HR1: only pyrite consumes oxidants ($f_{pyrite} = 1$; $f_{biotite} = 0$)

Case HR2: only biotite consumes oxidants ($f_{pyrite} = 0$; $f_{biotite} = 1$)

Case HR3: both pyrite and biotite consume oxidants ($f_{pyrite} = f_{biotite} = 1$)

CaseHR1: only pyrite consumes oxygen

The difference of this case with the fractured media is that the main oxidant acceptor is pyrite instead of chlorite, which will affect to the results obtained from compartment C, i.e., the reducing zone. The results indicate that, as expected, the pe of the groundwater equilibrated with pyrite is lower than in the case of considering chlorite as reductant in the media

The chemistry of the system is buffered to the following values in the reduced zone:

pH	pe	Ca_{tot}	Fe_{tot}	HCO_3^-
8.17	-4.36	$7.11\cdot10^{-4}$	$2.74\cdot10^{-6}$	$1.13\cdot10^{-3}$

In any case, the migration of the redox front does not occur until pyrite is exhausted in the media.

The rate at which pyrite is dissolving in the system is on the order of $9.7\cdot10^{-6}$ moles per liter per year. By taking into account the initial pyrite content in each cell, we can see that it will be exhausted in 464327 (470000) years in one cell. Therefore, the velocity of migration of the redox front is calculated to be: $4.3\cdot10^{-5}$ meters per year through the reduced zone. This implies that the time needed to reach the repository depth will be some $1\cdot10^{7}$ years if the main groundwater flow occurs through the host rock. We can proceed as in the case of fractures and compare this figures with the ones obtained in the stationary-state approach when only pyrite is considered to be present in the host-rock. The comparison is as follows:

	v_{RF} (m/y)	t (y)
Stationary-State*	9.7×10^{-3}	4.12×10^{4}
Equilibrium	4.3×10^{-5}	1.0×10^{7}

*values taken from table 3.2.

We can see that in this case there is a difference of three orders of magnitude, due to the lower rate of pyrite dissolution, what implies that pyrite is a very efficient oxygen scavenger and, therefore, it is going to be a very good redox buffer if it is allowed to equilibrate with the flowing groundwater.

According to these calculations, we can see that the velocity of migration of the redox front is slower if we assume an homogeneous porous media than when considering that groundwater flows preferentially through fractures. This result was already expected, due to the efficiency of the pyrite oxidation process.

As previously discussed one of the main uncertainties of the system is related to the concentration of oxygen in the glacial meltwater. In order to test the influence of this parameter on the velocity of migration of the redox front, we have performed several calculations by assuming that the oxygen content in the recharge is three times the atmospheric value, i.e., fO_2 (g) = 3 x 0.21 = 0.66 atm. The comparison of the results obtained in one and in the other case is shown in figure 3.8.

We can see that the oxidised zone extends up to 100 m depth, characterised by the absence of pyrite. At depths larger than 100 m, the initial pyrite content is of approximately 4 moles. As the system evolves pyrite is depleted as indicated by the contour concentration lines with values lower than 4. Due to the larger oxygen input in the case plotted in the right hand side of the figure (2), the rate of pyrite dissolution is faster and consequently the calculated isolines reach lower values for the same period of time.

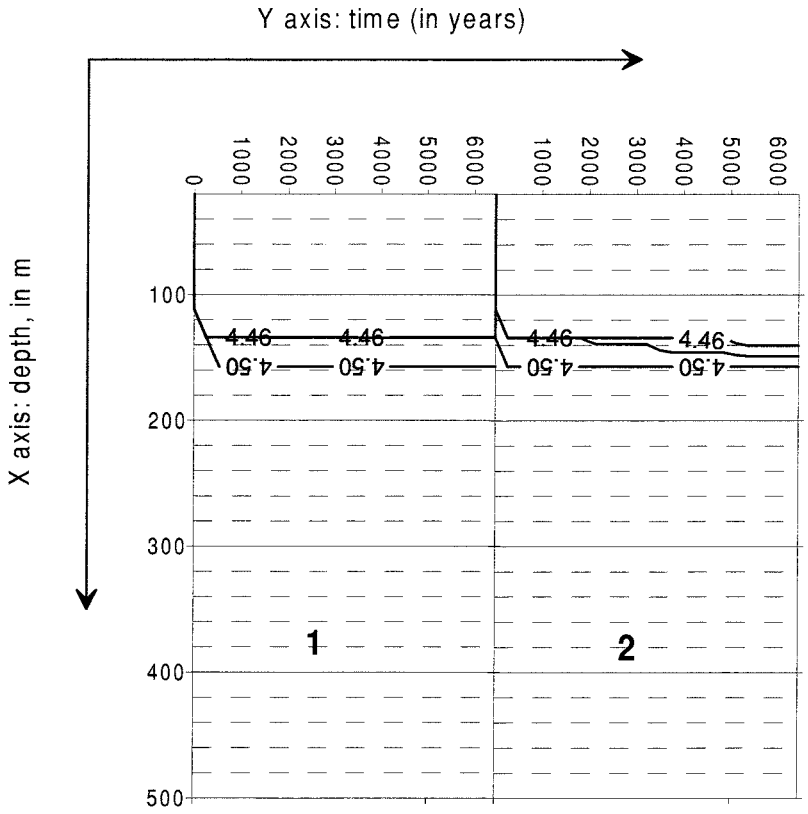

Figure 3-8. *Comparison between the moles of pyrite present in the system as a function of depth and time. (1): the fugacity of oxygen equals the atmospheric value (0.21 atm); (2): the oxygen content of the infiltrating groundwater is three times larger (0.66 atm).*

The velocity of migration of the redox front in these two cases is:

Case 1: $4.3 \cdot 10^{-5}$ m per year through the reduced zone, i.e., 10 million years to reach the repository.

Case 2: $1.3 \cdot 10^{-4}$ m per year through the reduced zone, i.e., 3 million years to reach the repository.

From these figures it seems clear that the difference in the initial oxygen considered in the calculations affects the velocity of migration of the redox front as expected, i.e., the largest the oxygen input, the fastest the velocity of migration of the redox front. In order to simplify the calculations, though, only one case will be assumed: considering that the infiltrating groundwater contains an oxygen concentration equilibrated with the atmosphere.

CaseHR2: only biotite consumes oxygen

The chloritization of biotite is a very well-known phenomenon in natural granitic environments. In fact, when studying the saturation state of the groundwater sampled in the reduced zone of Äspö with regard to these two minerals (biotite and chlorite) we can see that it is very close to equilibrium (see figure 2.4. in the previous section). Nevertheless, we must take into account that biotite is slowly altered in an incongruent fashion, producing a large variety of secondary minerals, depending on the weathering environment. In order to simulate the oxidant consumption due only to biotite, we have not considered the presence of chlorite. The aqueous chemistry of the reduced zone is very efficiently buffered to the following values:

pH	pe	Ca_{tot}	Fe_{tot}	HCO_3^-
9.13	0.64	$1.4 \cdot 10^{-4}$	$4.92 \cdot 10^{-8}$	$6.02 \cdot 10^{-4}$

From the uncommon alkaline pH value obtained in this case, it seems that this simulation does not represent a reallistic situation. On the other hand, the redox potential is buffered to a positive value and the comparison with the other cases, where negative redox potentials are achieved, is difficult to do. Therefore, we prefer to skip this case in the equilibrium calculations and to simulate the combined effect of pyrite and biotite as oxidant acceptors in the system.

CaseHR3: both, pyrite and biotite consume oxygen

In this case, the chemistry of the system is very efficiently buffered to the following values:

pH	pe	Ca_{tot}	Fe_{tot}	HCO_3^-
8.27	-4.37	$6.00 \cdot 10^{-4}$	$8.03 \cdot 10^{-5}$	$1.07 \cdot 10^{-3}$

And, as we can observe, these values are very similar to the ones obtained in case HR1.

The rate of pyrite dissolution at steady-state is of $9.7 \cdot 10^{-6}$ moles of pyrite per liter and per year, i.e., the same value obtained in case HR1 from where we can infere that the redox effect exerted by biotite is negligible if pyrite is present in the system.

The equilibrium approach can be regarded as a useful way of understand the system, however it presents severe limitations with regard to the validity of the results obtained:

a) The water replacement is complete, i.e., the water initially contained in cell 1 passes to cell 2 and so on. Therefore, the approach will be more valid as more cells are considered in the system. This problem can be solved by increasing the number of cells which causes a dramatic increase in the calculation time.

b) No dispersion is considered in this approach. As we will see later when analysing the results obtained from the reactive transport approach, the dispersion term can have important effects in the movement of the constituents of groundwater.

c) Water is assumed to equilibrate with the minerals present in the system. This assumption is valid only when the characteristic times of reaction are lower than the residence times of groundwater, i.e., when the water flows at a velocity slow enough as to allow equilibration with the mineral. This can be useful when dealing with fast heterogeneous systems, such as dissolution/precipitation of calcite or $Fe(OH)_3(s)$, but can led to important misinterpretations when considering dissolution of aluminosilicates (such as chlorite and biotite) or sulphides (e.g. pyrite) due to their slow kinetics of dissolution under most natural groundwaters conditions.

In order to estimate whether the equilibrium approach is more or less appropriate than a kinetic approach it is very useful to compare the residence time of groundwater versus the time needed for the system to reach equilibrium. These calculations are shown below:

3.3 Equilibrium vs. Kinetics

We will analyse here whether an equilibrium or a kinetic approach will more reallistically describe the system in cases where either chlorite (fractured media) or pyrite (host rock) are the main oxidant acceptors.

3.3.1 Fractured media

In the case of water flow through fractures, the main oxidant acceptor we have considered is chlorite. In order to reach equilibrium, we have estimated that the rate of dissolution of chlorite must be $9.05 \cdot 10^{-4}$ moles of chlorite per liter per year and that the pH value is buffered at 8.34.

We have assumed that the rate of dissolution of chlorite is very similar to the rate of dissolution of biotite (Malmström et al., 1995) and, therefore, the following rate law can be applied:

$$R_{diss} = 0.08457\ [H^+]^{0.51} + 6.437 \cdot 10^{-11}\ [H^+]^{-0.65}\ mole \cdot m^{-2} \cdot y^{-1}$$

and, at pH = 8.34:

$$R_{diss} = 2.16 \cdot 10^{-5}\ mole \cdot m^{-2} \cdot y^{-1}$$

By using the porosity and the surface area of chlorite per volume of rock, we can estimate the rate in terms of moles per liter of water per year in order to compare it with the rate of dissolution obtained from the equilibrium analyses. The most difficult parameter to estimate is the surface area. We have used the largest value of surface area shown in Table 2.2 (10, 1 and 0.1 m2/m3 of rock). In any case, the values obtained by using these surface area will be overestimations of the actual rate and, therefore we will be sure that if by using these values for the surface ares the rate of dissolution of chlorite is not high enough as the rate required for the system to reach equilibrium, a kinetic approach will be more appropriate to simulate the system. The results of the calculations are shown below:

$S_A(m^2/m^3)$	$R(moles \cdot dm^{-3} \cdot y^{-1})$	To compare with:	More appropriate approach:
10	$2.16 \cdot 10^{-5}$		Kinetics
1	$2.16 \cdot 10^{-6}$	$9.04 \cdot 10^{-4}$	Kinetics
0.1	$2.16 \cdot 10^{-7}$		Kinetics

As we can see, the rate of dissolution of chlorite is not fast enough as to allow the equilibration of the system and, therefore, the use of kinetics is advisable.

3.3.2 Host rock

According to the equilibrium calculations, the rate of dissolution of pyrite was $9.7 \cdot 10^{-6}$ mol per liter and per year. The rate of dissolution of pyrite is given by the following expression:

$$R_{diss} = 0.044 \cdot [O_2]_{aq} \ mole \cdot m^{-2} \cdot y^{-1}$$

Proceeding as in the previous case, and by taking into account the oxygen content in the oxygenated water, we can calculate that the rate of dissolution of pyrite would be:

$SA(m^2/m^3)$	$R(moles \cdot dm^{-3} \cdot y^{-1})$	To compare with:	More appropriate approach:
10	$5.54 \cdot 10^{-71}$		Kinetics
1	$5.54 \cdot 10^{-72}$	$9.7 \cdot 10^{-6}$	Kinetics
0.1	$5.54 \cdot 10^{-73}$		Kinetics

And, as in the previous case, it seems clear that a kinetic approach is more advisable in the case of assuming the dissolution of pyrite as the main oxidant acceptor.

This is the reason why, in the reactive transport calculations, we will assume dissolution of these minerals according to their kinetic rate laws instead of assuming instantaneous equilibration of the system with those solid phases.

4 Numerical model

This chapter deals with the simulation of redox front migration by means of reactive transport models. First, the approaches to the reactive transport simulation are reviewed with special emphasis to cases pertinent to the present project. Second, a brief description of the used code is given. Third, we describe the common features to all cases studied, basically definition of the problem and structure of the models. In section four, the most relevant results achieved with different conceptual models are described and discussed. Finally, the results of the simulations are summarised and compared.

4.1 Background on modelling of reactive transport

An extensive dissertation on the topic would be too ambitious and it is out of the scope of the report. However, a brief summary is provided for completeness in the framework of the report.

The modelling of solute transport with many chemical reactions has experienced a vast growth since Rubin (1983) stated early quantitative approaches to the problem. The problem admits at least, two approaches, and a third one as a combinations of the former two: The geochemical system is in equilibrium -the chemical reactions happens so fast that may be considered instantaneous- or the rate at which they occur is governed by a "slow" kinetics, that does not permit the former approach. Indeed, many geochemical systems display a combination of both types of reactions. The former are homogeneous aqueous reactions, while the second are usually heterogeneous water/rock interactions. Additionally, sorption and/or ion exchange reactions can be present.

The problem admits several numerical treatments (Friedly and Rubin, 1992; Steefel and McQuarrie, 1996). Usually, the direct or forward problem formulation is most extensively used. Basically, this formulation admits either direct sequential substitution (Saaltink and Carrera, com.pers.), where both chemical and transport equations are solved together, or successive iterations, where the equations are solved separately. When sufficient information is available, the inverse geochemical modelling provides a better understanding of the system (Glynn and Brown, 1996). Similarly to applications of inverse problem in hydrogeology (Carrera and Neuman, 1986) inverse geochemical modelling uses existing ground water chemical and isotopic data, which are assumed to be representative of the chemical and isotopical evolution of a ground water along a given flow path, and attempts to identify and quantify the reactions that may have been responsible for the evolution of ground water. Although an aqueous speciation code may be used to identify thermodynamically possible -or impossible- reactions and to determine the dissolved inorganic carbon content and the redox state of a given groundwater, the inverse modelling approach does not require that reactions proceed to thermodynamic equilibrium. Indeed, mass balance constrains and the expert judgement of the user concerning the possibly occurring reactions are the only constrains in the inverse modelling approach.

Reactive transport applications to real cases are widespread. One of the most known cases involving redox evolution is the Poços de Caldas Natural Analogue System

(Waber et al., 1990). One of the characteristic features of redox fronts observed in Poços de Caldas is the presence of a narrow bleached zone millimetres or less in thickness sandwiched between the iron oxide zone formed from oxidation of pyrite and the deposition of uraninite. The bleached zone is presumably caused by oxidising pyrite without deposition of iron oxide or uraninite. Cases dealing with redox evolution, frequently involve pyrite oxydation. Hence, Engesgaard and Kipp (1992) use data on chemical denitrification produced by pyrite presence to validate a geochemical transport model. Nitrate removal has often lead to geochemical transport modelling, as stated by Trudell et al. (1986). Appelo and Postma (1993) present several cases where reduction of a given metal is the subject of aquifer remediation and cleaning-up techniques. Similarly, Friedly et al (1995) compare the results of chromium reduction in field scale studies to laboratory experiments.

In fact, many problems in contaminant hydrology are being addressed by multicomponent reactive codes (Clement et al., 1998). The scope of the problems are as detailed as mineral-fluid interactions at the molecular scale (Sherman, 1998) and as broad as fluid processes in sedimentary basins (Bjørkum, 1998).

The system we attempt to model is controlled by more than one redox sensitive mineral and multiple species and aqueous complexes have to be taken into account. Differently to the redox cases mentioned above, our system involves chlorite as redox control phase in the fracture filling marterial, as well as biotite -and pyrite in the host rock.

4.2 The ARASE code

The ARASE application has been designed to model geochemical performance of engineered barriers within host rock environments (Grindrod et al., 1994). Such systems may be represented by a heterogeneous reactive transport model. Despite the original concept, ARASE has proven to be capable of handling several problems in different formations.

The input parameters for an ARASE calculation can be broken into chemical reactions, geometry of the region of interest, physical properties of the region of interest, fluid boundary conditions, chemical transport boundary conditions, mesh properties and result output times.

The chemistry -the reactions which may take place- is assumed to be the same in all regions, although the initial conditions of the chemical concentrations may be varies between regions. The reactions of interest are selected from lists generated from the HATCHES database (Cross and Ewart, 1989) and a small mineral database provided with ARASE and that can be easily modified by the experienced user. Two types of reactions are performed. The first type is of equilibrium or instantaneous reactions. These reactions are generally aqueous complexation reactions which are assumed to be in equilibrium throughout the calculation. The second type are the kinetically controlled processes. These reactions take place at a rate which may be governed by parameters such as the concentration of other chemical species in the system. A useful feature of ARASE is the automatic suggestion of additional equilibrium reactions which may take place, given the initial choice of components. This is an additional check for the expert user regarding the completeness of the chemical model.

ARASE requires a two dimensional area of study, which can be composed by several regions or sub-domains, each of them displaying different physical and chemical properties. Boundary conditions are of fluid flow and of chemical transport type. The former consists of prescribed head or flow, while the latter is of fixed concentration of chemical)

An automatic gridding routine is included in ARASE, which produces triangles of different areas and shapes so as to cover the region boundaries defined by the user.

In this context, ARASE is used to integrate the hydrogeological and geochemical conceptual models and to analyse the impact of the reactive transport of the oxygen-containing melt-water on the RDC of the granite host-rock (geosphere). Quantitative estimates of the redox front were produced for the time scales involved in a HLW repository conditions (thousands of years).

4.3 Definition of the problem

The problem is analysed under 1D and 2D approaches. On one hand, 1D cases provide a simple and efficient description of the most relevant processes occurring. The counterpart is that a regional flow scheme is hardly reproduced in one dimension. On the other hand, 2D models permit to simulate hydrogeological conditions more resembling to reality, although they still present some limitations that will be discussed below.

As stated in section 4.2, given problem can be divided between the geochemical system and the physical definition of the system. The first refers to the definition of the chemical components, the mass law and stoichiometric relationships and the thermodynamic and kinetic relationships. The structure of the model can be viewed as the extent of the domain, zones of parameters, and flow and transport conditions. For consistency, we split the description of the structure of the models into 1D and 2D types, but the chemistry of the systems can be outlined singly.

4.3.1 Chemistry

The geochemical system attempts to simulate those processes described in chapters 2 and 3 in the most resembling manner. For that, we first represent a system with a pH buffered by calcite and where iron controls the RDC of the system. The thermodynamical equations of the system are described in Table 4.1. The presence of minerals (chlorite, biotite and pyrite) is constrained to fracture filling or host rock.

Weathering of chlorite and biotite is described under two assumptions: On the other hand, the kinetic rate law depends on the saturation index, i.e., the rate of dissolution decreases as the system approaches equilibrium. Second, the mineral is assumed to dissolve independently on the state of saturation of the system. Some differences were observed making use of both approaches and they are consequently discussed. Equations describing the kinetics of the reactions are also shown in Table 4.1. Note that the weathering of both, chlorite and biotite describe a parabolic function which

minimum lays at neutral pH values, when they are assumed to dissolve independently on the degree of saturation of the system (Figure 4.1).

Table 4-1. Thermodynamic and kinetic equations of the geochemical system buffered by calcite (aqueous phases)

Log k	Charge	Stoichiometry
11.40	1	MGHCO3+ <=> MG+2 H+ CO3-2
-14.00	-1	OH- <=> H2O -H+
-86.08	0	O2(AQ) <=> 2H2O -4H+ -4E-
10.33	-1	HCO3- <=> CO3-2 H+
16.68	0	H2CO3 <=> CO3-2 2H+
33.65	-1	HS- <=> SO4-2 9H+ 8E- 4 H2O
2.25	0	MGSO4 <=> MG+2 SO4-2
-11.48	2	Ca+2 <=> CALCITE -CO3-2
-9.17	0	cASO4 <=> CALCITE -CO3-2 SO4-2
-0.13	1	CAHCO3+ <=> CALCITE H+
3.80	1	FeOH+ <=> HFO 2H+ E-
-12.29	0	Fe2O3(AQ <=> Fe2O3
12.52	1	FeCL+ <=> FeO 3H+ E- CL- -3H2O
13.30	2	Fe+2 <=> FeO 3H+ E- -3H2O

Stoichiometry of biotite and chlorite:

2×n mineral <=> nFeO 3×nH+ nE- -3×nH2O

Kinetic equations for biotite and chlorite (units in mol m^{-2} $year^{-1}$):

$$Rate = -0.08457 \cdot [H^+]^{0.51} - 6.437 \cdot 10^{-11} \cdot [H^+]^{-0.65} + (term\ on\ SI)$$

$$Term\ on\ SI = 14.7 \cdot [H^+]^{0.51} \frac{[Fe^{+2}]^n}{[Mg^{+2}]^n} + 1.12 \cdot 10^{-8} [H^+]^{-0.65} \frac{[Fe^{+2}]^n}{[Mg^{+2}]^n}$$

n=number of moles of Fe^{+2}

chlorite: n=1.5

biotite: n=1

Stoichiometry of pyrite:

pyr <=> FeO 2SO4-2 -8H2O 16H+ 14E-

Kinetic equations for pyrite:

$$Rate = -0.044 \cdot [O_2(aq)] - 6.437 \cdot 10^{-11}$$

The way in which pyrite kinetics is described may have some implications that are worth commenting. Pyrite kinetics depends on the aqueous oxygen content (Stumm and Morgan, 1981) as indicated in Table 4.1. In this context, pyrite oxidation will take place under highly oxidising conditions, yet oxygen contents below 10^{-7} mol/l would prevent the reaction to occur. The initial groundwater composition of the conceptual model adopted is highly anoxic at the reduced zone, with pe = -2; thus, pyrite oxidation does not progress.

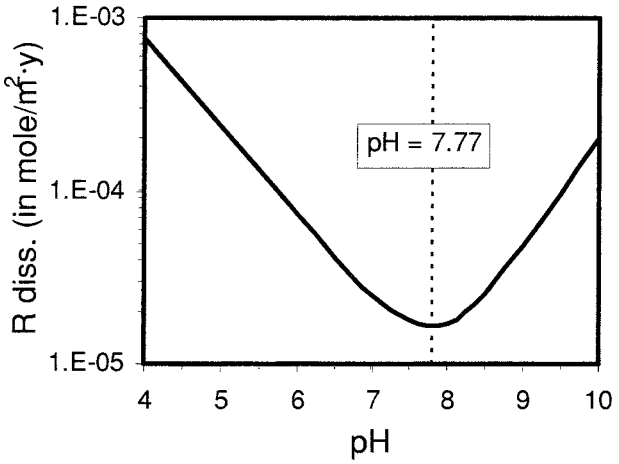

***Figure 4-1**. Weathering rate of chlorite as a function of pH. Note that the minimum lays at neutral - slightly alkaline values of pH and that for both alkaline and acidic conditions, the rate increases.*

Additionally, a system not buffered by calcite was attempted. The objective was to check the effect of a low pH on the weathering of chlorite and consequently on the release of Fe(II) and on pe values. For the sake of comprehensiveness the aluminosilicates system was included. Finally, a third geochemical conceptual model of iron release was attempted, consisting of equilibrium among magnesian and ferrous chlorites. Thermodynamic and kinetic equations describing these systems are expressed in Table 4.2.

Table 4-2. Thermodynamic equations of the geochemical system not buffered by calcite (see Table 4.1 for kinetic equations)

Log k	Charge	State (*)	Stoichiometry
-86.08	0	0	O2(AQ) <=> 2 H2O -4 H+ -4 E-
10.33	-1	0	HCO3- <=> + CO3-2 + H+
33.65	-1	0	HS- <=> + SO4-2 9 H+ 8 E- -4 H2O
11.35	1	0	CAHCO3+ <=> + CA+2 + CO3-2 + H+
2.31	0	0	CASO4 <=> + CA+2 + SO4-2
11.40	1	0	MGHCO3+ <=> + MG+2 + H+ + CO3-2
-14.00	-1	0	OH- <=> + H2O - H+
2.25	0	0	MGSO4 <=> + MG+2 + SO4-2
-9.50	1	0	FE(OH)+ <=> + FE+2 + H2O - H+
-25.59	0	0	FE(OH)3 <=> + FE+2 3 H2O -3 H+ - E-
-16.90	0	0	AL(OH)3 <=> + AL+3 3 H2O -3 H+
-22.70	-1	0	AL(OH)4- <=> + AL+3 4 H2O -4 H+
0.78	1	0	FECL+ <=> + FE+2 + CL-
8.48	0	1	calc <=> + CA+2 + CO3-2
-16.30	0	1	Fe(OH)3(s) <=> + FE+2 3 H2O -3 H+ - E-
-10.80	0	1	gibbs <=> 3 H2O -3 H+ + AL+3
2.70	0	1	quartz <=> -2 H2O + H4SIO4
-7.43	0	1	KAOLINITE <=> 2 AL+3 2 H4SIO4 + H2O -6 H+

(*) 0=aqueus 1=solid

Minerals in equilibrium:

-61.00	0	1	Chlorite_14A	<=>	1.50FE+2 3.50MG+2 2AL+3 +3H4SIO4 6H2O -16H+
-63.24	0	1	Chlinochlore_14A	<=>	5MG+2 2AL+3 +3H4SIO4 6H2O -16H+

4.3.2 Structure of the 1D models

The dimension -depth- of the domain was set to 400 m, which is the minimum extent of the reducing conditions below an oxidising zone of some 100 m, at which a potential repository site is planned. The selected grid considered a set of regular triangular cells of "length" smaller than 10 m. Such a size was selected after a sensitivity analysis, since it made no significant differences at the input boundary, where most of the chemical transport changes occur and where the concentration gradients are higher. In this respect, coarser grids (L ≈ 50 m) showed that differences in one pe unit could be achieved at the input boundary (Figure 4.2). Such difference becomes negligible some

distance away from the boundary (repository depth). One could contend that the coarser grid would have been more CPU-time efficient; however, we selected the finer grid for the 1D simulations since the evolution along the whole domain is reported. This discussion is extended in the case of the 2D models, where coarser grids were imposed due to computational requirements.

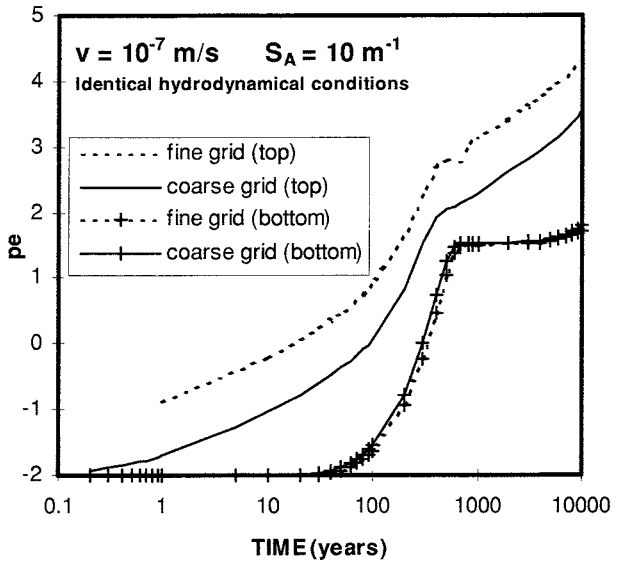

***Figure 4-2**. Sensitivity analysis of the arrival time and magnitude of the redox front at different positions of the grid. Bottom is the depth of the repository and top is immediately below the input boundary. Average size of the coarse grid cells is aproximately 10 times the fine grid. Note that differences observed in the coarse grid at 400 m (some 10 cells away) are negligible compared to those at the input boundary where concentration gradients are maximum.*

1D simulations were homogeneous and isotropic. The reasoning behind the groups of parameters used has been discussed in Chapter 2. The number of cases analysed is displayed in the next section (Table 4.6). Hydraulic conductivity, porosity and hydraulic gradient are combined so as to produce groundwater velocities ranging from 10^{-5} to 10^{-10} m/s.

The hydrodynamical dispersion coefficient always fall in the order of meters up to few tens of meters. In this respect, a sensitivity analysis was carried out in combination to the previously mentioned for the grid size. Figure 4.3 shows the effect of increasing twice the value of α_L. Some differences are found at the first arrival time of the redox front at repository depth. However, no changes are displayed for the final value of pe.

Chemical composition of groundwater and of boundary input water were selected according to reference Äspö groundwater (Banwart et al., 1995) and to highly oxidising ice melt water with 45 ppm O_2 (Ahonen and Vieno, 1994; Yang et al., 1996) respectively. In fact, the input groundwater into the reducing domain is pressumably equilibrated with the oxidising zone laying below the ice sheet and above the modeled domain (see Figure 2.1). In order to properly simulate such composition, we first equilibrated the ice melt water with calcite and iron oxides. Their composition is expressed in Table 4.3

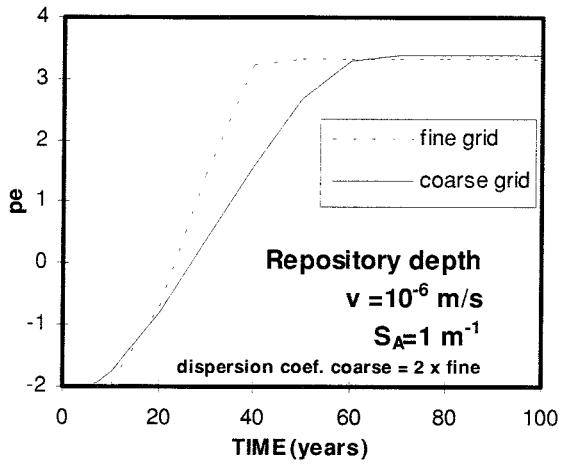

Figure 4-3. Comparison of diferent dispersion coefficient for different grids at the same depth (400 m from the input boundary). While the arrival time is affected, the final value of the pe does not display significant changes.

Table 4-3. Compositions of groundwater used in the models

Compound	Ice melt water ($\times 10^{6}$ mol/l)	Boundary ($\times 10^{3}$mol/l)	Domain (mol/l)
Cl^-	0.65	0.169	0.181×10^{0}
NO_3^-	1.77		
SO_4^{-2}	0.875	0.180	0.583×10^{-2}
HS^-			0.455×10^{-5}
Na^+	0.37	0.446	0.913×10^{-1}
K^+	0.05	0.00005	0.205×10^{-3}
Mg^{+2}	0.06	0.132	0.173×10^{-2}
Ca^{+2}	0.25	0.848	0.473×10^{-1}
$Si(OH)_4$		0.237	0.146×10^{-3}
Fe^{+2}			0.43×10^{-5}
pH		8.15	7.7
pe		12	-2

Flow and transport boundary conditions are constant over time. Therefore, when modelling the evolution of the redox front, oxidising water enters with the same composition and at the same rate during the whole period, independently of the duration of the simulation. This is extended for 2D models.

4.3.3 Structure of the 2D models

The main objective of such 2D analysis was to combine the presence of materials with different hydrodynamical and geochemical properties and the distribution of certain flow conditions, which was prevented in 1D cases.

Three different conceptual models are attempted in 2D. The domain of the model 1 cover a cross section of 500 × 500 m. The system is described as a top zone and a rock mass of 100 and 400 m thick respectively. The rock mass is composed of host rock and a vertical zone which mimics a fracture. Figure 4.4 illustrates the distribution of material zones, zones of boundary conditions and the grid used. In models 2 and 3, boundary conditions are imposed on top of a fracture zone, with homogeneous hydrodynamical properties and chemical conditions according to oxidising the top 100 m and reducing the rest. Dinmensions of models 2 and 3 are 500 m deep × 350 m wide.

One could contend that the dimensions of the domain does not permit to fully represent regional flow conditions. For that, we rely in a conventional scheme given by Tóth (1963) with modifications according to the presence of a thick ice overburden (Boulton and de Marsily, 1997; Svensson, 1996). Figure 4.5 illustrates how regional flow conditions are taken into accout into the 2D models.

Differently to the 1D cases, the system in 2D is viewed as if truly ice melt water infiltrates into the rock mass. Therefore, very diluted and oxidising water recharge the domain through an oxidising zone, presumably laying above the reducing medium. According to how this recharge is produced, two different conceptual models are analysed:

Water infiltrates through the rock mass surface (conceptual model 1)

Water infiltrates through a fracture zone of "high" permeability (conceptual model 2)

In the first case, water moves preferentially through the oxidising top zone which homogenises the composition of groundwater moving deeper into the host rock and fracture. The second case attempts at simulating a highly preferential flow through the fracture, which is prescribed at the recharge surface. It is expected that the results will not be extremely different one from each other, especially at repository depths after a period of 1000 years, but they will be more sensitive to the hydrodynamic conditions which in turn, control the residence time.

A third conceptual model was attempted imposing parallel flow across a domain composed of a fracture and host rock, the flow being parallel to the fracture major axis. In principle, such model is analogous to two 1D cases of similar groundwater flow velocities. However, hydraulic and solute concentration gradients between the two materials are considered, which are not in the former one dimensional analyses.

As regards parameters and water composition, the first have been kept as close as possible to realistic values either to field measurements (Rhén et al., 1997) or to expected values during glaciation periods (Boulton and de Marsily, 1997). For consistency, water composition has been fixed to values described in Table 4.3: composition at the input boundary is the ice melt water, composition at the top oxidising zone is the one depicted as "boundary condition" in Table 4.3 and the host rock and

fracture below the upper 100 m display initial composition depicted as "domain". However, such composition distribution created some numerical convergence problems since pe differences were extreme between a certain number of cells. For that, after a sensitivity analysis, we were forced to accommodate the pe of the top oxidising zone to a value of 5. Such change has no major implications for the final results, since the pe at the input boundary is kept oxidising enough (pe = 15.7).

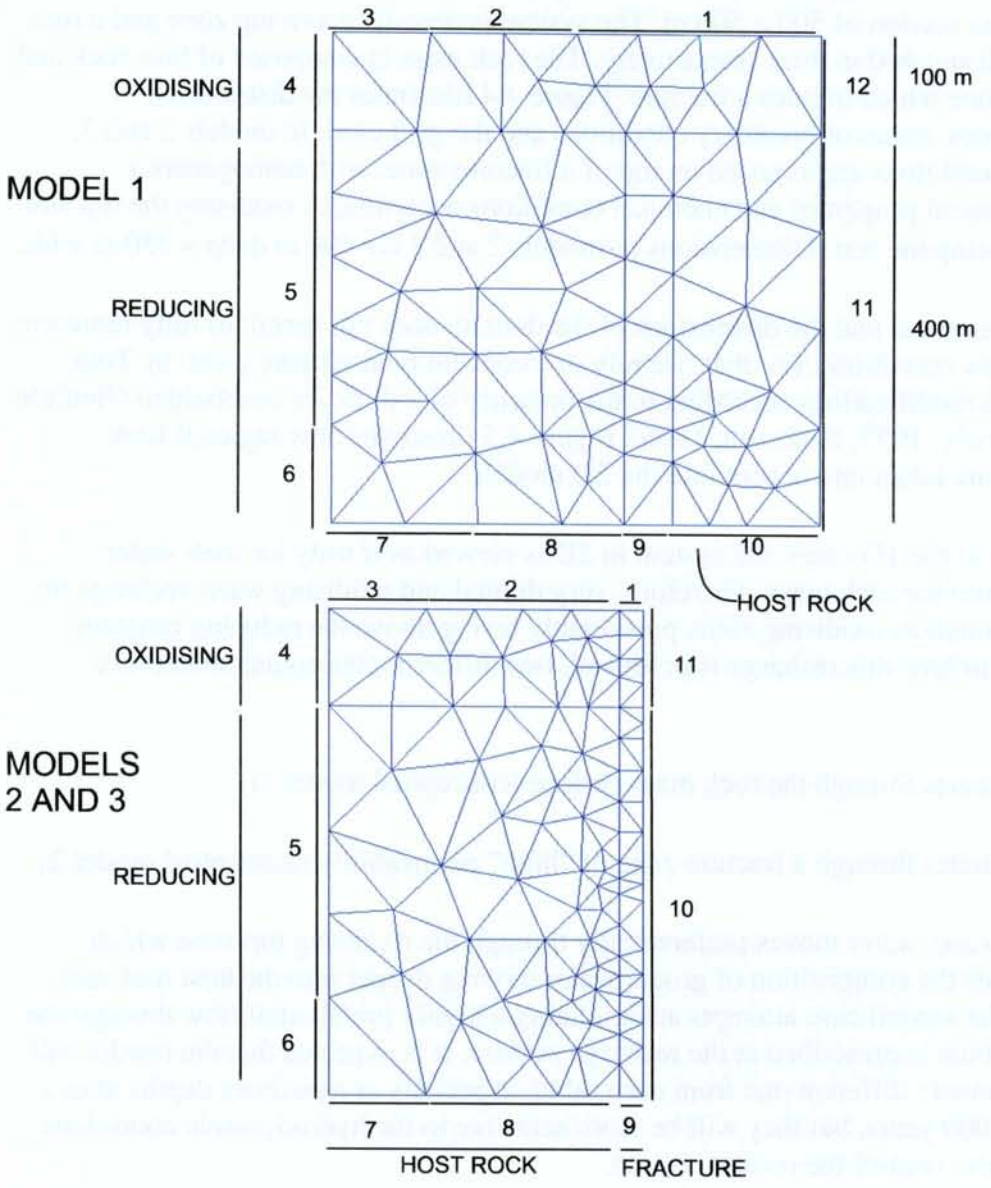

***Figure 4-4**. Distribution of material zones, grid used and number of flow boundaries. Conditions for these boundaries varied along the analyses and they are expressed in Table 4.4.*

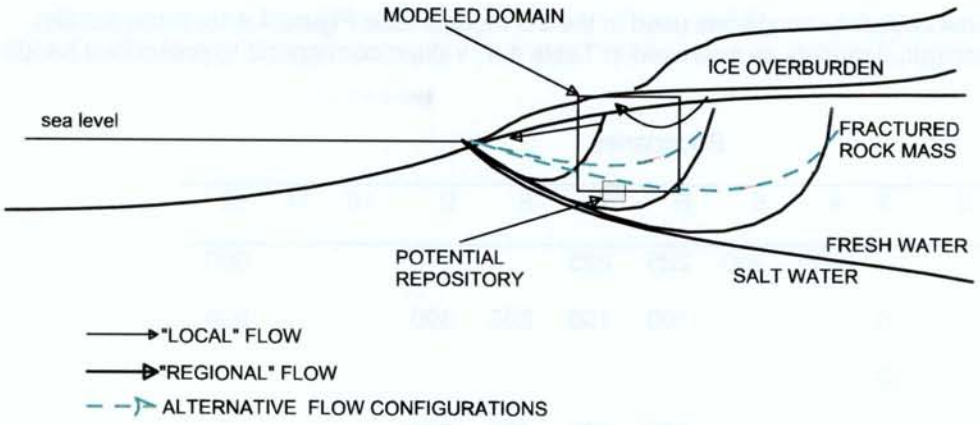

Figure 4-5. *Groundwater flow at regional scale (several km) and idealisation of the modeled domain in this report.*

The presence of minerals described by kinetics was adopted as in 1D cases: initial content of chlorite in fracture fillings is 91.8 mol/l groundwater and pyrite and biotite in the host rock are 22.5 and 447 mol/l groundwater respectively. The dissolution rate law was always limited by the saturation index.S_A values are not varied as in 1D cases, but fixed according to previous results which are described latter on. S_A for chlorite i 10 m^{-1}, while for biotite and pyrite is 0.1 m^{-1}. The reasoning for such low values in the host rock is that we expect a decrease of S_A proportional to the scale of our domain and accordingly, to the presence of flowing features (see Banwart et al., 1998 for further discussion).

Table 4-4. Parameters used in 2D simulations. Runs 5, 7 and 8 pertain to conceptual model 1; runs 9 and 10 correspond to conceptual model 2 and run 11 to conceptual model 3. Values in m and years

run	K_{top}	$K_{fracture}$	K_{host}	D_{top}	$D_{fracture}$	D_{host}
5				5	1.	0.21
7				6	2	0.21
8	0.0310	0.3100	0.0031	6	2	0.3
9				-	6	0.6
10				-	6	0.6
11	-	31	0.0031	-	70	10

Table 4-5. Flow boundary conditions used in the 2D models (see Figure 4.4 for more details). Runs and conceptual models as expresed in Table 4.4. Values correspond to prescribed heads in m H_2O

	Boundaries											
run	1	2	3	4	5	6	7	8	9	10	11	12
5	500			400	300	225	225					500
7	500		0			100	100	200	300			500
8	800		0									
9	800		0			300	300	400	500			
10	500		0			200	200	300	400			
11	500	500						450	450			

4.4 Results

Following, the results are presented according to the different models adopted. 1D cases are explained first, followed by the 2D ones.

4.4.1 1D cases

Prior to any description or discussion of the results, it should be recalled the structure of the model, since it has some implications on the results. The modelled domain extends over 400 m above the repository depth, which is considered the minimum domain where reducing conditions will be present in real conditions. The oxidising zone between the ground surface -bottom of ice- and the reducing zone extends over 100 m. Thus, the modelled domain accounts for 80% of the total travel zone -500 m-. The arrival times thus calculated, should be corrected by adding 3, 30 or 300 years to the results - corresponding to velocities of 10^{-5}, 10^{-6} and 10^{-7} m/s-. We demostrate that this effect is negligible in all of the cases considered and consequently, corrections have not been made. Table 4.6 summarizes the cases analysed.

The system buffered by calcite

The evolution of the system is descrtibed in terms of dependence of the redox conditions on groundwater velocity, reactive surface area and kinetic formulation of the controlling mineral phase. The RDC of the system is described as well.

Figure 4.6 compares the results of different cases. The effect of groundwater velocity is notorious not only for the arrival time of the redox front (time at which formation's pe starts to denote any change), but also for the values of pe achieved. Hydrodynamic dispersion of cases at velocity 10^{-7} m/s was 1 order of magnitude higher than that adopted for v=10^{-6} m/s and accordingly, the shape of the breakthrough curves becomes less steep (α_L = 10 m compared to 1 m). Despite the relevance of the first arrival time of the redox front, we observe that the effect of velocity on the final pe value is important when the kinetic reaction is not limited by the saturation index of the mineral dissolving: differences of one unit pe are achieved. When the reaction rate is limited by SI, the final pe values are exactly the same.

Table 4-6. Summary of the 1D cases analysed according to geochemistry, flow conditions and surface areas considered. Times at which pe reaches a stable value and the value at repository level obtained are expressed in columns 5 and 6

Case	v (m/s)	S_A (m^{-1})	Mineral	Time (y)	pe
Not buffered					
B1		0.001			7
C1		0.01			6
A1	10^{-5}	1		5	4
B1_b		10			3.2
C1_b		100			2.1
C2		0.01	Chlorite		5.2
A2		1			3.2
B2	10^{-6}	10		50	2 (2)
C2_b		100			1.7 (2)
D2		10	(1)		2 (2)
C3		0.01			(3)
A3	10^{-7}	1		500	2.3
B3					1.5
PB_B1	10^{-6}	10	Pyr-biotite	150	2.7
PB_B2	10^{-7}			90	1.7
DC_4	10^{-5}	-	Eq. Mg-Fe	20	1.7 (4)
DC_3	10^{-6}	-	chlorites	200	1.7 (4)
Buffered					
B2_doc5		10	chlorite	40	2
B2_doc6			chlorite-SI	40	2.2
C2_doc4	10^{-6}	100	chlorite	40	1
C2_doc6			chlorite-SI	40	2.2
B3_doc3			chlorite	700	1
B3_doc4		10	chlorite-SI	700	2.2
PBD1dc22	10^{-7}		biotite	300	3
PBD1dc11		1	biotite-SI	300	3
PBD1doc3		1	biotite		(5)
PBD1doc1	10^{-10}	10	biotite-SI		(5)

(1) Chlorite content = 1/100 other cases

(2) Chlorite is exhausted

(3) Steady state not reached after 400 years

(4) Sligth increase

(5) Steady state not reached after 1000 years

The redox state of the system is strongly dependent on the way which we describe the kinetics of the mineral (either limited by SI or just dependent on the pH). Differences thus obtained attain up to 1.3 pe units for chlorite with an assumed value of S_A of 100 m-1. For slow groundwater velocity differences are important as well. Nevertheless, such differences are not extremely relevant for the geochemical stability of the spent fuel, as we discuss latter.

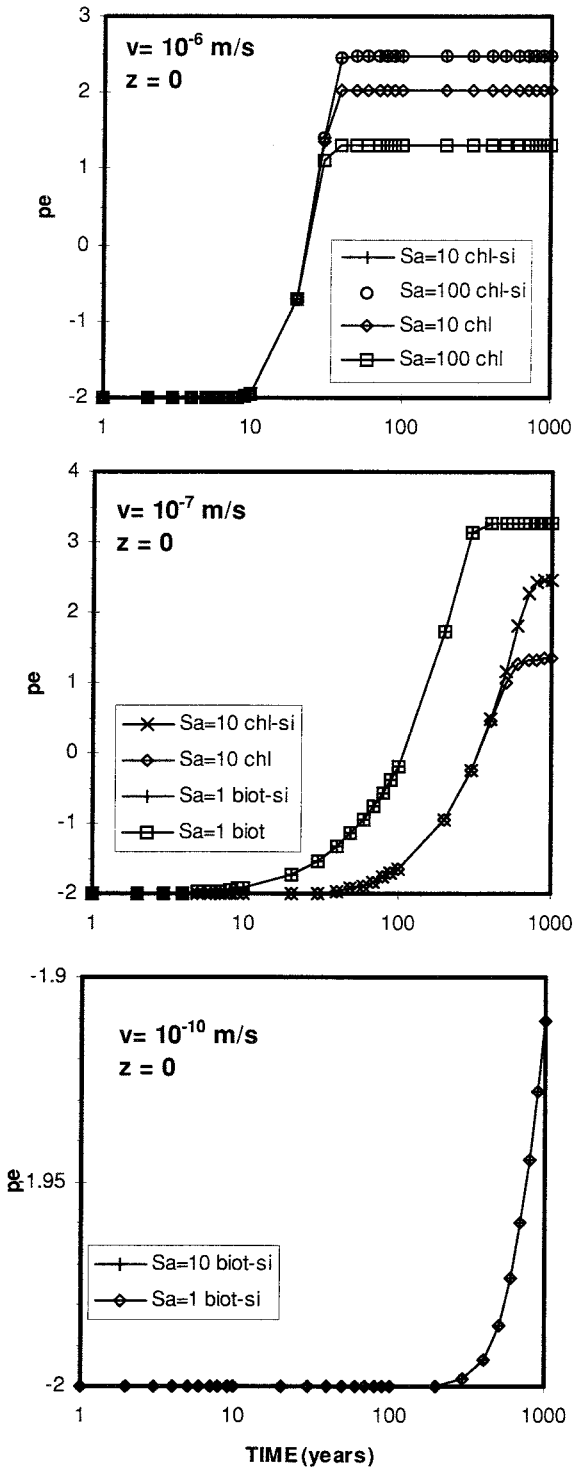

Figure 4-6. *Comparison of the evolution of the pe for different cases. Note that different minerals and reactive surface areas are compared across the graphs.*

All cases analysed -including those not buffered and also the 2D models-return a dissolved oxygen content below 10^{-20} mol/l at relatively early times, due to the initial pe values. Such content has two main implications: First, that the oxidants of the system will not be those entering within the recharge water, but those resulting from the water rock-interaction. Second, that pyrite does not take part in the geochemical system, since we expresses pyrite kinetics as a function of dissolved oxygen concentration.

Biotite contrasts with chlorite despite the fact that their kinetic expression is remarkably resembling. Biotite does not show dependence nor on the saturation index neither on the reactive surface. Such effect -or better, lack of effects- is explained by the fact that water stays far from saturation in biotite. As a matter of fact, since the kinetic expression takes on the form:

$$R = R(1-\Omega) \qquad [4.1]$$

the saturation state Ω becomes negligible since it takes values on the order of 10^{-16}. Therefore, both results -limited and not limited by SI- are comparable.

Figure 4.6 also illustrates that the pe evolution controlled by biotite at very low velocities barely displays any difference after 1000 years, which is a consequence of the low mass flow of oxidants.

The evolution of the Fe(II) system is described in Figure 4.7. A striking feature is the different trends displayed by both systems: as long as the release of iron is only controlled by pH, it increases monotonically. On the contrary, when kinetic dissolution of chlorite is limited by the saturation index, a steady state is rapidly reached. Such fact has implications on the RDC of the system. Recall that we define:

$$RDC = 1.5[\text{chlorite}] + \Sigma \left| Fe^{II} \right|^{tot}_{aq} \qquad [4.2]$$

therefore, the variation of RDC, that is, the difference between the initial and final reductants, is -1.77 when the mineral is not limited by the SI and pe values close to 1 are attained. For a mineral dissolution limited by the SI, the difference is smaller, -6.75×10^{-5}, and pe values attained are slightly more oxidant, close to 2.5. In fact, the dissolution of chlorite limited by SI becomes null far from the boundary and after 100 years some precipitates (few milimoles) are produced.

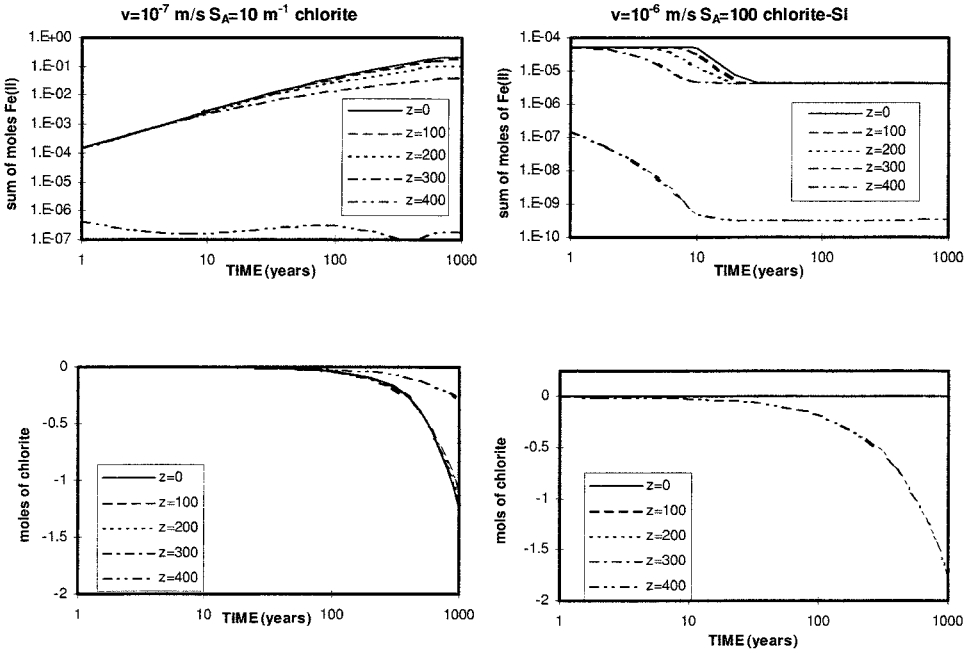

Figure 4-7. Fe(II) variation in the systems which have returned more extreme values of pe.

For comprehensiveness, Figure 4.8 describes the evolution of sulfate ion. Although redox processes related to sulfate are relevant in presence of bacteria, it is worth

commenting the effect of mixing and reduction. Input concentration at 400 m and the initial content of the domain are of 2×10^{-4} and 3×10^{-3} mol/l respectively. While the boundary rapidly changes and slowly attains the value of the prescribed concentration, the system at different depths follow almost the same trend as the pe curves (see Figure 4.6). Note that sulfate reduction is important when chlorite kinetics is not limited by the SI: the prescribed concentration decreases down to one order of magnitude (from 2×10^{-4} to 1.5×10^{-5} mol/l). Such reduction is less remarked when the SI is taken into account (1/2 order of magnitude) in spite of the higher S_A.

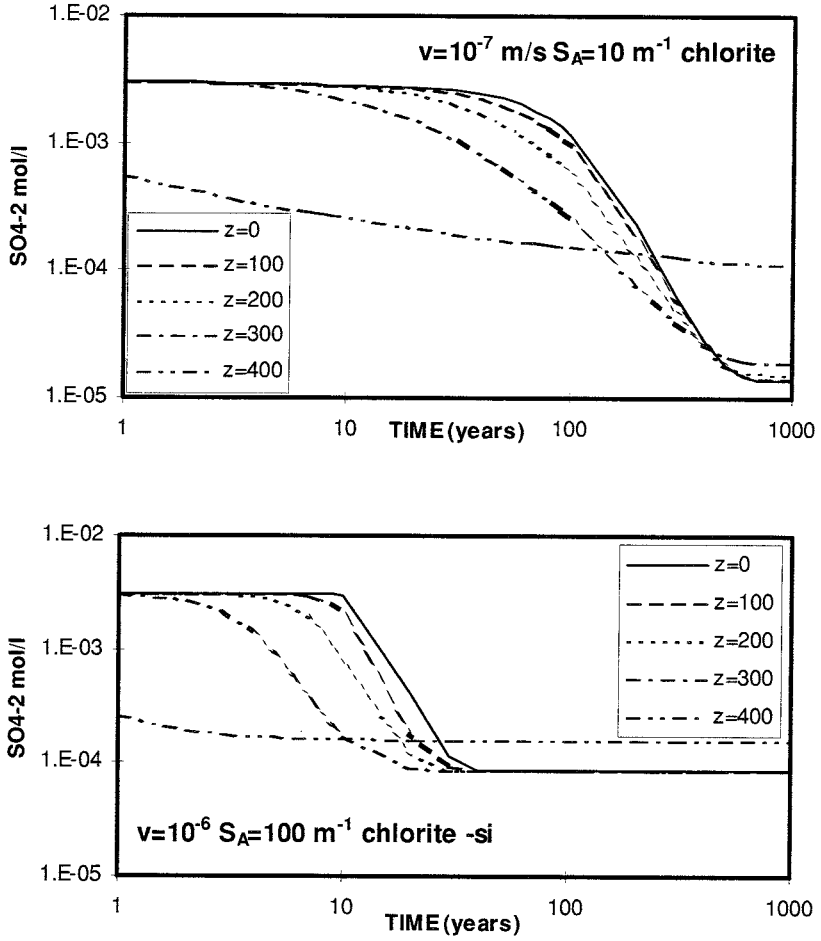

Figure 4-8. *Sulfate evolution for different systems. Input concentration is 2×10^{-4} mol/l at z=400 m and initial content is 3×10^{-3} mol/l. Note that the final values are far from initial content, since reduction occurs.*

The system not buffered by calcite

The results of the analysis of the system not buffered by calcite are shown in Figures 4.9 and 4.10. The number of chlorite cases has been extensive and they show that the arrival time of the redox front is almost independent of the surface area of the system. As a matter of fact, the diagrams for the three groundwater velocities show differences in terms of pe values of the front, but not in terms of time. Hence, the arrival of the front is proportionally delayed with decreasing groundwater velocity -one order of magnitude of time to one order of magnitude of velocity-. The value of pe, which imposes the "threatenability" of the geochemical conditions of the repository in the immediate vicinity of the far field varies almost proportionally with the surface area considered

-one unit of pe to one order of magnitude of S_a-. Therefore, pe values higher than 2.5 - 3 are achieved during the time span considered when either groundwater velocity is high (10^{-5} m/s) or surface area is low (equal or lower than10 m^2/m^3). The above statement is valid whenever the mineral abundance is enough to fulfil the system demands. Case D2, where the abundance of mineral is 1% of the rest of the cases, illustrates the rapid increase of pe when chlorite is exhausted.

The cases where biotite controls the evolution of the system behaves similarly to the chlorite cases described. Also, the differences in pe values compare well with the values of the surface area considered. Values of pe lower than 3 are attained in both cases. The influence of the selected stoichiometry for both biotite and chlorite, can easily be compared for a given combination of velocities and surface areas. For instance, when $v=10^{-7}$ m/s and $S_a=10$ m^{-1}, the stable value of pe is 1.7 and 1.5 for biotite and chlorite respectively, the time after which is reached being 125 and 500 years.

The differences between the cases that consider equilibrium (Figure 4.10), appear as a function of groundwater velocity. Similar values of pe are reached after a certain log time period, equally varying as a function of velocity.

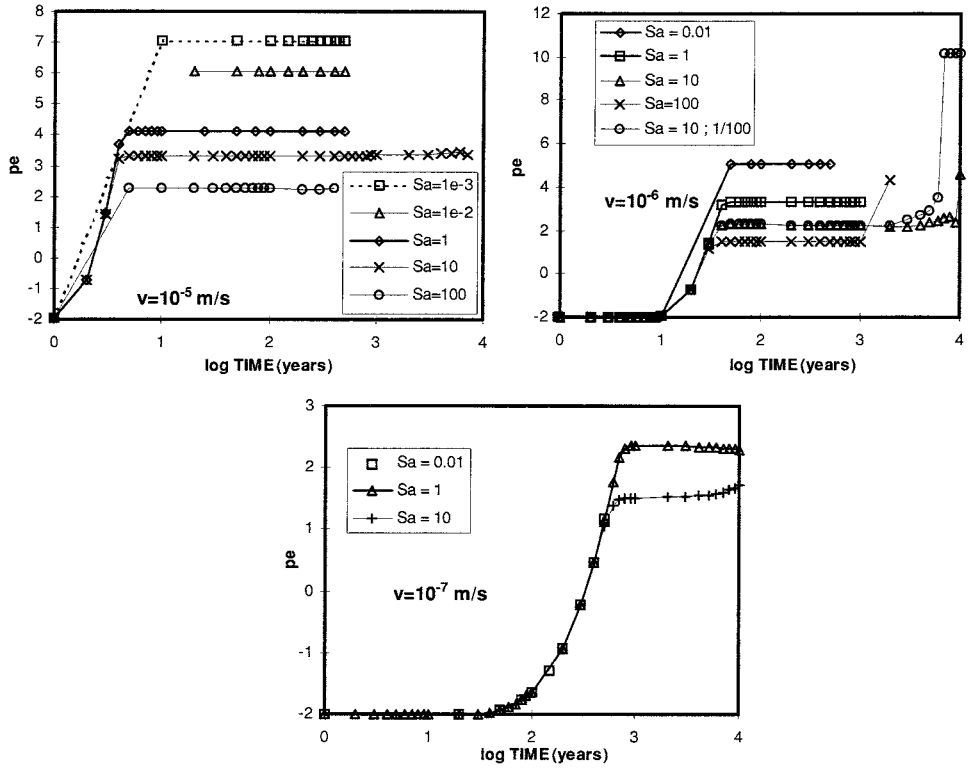

***Figure 4-9**. Summary of the runs of the system not buffered by calcite. Weathering of chlorite progresses independently on the saturation index.*

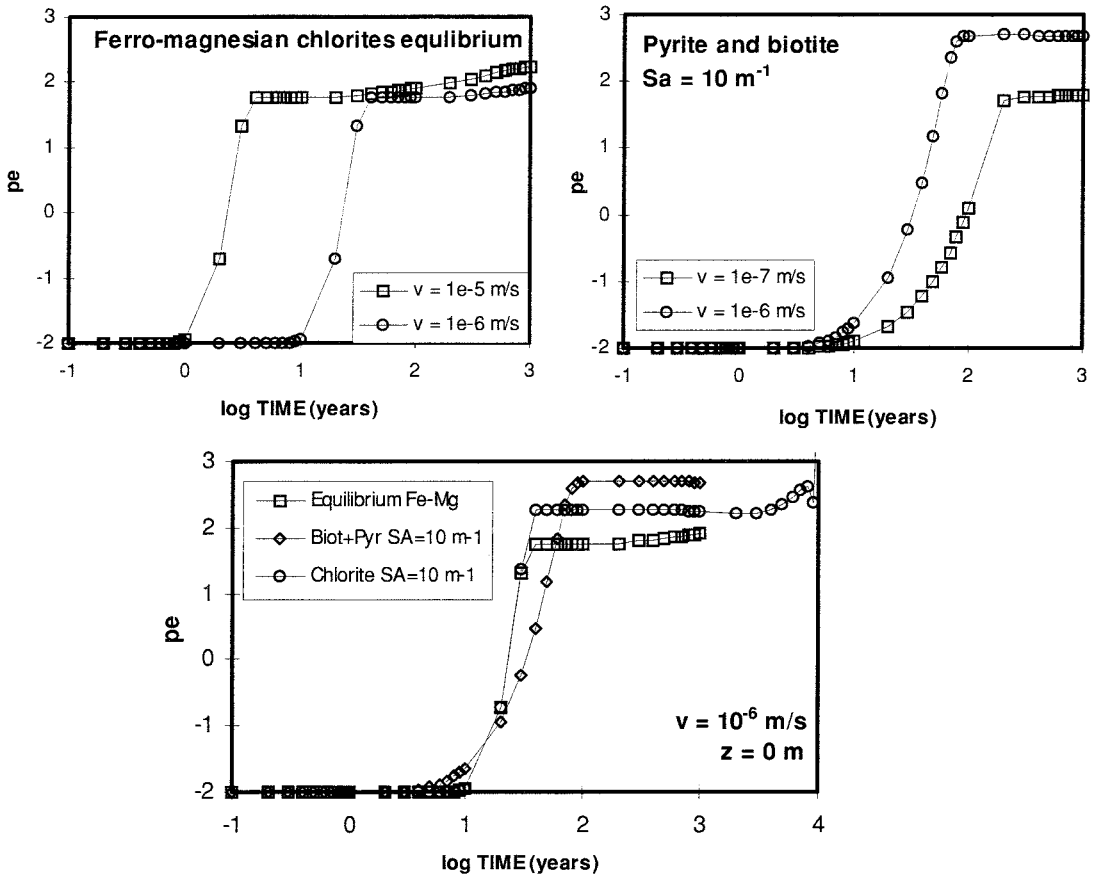

Figure 4-10. *Summary of the runs of the system not buffered by calcite. Top rigth: evolution with biotite not kinetically limited by SI. Top left: Evolution assuming equilibrium between magnesian and ferrous chlorites. Bottom: Comparison of the results for a given groundwater velocity and surface area (when available). Not that the biotite evolution is affected by a slightly higher dispersivity (about twice the other two curves). In terms of resulting pe values, the equilibrium model is the one displaying more reducing conditions.*

Finally a case of each of the three conceptual models are compared. There, the relative behaviour of each model can be appraised in terms of safety assessment. In terms of pe value after a give time of 1000 years, the most favourable case is the equilibrium one, since pe is always kept below 2. Contrarily, biotite is the most unfavourable, since displays higher pe values (pe>2.5). In any case, such values have to be treated quantitatively in order to know the amount of oxidants transfer to the vicinity of the repository.

Figure 4.11 displays the evolution of the system in depth and time also for pH, mineral content and they are compared with a conservative solute of the system. The acidification of the system is shown as a consequence of the poor buffering. Consumption of chlorite progresses as a function of pH, a fact that is evidenced in all cases and explains why pe is buffered to a value around 2-3. At latter times, pH becomes more and more acidic, which in turn affects the consumption rate of chlorite (see Figure 4.5). As a consequence of the function controlling chlorite kinetics, a "precipitation" front -slow dissolution- is formed whenever pH becomes close to 7.7. Such circumstance occurs at depths of 300 m, which is depicted by a change of the trend of the contour lines.

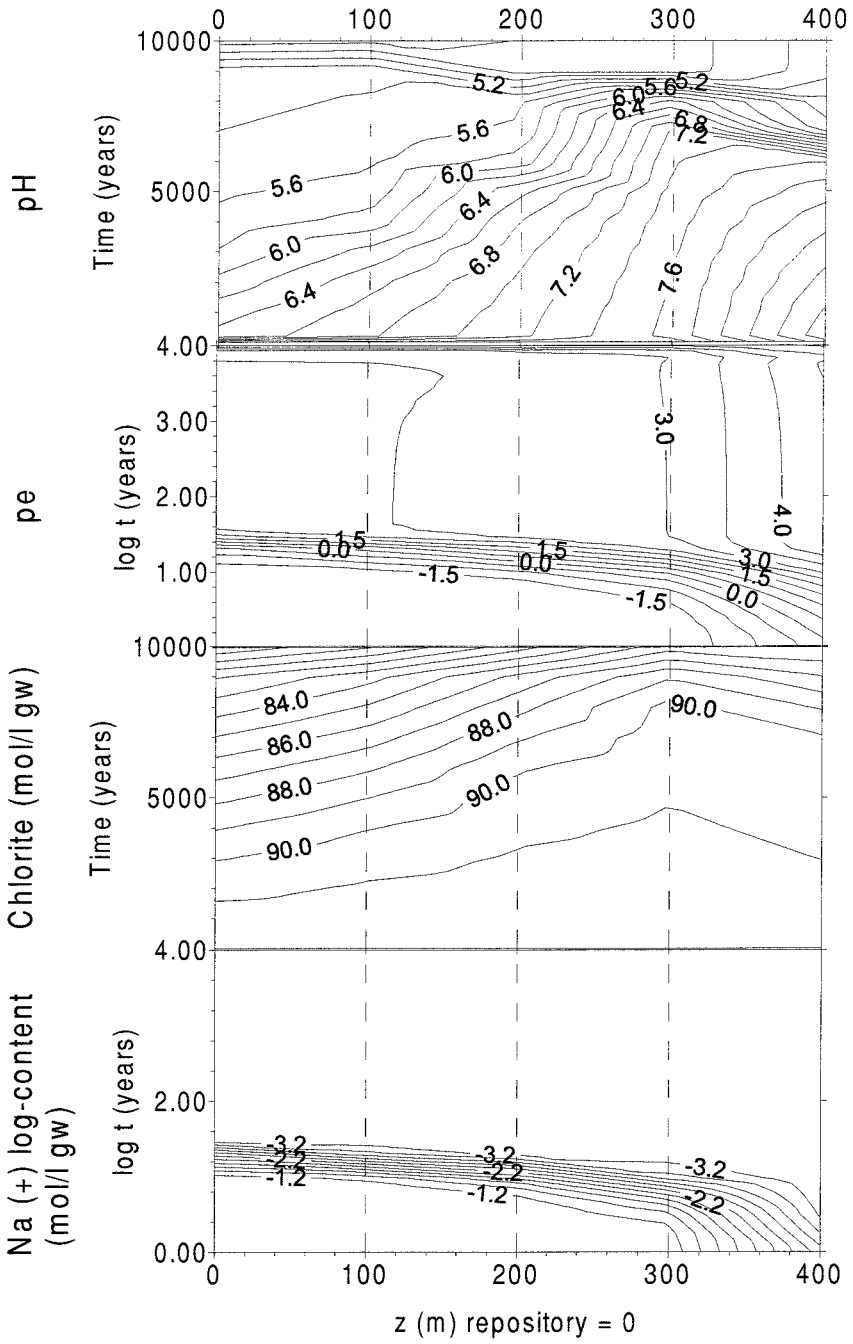

Figure 4-11. *Case B2. Time and space evolution of the system. t and log t values are used to illustrate the rate of change of the variables.*

Results achieved with the EXCHANGE code

Some of the cases are analysed by means of a second multicomponent reactive transport code: the EXCHANGE code (Saaltink et al., 1997). EXCHANGE is based on the direct substitution approach (DSA) to solve the coupled equations for hydrological transport processes and chemical reactions. The chemical equations are substitued as a source/sink term in the transport mass-conservation equations which are solved at the same time. Solution of these non linear partial-diferential equations is carried out using Newton-Raphson iterative procedures. After convergence, the chemical source term is updated.

EXCHANGE can cope with problems having irregular boundaries and composed of nonuniform physical and geochemical properties. The code can handle heterogeneous and anisotropic media in two-dimensional horizontal plane for confined or unconfined aquifers, in two-dimensional vertical planes and in three dimensional regions exhibiting axial symmetry for confined aquifers. Prescribed head, water flux boundary and mixed boundary conditions are included. Both point and areal fluid sources can be specified. Implicit, explicit and general finite difference schemes are used for time discretization.

Transport processes included in the code are: advection, molecular diffusion and mechanical dispersion. Solute transport boundary conditions include: (1) specified solute mass fluxes, (2) specified solute concentrations and (3) solute sources associated to fluid sources. The code can handle the following types of reactions under the local equilibrium assumption: acid-base, aqueous complexation, redox, mineral precipitation or dissolution (including gas), and sorption or desorption reactions. The code also handles mineral precipitation and dissolution reactions under a large set of experimental kinetics laws. EXCHANGE can take into account a user-limited number of aqueous and sorbed species, minerals and gases.

The geometry and conceptual model used for the simulated case were maintined as close as possible to the case C2 analysed with the ARASE code (see Table 4.6). However, chlorite dissolution was limited by the saturation index while C2 was not. Figure 4.12 show the main results in terms of pe and pH evolution at repository depth. The results are consistent with those obtained for case C2 but obviously, they do not match one each other. The dispersivity was higher by approximately one order of magnitude and, accordingly, the shape of the curve changes causing earlier first arrival times (some 10 years compared to 50 for case C2). The pe value attained is lower, yet the release of iron is limited by the saturation index of chlorite. Therefore, values of 4 are achieved while case C2 attains values up to 5.2. pH evolution also changes according to the release of iron, reaching values of 7.9.

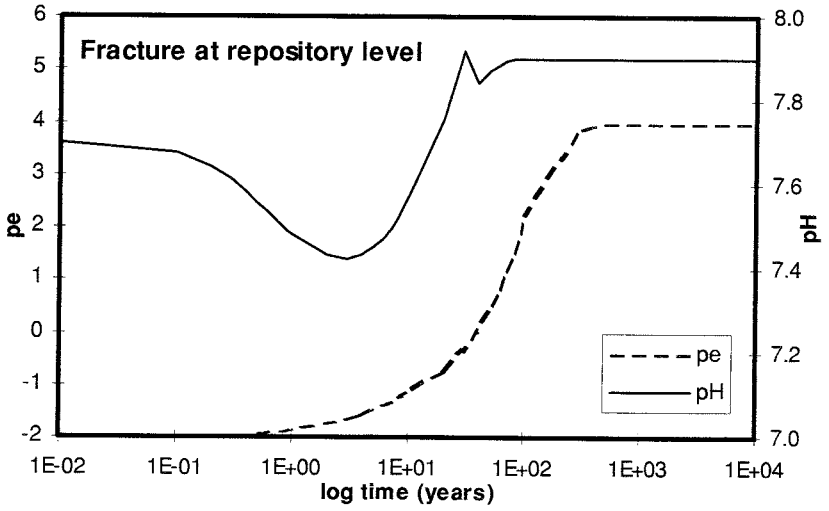

Figure 4-12. *pe and pH esults achieved with the EXCHANGE code at repository level with the geochemical system dominated by chlorite.*

4.4.2 2D cases

Flow field configurations tried to match as much as possible the regional flow field trends displayed in Figure 4.5. Similarly to 1D cases, different flow fields in 2D produced different groundwater residence time, transit time across and along the chlorite-rich material zones and therefore, different redox state results. Following we describe the results obtained according to the three different conceptual models analysed.

Conceptual model 1

The differences among the runs of this conceptual model, consisted of a set of inflow conditions which produced flows approximately normal to the fracture zone (run 5); flows which crosses the fracture zone under a certain angle (run 7) and flows which were forced to follow a "Tóth scheme" (run 8). The results are compared in terms of groundwater renovation and pe and pH values attained. Figures 4.13 and 4.14 show the two latter. At first glance, results returned at the "monitoring points" of the domain are rather comparable for each run: they display similar values independently of the position within the domain. This is likely because hydraulic conductivity values are not far one from each other (2 orders of magnitude) and because the size of the cells composing the fracture zone is slightly large. Flow in runs 5 and 8 occurs mostly in the top zone, and renovation at the repository altitude is low (less than 10% in terms of chloride mass balance). On the contrary, run 7, in which flow is forced diagonally across the fracture, attains renovation values of 75%. Accordingly, for low renovation values, pe attains lower values than high renovation. For high renovation values, although not complete, pe raises up to 3 but it does not become stable within the period simulated. When groundwater flow occurs mostly on the top zone, pe at repository depths reaches values up to 0.5.

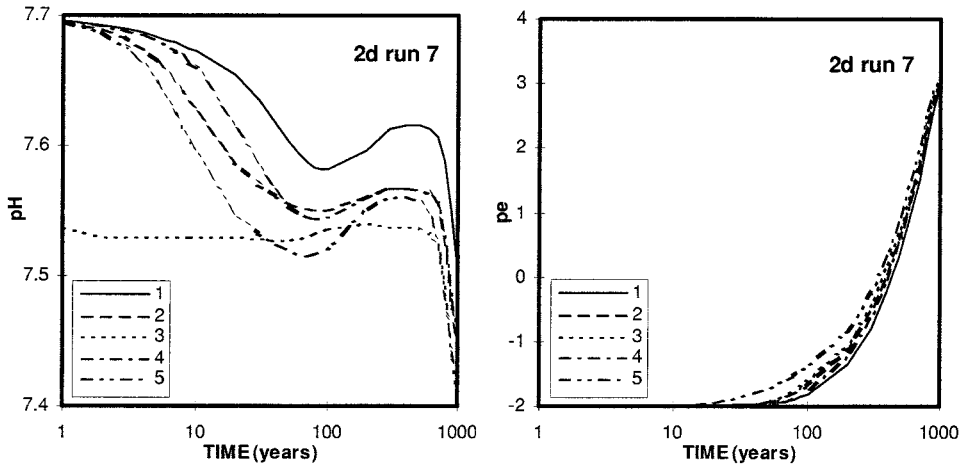

*Figure 4-13. pe and pH values at repository altitude control points when groundwater flow is forced across and along the fracture zone (run 7). Note that neither the values of pe nor the values of pH become stable. Point **1**: host rock, close to discharge of the domain; point **2**: host rock, 100 m downstream of the fracture; point **3**: fracture; point **4**: host rock fracture upstream; point **5**: host rock, center of the domain.*

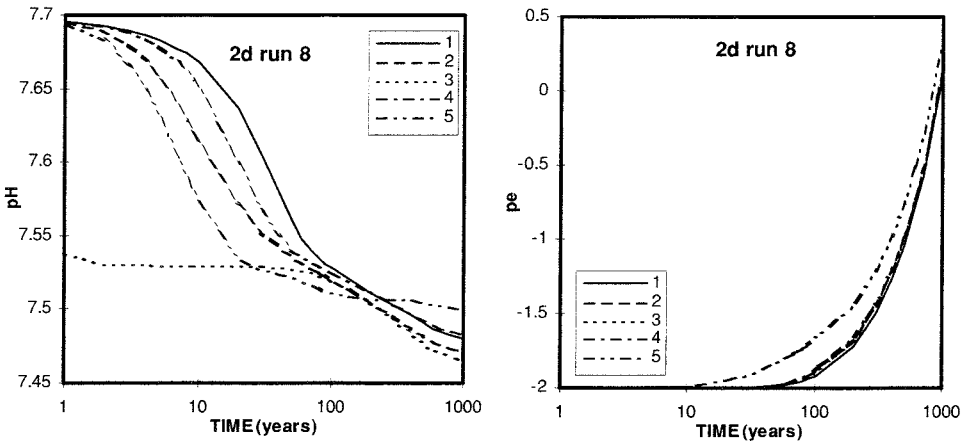

Figure 4-14. pe and pH values at repository altitude control points when groundwater flow mostly circulates by the top zone (run 8). Note that pH values reach a quasy steady state, while pe values remain below 0.5, as a consequence of the low renovation of groundwater. Similarly to to run 7, pH value at the fracture remains controlled by the chlorite kinetics. See Figure 4.13 for monitoring points location.

pH values also vary accordingly to groundwater renovation and to the presence of mineral. Fracture values (point 3 in Figures 4.13 and 4.14) are affected by the mineral presence and its evolution is buffered by the release of Fe^{+2}. On the contrary, variation of pH in the host rock is more dependent on water renovation rather than water-rock interaction and display higher variability.

The mineral content does not vary significantly, neither the $Fe(OH)_3$ (aq) does. The former remain close to its initial value for all cases considered and the log content of the latter around -9.5 (mol/l). So that, the effect of the redox front migration can be described in terms of variation of the RDC of the system, that is to compare the final value to the initial one. Figure 4.15 shows the evolution of the Fe(II)aq species, which in turn are the main controlling factors of the RDC given that the mineral content variation is negligible. Thus, ΔRDC is in the order of 5×10^{-7}, expressed in mol/l of Fe^{+2}.

Conceptual model 2

Two different simulations are performed with this conceptual model, the groundwater flow differences being the head distribution: while run 9 has a prescribed head of 800 m on top of the fracture, run 10 has only 500. Consequently the residence times will be different, although complete renovation is achieved for both of them after 1000 years. Renovation expressed in terms of chloride concentration for run 10 is expressed in Figure 4.16

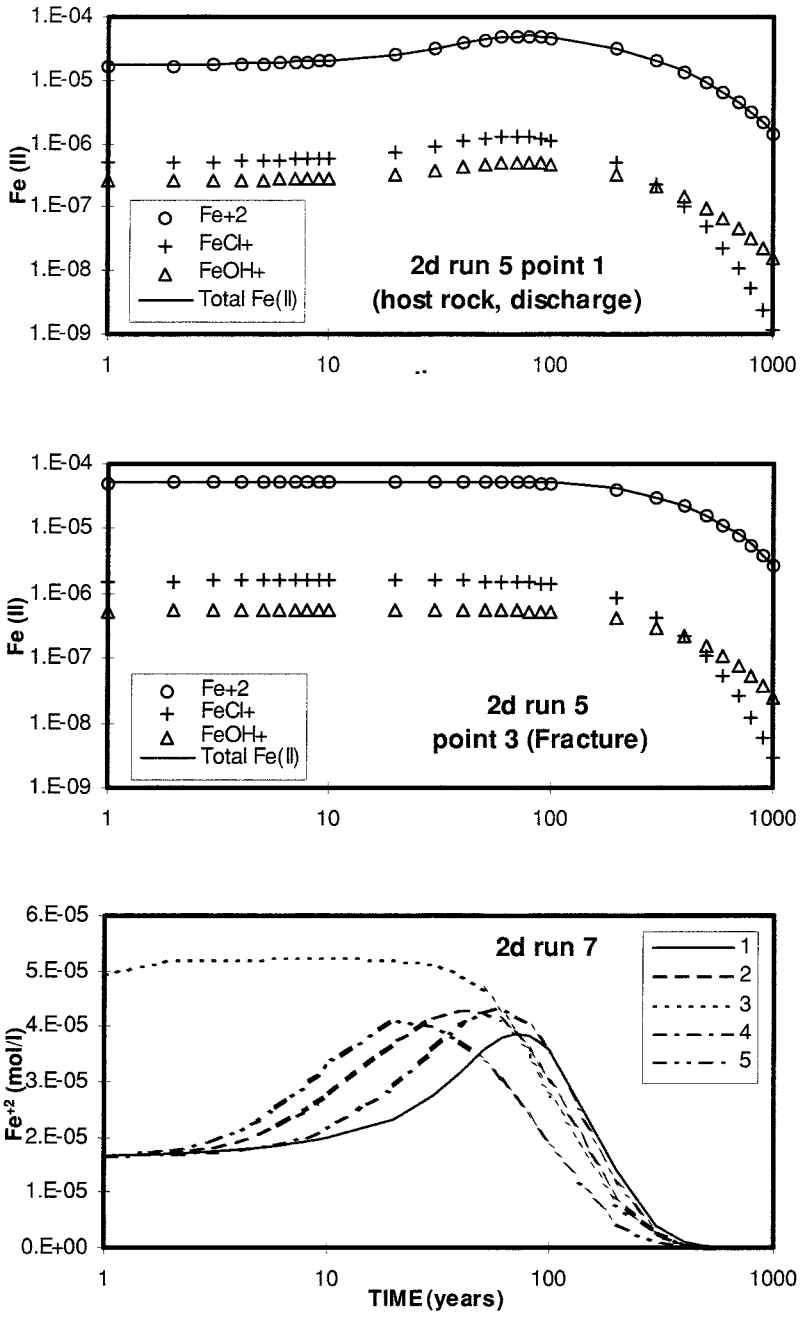

Figure 4-15. *Evolution of the Fe(II) species for runs 5 and 7. Note that run 5 displays the* Fe^{+2} *content given that it is the main specie.*

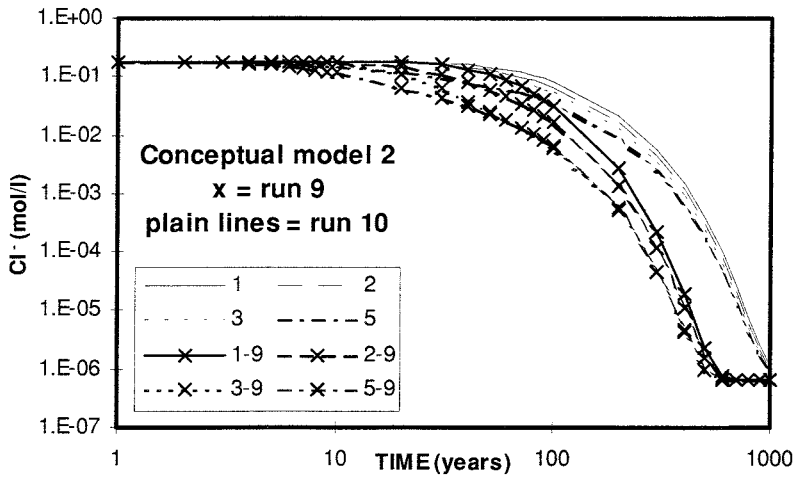

Figure 4-16. *Chloride concentration at run 10. Input concentration at the boundary is 6.5×10^{-7} mol/l.*

pH and pe values reflect the effects of such renovation. Although pH values does not reach steady state, pe values. attained are close to 3 in both cases but for different times and steady state conditions as well (see Figure 4.17 for run 10, where steady state is not reached).

In general terms the results are comparable to run number 7 - conceptual model 1 -. The mineral dissolution is negligible and the Fe(III)aq contents are lower than $10^{-9.5}$ mol/l due to the low mass flow of oxidants. Again, the effect of the redox front migration has to be assessed in terms of RDC variation, the Fe^{+2} being the main specie controlling the RDC of the system. In run 9 the difference between initial and final Fe^{+2} content are comparable for both, fracture and host rock (from 5×10^{-7} to 5×10^{-11} mol/l). The variation in iron is of the order of 5×10^{-7}, which is some two orders of magnitude below the difference attained by the cases analysed in conceptual model 1. However, run 10 does not attain stable values of iron after 1000 years, although the dominant specie is Fe^{+2} (Figure 4.18). For this conceptual model, ΔRDC is around 1.2×10^{-5}.

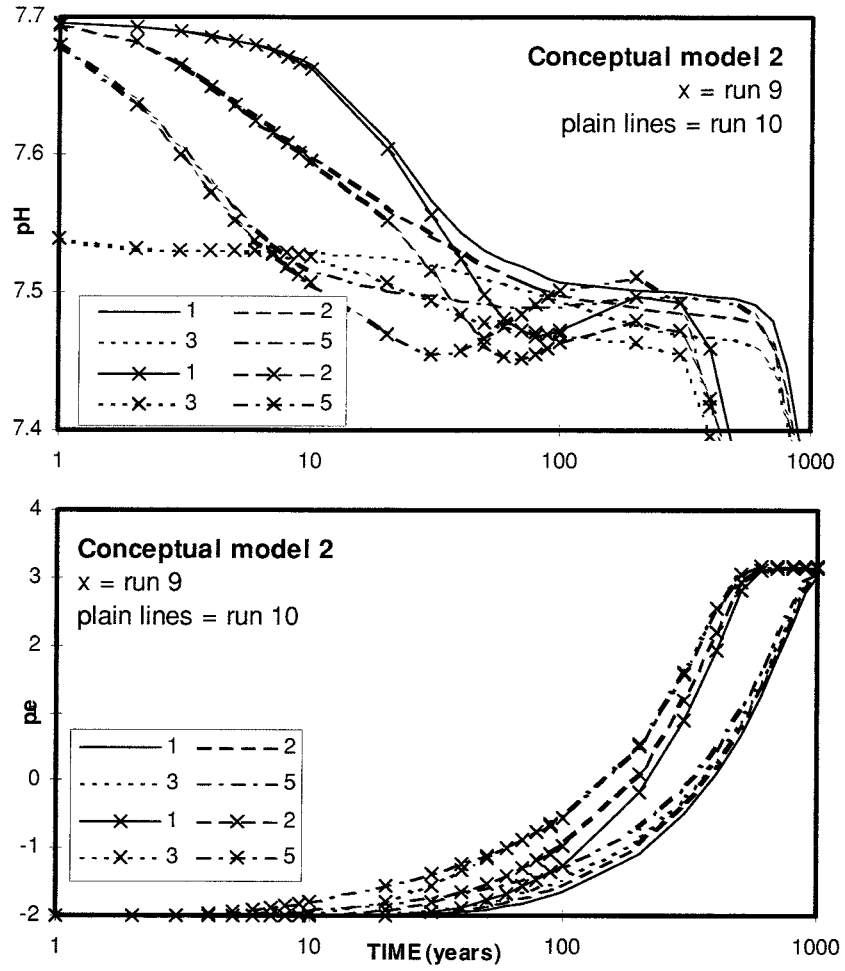

Figure 4-17. *Evolution of pe and pH assuming slow groundwater flow.*

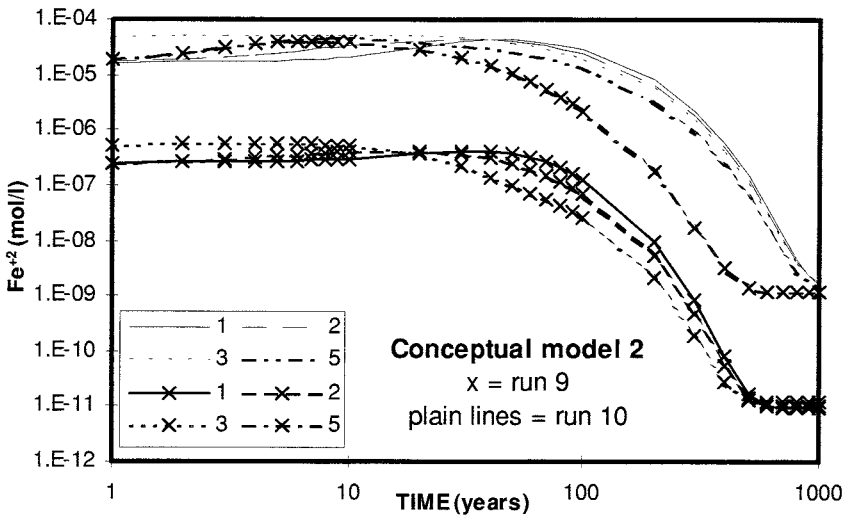

Figure 4-18. *Evolution of the dominant specie of Fe(II) assuming slow groundwater flow.*

Conceptual model 3

This conceptual could be envisaged as two 1D models, corresponding to host rock and fracture features, since flow is imposed almost parallel along the 2D domain form top to bottom. However, concentration gradients perpendicular to the main direction of flow are allowed and they may become important. The mass flow of oxidants is some 4 orders of magnitude higher in the fracture zone than in the host rock, which enhances the differences in the results obtained within both materials. Also differently to the 1D cases, the oxidant top zone is included. Figures 4.19 and 4.20 show the evolution of pe and pH at certain fracture and host rock locations. A striking feature is the parabolic shape of the pe evolution in the oxidising zone of the host rock. Such trend is a result of the artifact of imposing a certain pe value so as to ensure numerical convergence. As a matter of fact, such evolution has no implications for the final results, yet it rapidly evolves to steady values imposed by the boundary conditions. In addition, the advance of the redox front in the host rock is so slow, that it barely changes within the first 100 years (see profiles in Figure 4.19). pe evolution in host rock and in the fracture differ by more than 3 units, reflecting the different groundwater flow. While fracture flow lays on the order of 10^{-7} m^3/s, flow though host rock is 4 orders of magnitude smaller. That would explain why the evolution of pe at the oxidising zone of the fracture does not display the same behaviour that in the host rock. Despite the large mass flow of oxidants in the fracture, the amount of chlorite consumed is small. Figure 4.21 shows that less than 0.25 moles of chlorite are dissolved in the repository level while biotite in the host rock does not display any change. Iron (III) displays slight changes in the fracture domain, but they are negligible in terms of oxidants mass balance. Fe^{+2} barely varies within the host rock; on the contrary, it decreases down to 4 orders of magnitude in the fracture, which consequently, implies a decrease of the RDC of the system from 10^{-4} to 10^{-8} mol/l of Fe^{+2}.

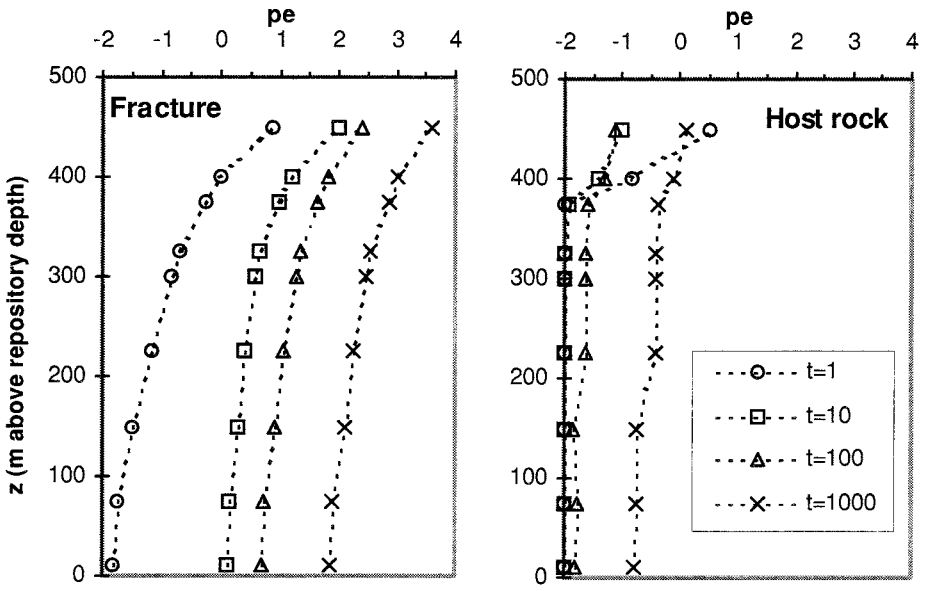

Figure 4-19. pe profiles at different simulation times (in years) for host rock and fracture respectively. Note that the top 100 m (from 500 to 400m) are the oxidising zone and the repository altitude is 0.

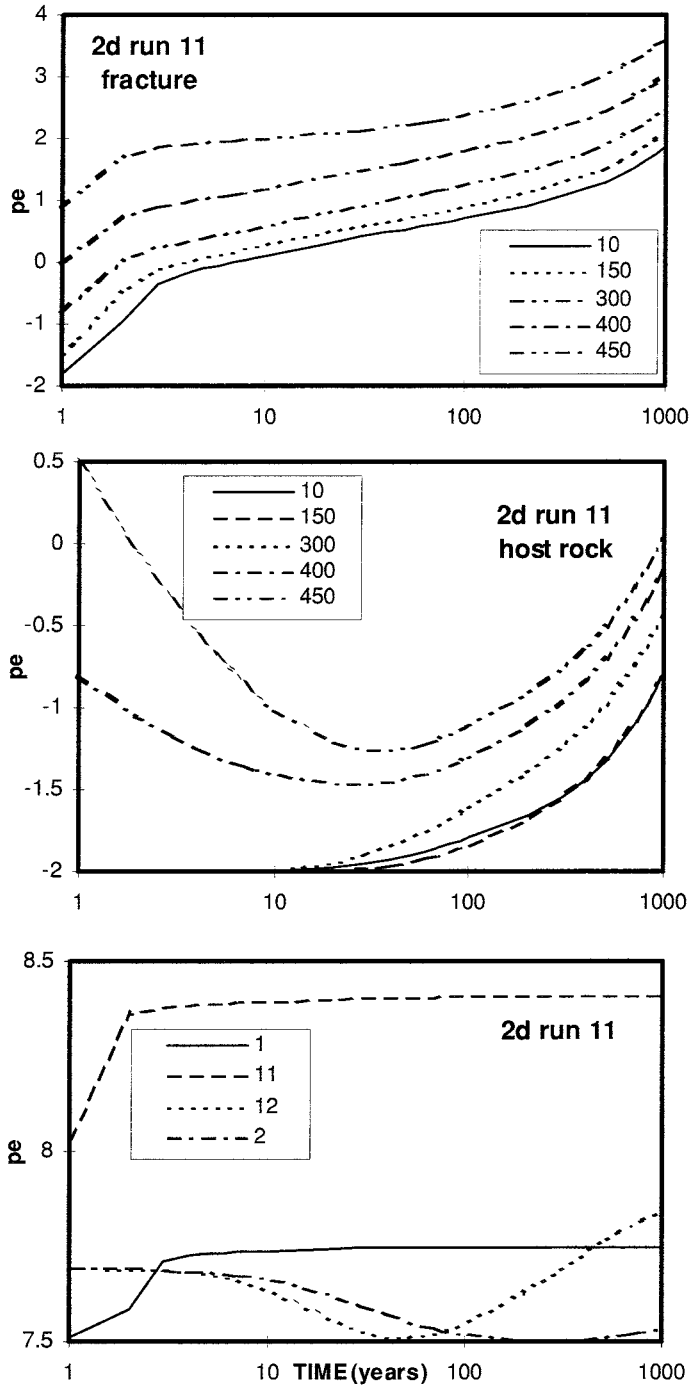

Figure 4-20. *pe and pH evolution at different depths of the domain. Above and centre: Monitoring points of the pe are located at the altitudes expressed above the repository level. Host rock points were selected 100 m away from the fracture (4-5 cells to avoid spureous effects due to grid size, see Figure 4.4). Bottom: points 1 and 2: repository level, fracture and host rock respectively; point 11 and 12: 325 m above repository level (and 75 m below the oxidising zone) fracture and host rock respectively.*

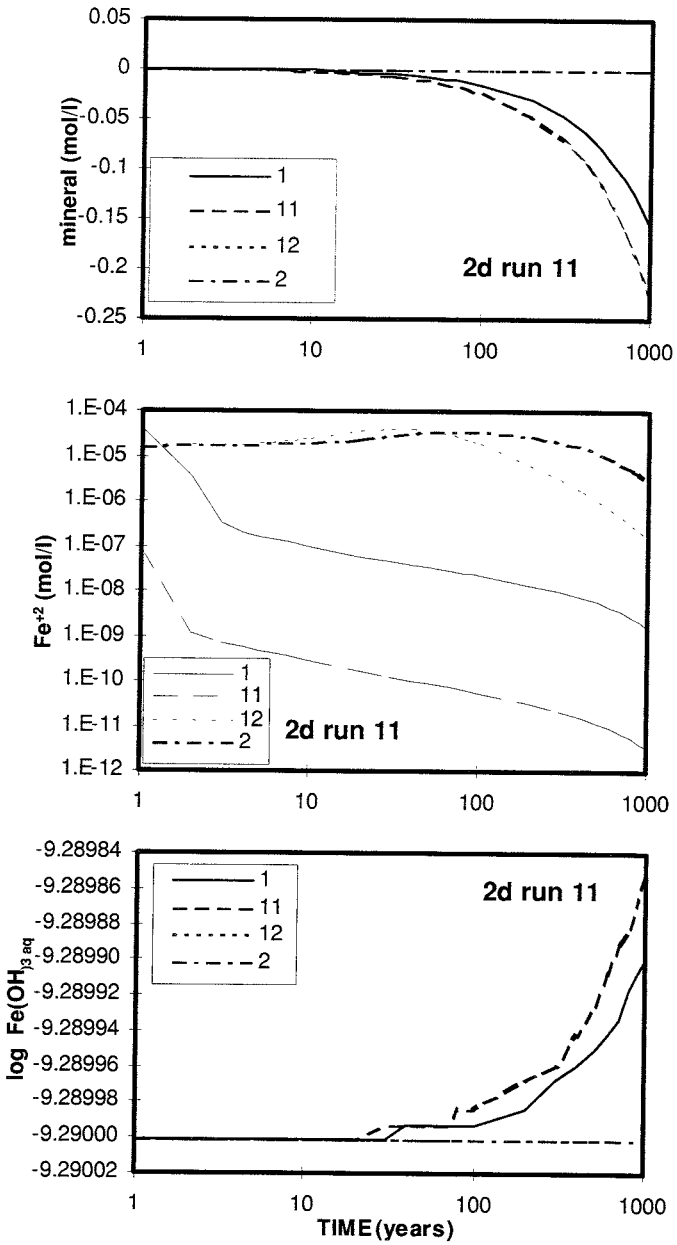

Figure 4-21. *Evolution of the RDC of the system. Above: moles of mineral dissolved (biotite for host rock and chlorite for fracture). Center: Fe^{+2} content in both, fracture and host rock domains at the same locations as in Figure 4.20. Below: Evolution of $Fe(OH)_{3\,aq}$ (log content). Note that the major change in the RDC of the system is explained by the change in Fe^{+2} content, and that the presence of oxidants in water is negligible after 1000 years.*

4.5 Summary of the calculations and mass balance analysis

The results of the cases considered in both 1D and 2D show that the groundwater reaching the repository which results from the mixing and reaction with infiltrating ice-melt water is generally anoxic but could become oxic (pe up to 3, Eh = 200 mV) in some extreme cases. The alkalinity of the groundwater is not affected during this process, because of the large acidity buffering pool present in the form of calcite and aluminosilicates.

What remains to be studied is which are the relative amounts of oxidants reaching the repository under the various hydrodynamic conditions and how they compare with the total reducing capacity present in the system. This will be done by a mass balance study based on the findings of the previous calculations.

4.5.1 Definition of the flow field distribution

There is an extensive research on flow through heterogeneous media - and consequently a vast amount of literature on the topic. One of the best documented field studies is the Stripa 3D experiment, where a number of tracers were injected in several borehole intervals and collected in plastic sheets attached to the walls of a tunnel (Abelin et al., 1991). Since monitoring was exhaustive, the flow distribution along a section of tunnel was well characterised. Actually, 10% of the total inflow took place in 0.3% of the total monitored surface (fast flowing fractures), 50 % of flow through 3% of the surface (minor fractures), while the remaining 40% was attributed to the remaining 96.7% (fractured host rock). Although similar figures have been recently obtained in the frame of other projects (FEBEX, Guimerà et al., 1997) we will use the flow distribution derived by Abelin et al. (1991) due to their geological analogy and relevance for the case under study.

In spite of the rigorous characterisation of the Stripa site, the flow distribution that we use for the present analysis is somehow ambiguous, due to conceptual simplifications. Two flow distributions are considered, depending on the presence and amount of flowing fractures. Table 4.7 shows the flow distribution and the resulting total groundwater flow towards the repository for both cases.

The distribution of the flow field and its prognosis is crucial for a proper safety assessment, since the oxidants mass balance results will directly depend on it. For a quantitative assessment such as the one carried out in this report, we have to rely on simplified figures –probably over-simplified- because we need to couple a generic calculation –the geochemical modelling- to a flow distribution. This is the reason why we use the figures of a well known hydrogeological experiment that in addition is supported by independent hydrogeological characterisation. Any extrapolation of the results beyond the numbers proposed below, would need site specific flow distributions and geochemical calculations, which are not the scope of this report.

Table 4-7. Flow distribution. Units in m and years

Medium	Case	Flow contrib.	Darcy flow ($K \cdot \nabla h$ per unit area)	Flow 1 Surface weight	Flow 1 Weighted flow	Flow 2 Surface weight	Flow 2 Weighted flow
Fast fractures	A2	0.5	3.1·0.1	0.003	$9.3 \cdot 10^{-4}$	0.03	$9.3 \cdot 10^{-3}$
Slow fractures	B2	0.1	3.1·0.1	0.03	$9.3 \cdot 10^{-3}$	0.003	$9.3 \cdot 10^{-4}$
Host rock	PBA1	0.4	0.031·0.1	0.967	$3.0 \cdot 10^{-3}$	0.967	$3.0 \cdot 10^{-3}$
Total		1		1	$1.3 \cdot 10^{-2}$	1	$1.3 \cdot 10^{-2}$

The resulting total flow 1.3×10^{-2} $m^3/y/m^2$ (or 4.12×10^{-10} $m^3/s/m^2$) falls within the same range as some other field measurements in similar conditions. For instance, in the FEBEX experiment (Guimerà et al., 1997) the total flow was estimated to be $24.8\cdot10^{-10}$ $m^3/s/m^2$ (a factor of 6 larger). It is likely that in a real repository the head gradient will be lower; however, we maintain the values for consistency with the observations and to match the conservatism of safety assessment exercises.

4.5.2 Oxidants mass balance

We have attributed the same Darcy flow to "Fast" and "Slow" fractures since the main difference between these two types of fractures is the reactive surface area, S_A. This is considered to be reasonable for the purpose of the present analysis.

Figure 4.22 shows the arrival time and magnitude of oxidants in terms of cumulative moles of O_2 per repository area in m^2 for both flow configurations. The net amount of dissolved oxygen reaching the repository is negligible, independent of the flow field conditions considered, as shown in Table 4.8. According to the conceptual and numerical models used in our analysis, the most relevant oxidant should be aqueous Fe(III), shown in Figure 4.23.

Table 4-8. Number of moles of oxidants after 1000 years per m^2 of repository

Medium	Flow 1		Flow 2	
	O_2	$Fe^{III}_{(aq)}$	O_2	$Fe^{III}_{(aq)}$
Fast fracture	$2.8\cdot10^{-37}$	$8.62\cdot10^{-9}$	$2.8\cdot10^{-38}$	$8.62\cdot10^{-10}$
Slow fracture	$3.7\cdot10^{-49}$	$1.02\cdot10^{-9}$	$3.7\cdot10^{-48}$	$1.02\cdot10^{-8}$
Host rock	$1.05\cdot10^{-53}$	$3.00\cdot10^{-9}$	$1.05\cdot10^{-53}$	$3.00\cdot10^{-9}$
Total	$2.8\cdot10^{-37}$	$1.26\cdot10^{-8}$	$2.8\cdot10^{-38}$	$1.41\cdot10^{-8}$

4.5.3 Implications for safety assessment

The calculations and discussion performed in previous sections indicate that the arrival of oxidising fronts to repository levels within a glaciation time span is feasible. Also, we have computed the amount of oxidants in the system in order to assess to which extent their presence could disturb the geochemical stability of the repository vicinity. At this point we should recall that the simulations presented in this report do not reflect the presence of the engineered barriers. Hence, the presence of oxidants at repository depths should be understood as an indicator of the redox conditions at the interface of the geosphere and the near-field (the disturbed zone).

If we bear these premises in mind, we may compare the geochemical conditions at this interface with the stability diagrams of some relevant species in the HRLW geochemistry. This should be a reasonable indicator of the degree of potential disturbance of the repository conditions.

Figure 4.24 shows the evolution trend of groundwater for the three conceptual models considered and the stability diagram of uranium solid phases. The three trends evolve

from the minimum oxygen fugacity value at initial times towards higher contents. Most of the calculated evolutionary waters remain in the stability field of UO_2 to $UO_{2.33}$ which is accepted to be the field of thermodynamic stability of the spent fuel matrix and the radionuclides therein contained (Bruno et al,1996).

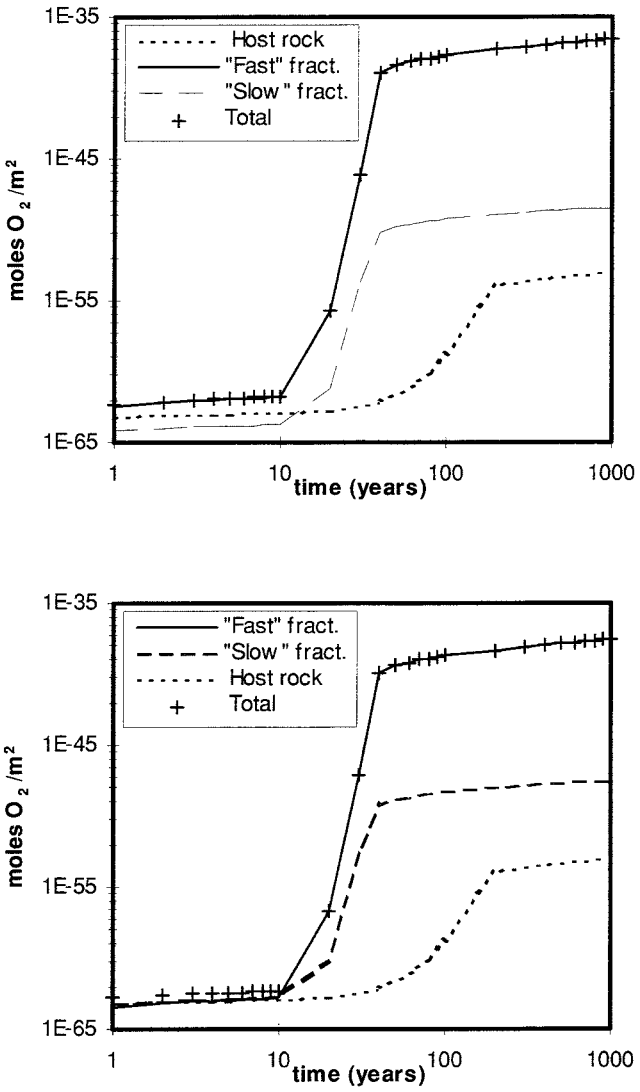

Figure 4-22. *Moles of O_2 which could reach the repository depth per unit area. Top: Flow 1; Bottom: Flow 2 (see Tables 4.7 and 4.8).*

Only in the case of flow through fast fractures the calculated oxygen fugacity reaches levels which could indicate the destabilisation of the spent fuel matrix due to the transformation to the U_3O_8 phase and the subsequent radionuclide release. This could be a potential threat provided the fast flow fracture water was put in direct contact with the spent fuel, without any further reaction with the bentonite and canister barriers. We consider this case unlikely since, it is reasonable to assume that underground repositories will not be excavated in fracture zones of hydraulic conductivity around 10^{-7} m/s (3.1 m/year). In any case, the spent fuel will not be placed in contact with the tunnel walls without engineered barriers.

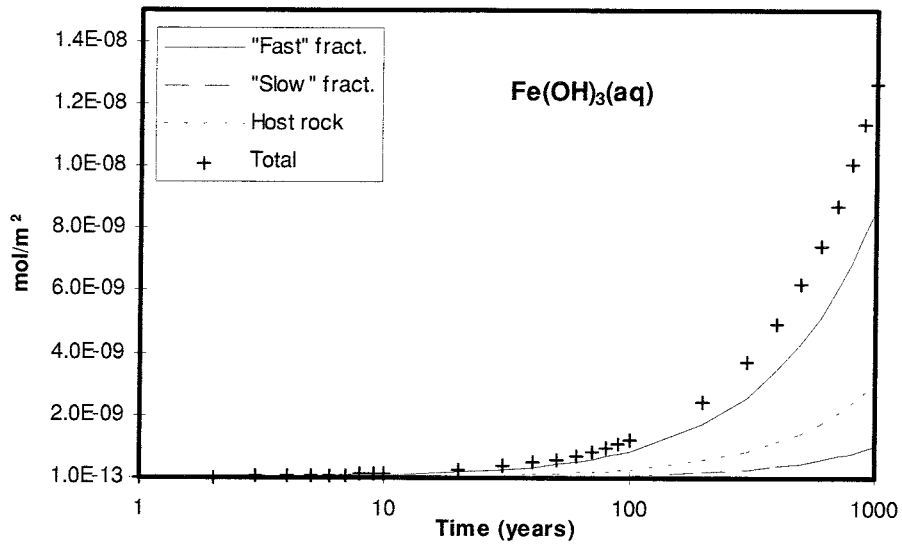

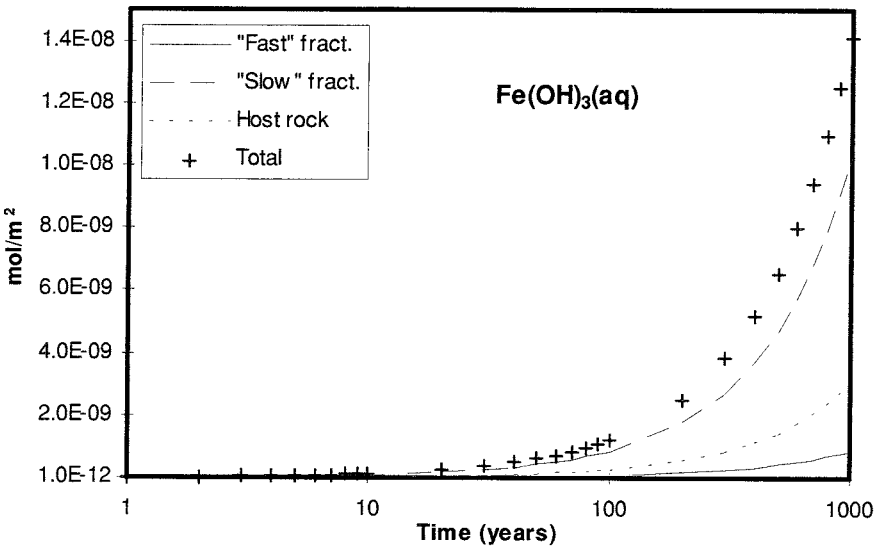

Figure 4-23. *Moles of* $Fe^{III}_{(aq)}$ *reaching repository depth per unit area. Top: Flow 1; Bottom: Flow 2 (see table 4.4 and 4.5).*

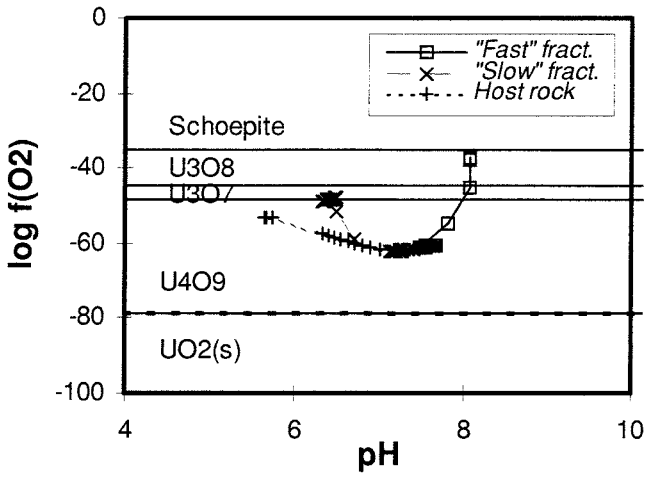

Figure 4.24. *Stability diagram of uranium species and evolution trends of groundwater for the three models considered up to t=1000 years.*

5 Conclusions

A thorough quantitative analysis of a redox front advance in a granitic environment has been done. Such a redox front is likely to originate due to melting of ice during deglaciation periods which eventually, could jeopardise the chemical stability of a repository at some 500 m depth. The analysis started assessing the geological, hydrogeological and geochemical conditions in the Fennoscandian Shield, with emphasis in the local conditions of the Äspö underground laboratory. Several conceptual hydrogeochemical models have been explored, based on hydraulic conditions, geologic domain and availability of minerals to flowing groundwater.

Three different approaches have been followed to assess the problem: the stationary state, the equilibrium approach, where the system is assumed to be in equilibrium with buffering minerals and the kinetically controlled system, where the dissolution (alteration) of such minerals is assumed to happen at a slower rate than groundwater flow. The geological systems considered have been preferential flow through fractures, where the redox system is dominated by the presence of chlorite and flow through the host rock, where the dominant redox controlling minerals are biotite and pyrite. The different calculation approaches included equilibrium and non-equilibrium reactive transport.

- If equilibrium is assumed, the redox front progresses slowly, and oxidising conditions do not reach the repository depth up to a million years. This assumption is largely optimistic since it presumes, that the whole mineral content is available to groundwater and it completely reacts until equilibrium is reached. The assumption of equilibrium showed the relative differences in the redox control exerted by the minerals considered on the migration velocity of the redox front. For instance, in host rock environment, pyrite becomes determinant while the effects of biotite are less important. The effects of chlorite in fracture fillings under a flow velocity 10 times faster than the one assumed in the host rock, are comparable to the effects of pyrite and biotite.

- A more realistic approach to the behaviour of the system is developed when assuming a kinetic control of the main redox processes. In this case the groundwater velocities in some of the domains are assumed to be faster than the characteristic reaction times of the heterogeneous redox processes involved.

- Concerning the use of multicomponent reactive transport, two parameters are deemed to be crucial for the sensitivity of the models considered: the reactive surface area (S_A) of the redox controlling minerals and velocity of groundwater. The reactive surface area S_A determines the steady state pe value which is reached and groundwater velocity controls the time at which certain steady state is reached, if ever. Hydrodynamic parameters such as dispersion are relevant to determine the first arrival times but they are not crucial in terms of final values of the redox state.

- Our present chemical models are unable to reproduce pyrite corrosion in anoxic environments. Hence, we could not include this process in our kinetic control approach, although it is considered to be extremely important when assessing the ReDuctive Capacity of repository systems. A dedicated experimental effort is recommended within the actual Nuclear Waste Management programmes.

- In most of the cases a steady state value of pe around 3 is, because the release of reductants compensates the mass flow of oxidants. This is not an indication that the system has reached equilibrium, it is likely that under natural conditions, mass flow of oxidants is not steady but it will happen through pulses.

- The assumed hydrodynamic conditions are conservative since in general terms, most of the cases assume relatively fast groundwater velocities. On the contrary, the geochemical model can be judged as optimistic: we consider that all the mineral content is available to reaction, that reactive surface area does not vary with time and the formation of corrosion coatings is not taken into account.

- The effects of the oxidising front migration have been analysed in terms of variation of the ReDuctive capacity (RDC) of the system. In most of the cases, the dissolution of minerals is negligible. Thus, aqueous Fe^{+2} is the main contributor to the RDC. The cases analysed show that RDC of the host rock barely changes due to oxidant mass flow. In contrast, changes up to four orders of magnitude are found in fractures. Such different behaviour between host rock and fractures has been corroborated by means of oxidant mass balance as well. This is important because a decrease of the available RDC in fractures -due to coating phenomena and/or diminished reactive surface area could have an impact on the amount of oxidants reaching repository levels through highly conductive fractures.

- Concerning the performance of the repository system, the hydrogeochemical stability of the repository systemis guaranteed in all cases except in the unlikely event of a fast flowing fracture crossing the repository.

References

Abelin H, Birgersson L, Gidlund J, Neretnieks I (1991) A large-scale experiment in granite 1. Experimental design and flow distribution. Wate Resour. Res. 27(12) 3107-3117.

Ahonen L, Vieno T (1994) Effects of glacial meltwater on corrosion of copper canisters. Report YJT-94-13, nuclear waste commission of Finish Power Companies. 20 pp.

Appelo C A J, Postma D (1993) Geochemistry, groundwater and pollution. A.A. Balkema, Rotterdam.

Arthur R C (1996) Estimated rates of redox front migration in granitic rocks (Site94) QuantiSci Internal Report.

Banwart S, Gustafsson E (1991) Scoping calculations of surface water and redox front breakthrough. Large scale redox experiment. SKB PR25-91-06.

Banwart S (ed.) (1995) The Äspö redox investigations in block scale. Project summary and implications for repository performance assessment. SKB TR 95-26.

Banwart S, Laaksoharju M, Nilsson A-C, Tullborg E-L, Wallin B (1992) The large scale redox experiment. Initial characterization of the fracture zone. SKB PR25-92-04.

Banwart S A, Destouni G, Malmström M (1998) Assessing mine water pollution: From laboratory to field scale Groundwater Quality: Remediation and Protection, International Association of Hydrological Sciences (IAHS) Conference, Tübingen, Germany, 21-25 September, pp 307-312.

Bindschadler R A, Alley R B, Anderson J, Shipp S, Borns H, Fastook J, Jacobs S, Raymond C F, Shuman C A (1998) What is happening to the W-Antarctic Ice Sheet? EOS, 79(22) p.257.

Björck S, Svensson N O (1992) Climatic changes and uplift patterns - past present and future. SKB Tech. Rep. 92-38.

Bjorkum P A (1998) Mineral diagenesis, thermodynamics, kinetics and fluid flow in sedimentary basins. ERC Geochmistry of crustal fluids, Crete, 22-27 May (abstract).

Blomqvist R, Frape S K, Nissinen P, Ivanovich M, Vuorela P, Blyth A, Ruskeeniemi T (1992) Crustal rebound-relate groundwater flow and calcite formation in the crystalline bedrock of the Fennoscandian shield: new observations from Finland. Paleohydrogeological methods and their applications. Proc. of NEA workshop, Paris, 9-10/11/92,161-167.

Blomqvist et al (1999) The Palmottu natural analogue project. Final report.

Boulton G, de Marsily G (1997) Hydrogeological aspects of glaciation. in King-Clayton et al. (eds) Glaciation and Hydrogeology. Workshop on the impact of climate change and glaciations on rock stresses, groundwater flow and hydrochemistry - past, present and future. Stockholm, April 1996.

Broecker W S, van Donk J (1970) Ice volumes and the 18O record in deep sea cores. Rev. of Geophys. and Space. Phys., 8(1):169-197.

Bruno J (1997) Trace element modelling, In Modelling in Aquatic Chemistry (I. Grenthe and I. Puigdomènech eds.)NEA OECD. Pp. 593-622.

Bruno J, Cera E, Duro L, Eriksen T E, Sellin P, Spahiu K, Werme L O (1996) A kinetic model for the stability of the spent fuel matrix under oxic conditions: model development against experimental evidence. Mat. Res. Soc. Proc. Vol. 465: 491-502.

Carrera J, Neuman S P (1986) Estimation of aquifer parameters under transient and steady-state conditions, 1. Maximum likelyhood method incorporating prior information. Water Resour. Res. 22(2) 199-210.

Cera E, Bruno J, Rollin C, Ahonen L, de Pablo J (1999) Redox measurements and redox controls at the Palmottu site.The Palmottu Project WP 6 TR.

Clement T P, Sun Y, Hooker B S, Petersen J N (1998) Modeling multispecies reactive transport in groundwater. Groundwater Monitoring Review, Spring 98, 79-92.

Craig H, Wharton R A, McKay C P (1992) Oxygen supersaturation in ice-covered Antarctic lakes: biological vs. Physical contributions. Science, 255: 318-321.

Cross J E, Ewart F T (1989) HATCHES - A Thermodynamic Database Management System. Proceedings of the Conference on Chemistry and Migration Behaviour of Actinides and Fission Products in the Geosphere.

Deer W A, Howie R A, Zussman J (1992) The rock forming minerals, 2nd edition, Longman Sci. & Tech.

Engesgaard P, Kipp K L, A Geochemical Transport Model for Redoxed-Controlled Movement of Mineral Fronts in Groundwater Flow Systems: A Case of Nitrate Removal by Oxidation of Pyrite, Water Resour. Res., 28(10), 2829-2843, 1992.

Fountain A G (1994) Borehole water-level variations and implications for the subglacial hydraulics of South Cascade Glacier, Washington State, U.S.A. J. of Glaciology, 40 (135)293-304.

Friedly J C, Rubin Y (1992) Solute transport with multiple equilibrium-controlled or kinetically controlled chemical reactions. Water Resour. Res., 28(6)1935-1953.

Friedly J C, Davis J A, Kent D B, Modeling hexavalent chromium reduction in groundwater in field-scale transport and laboratory batch experiments, Water Resour. Res. 31(11), 1995.

Glynn P D, Voss C, Provost A (1997) Deep penetration of oxygenated meltwaters from warm based ice-sheets, in "Use of hydrogeochemical information in testing groundwater flow models" OECD/NEA SEDE workshop, 1-3 September, Borgholm.

Glynn P D, Brown J (1996) Reactive transport modelling of acidic metal-contaminated ground water at a site with sparse information. In Lichtner et al. (eds) Reactive transport in porous media. Rev. In Mineralogy. Vol. 34 series ed. P.H.Ribbe. Min. Soc. Am. P. 83-130.

Grenthe I, Hummel W, Puigdomènech I (1997) Chemical background for the modelling of reactions in aqueous systems. Grenthe and Puigdomènech (eds) Modelling in aquatic chemistry. NEA, OCDE, Paris. 724 p.

Grindrod P, Crompton S P, Woods J A, Arthur R C (1994) ARASE: Multibarrier geometry in two dimensions. QuantiSci rep ID3830-4 Version 2.

Guimerà J, Carrera J (1997) On the empirical relationship among hydrodynamical parameters of rock masses, 5th Sci. Assemb. IAHS, Rabat, Morocco, 23 April-3 May. IAHS pub. no. 241, 123-134.

Guimerà J, Carrera J, Martínez L, Vázquez E, Ortuño F, Fierz T, Bülher C, Vives L, Meier P, Medina A, Saaltink M, Ruiz B, Pardillo J (1997) Hydrogeological characterisation and modelling. FEBEX project, 70-UPC-M-1-1001. ENRESA.

Herron S, Langway C (1979) The debris-laden ice at the bottom of the Greenland ice-sheet. J. Glaciol. 23 (89):193-207.

Holland H D (1984) The chemical evolution of the atmosphere and oceans. Princeton series in geochemistry, Princeton Univ. Press, 582 pp.

Lichtner P C (1988) The quasi stationary approximation to coupled mass transport and fluid-rock interaction in a porous medium- Geochim. et Cosmochim. Acta, 52, 143-165.

Malmström M, Banwart S, Duro L, Wersin, P, Bruno J (1995) Biotite and chlorite weathering at 25°C. SKB TR 95-01.

Martínez-Landa L, Guimerà J, Vázquez E, Vives L, Carrera J (1997) Consistency between different hydraulic characterisation methods of a granitic rock mass. Workshop on Hard Rocks hydrogeology, IAH Iberian sub-group, Madrid, 11-13 Sept.

Nicholson R V, Gillham R W, Reardon E J (1990) Pyrite oxidation in carbonate-buffered solution: 2. rate control by oxide coatings. Geochim. Cosmochim. acta, 54, 395-402.

Parkhurst D L (1995) User's guide to PHREEQC - A computer program for speciation, reaction-path, advective-transport, and inverse geochemical calculations. USGS, Water-Resources Investigations Report 95-4227. Lakewood, Colorado.

Peltier W R (1985) New constraints on transient lower mantle rheology and internal mantle buoyancy from glacial rebound data. Nature, 318, 614-617.

Raynaud D, Lebel B (1979) Total gas content and surface elevation of polar ice sheets. Nature, 281: 289-291.

Rhén I (ed), Bäckbom G (ed), Gustafson G, Stanfors R, Wikberg P (1997) Äspö HRL Geoscientific evaluation. 1997/2. SKB TR 97-03, Sweden.

Rubin J (1983) Transport of Reacting Solutes in Porous Media: Relation Between Mathematical Nature of Problem Formulation and Chemical Nature of Reactions, Water Resour. Res., 19(5), 1231-1252.

Saaltink M, Benet I, Ayora C (1997) EXCHANGE: Fortran code for solving reactive transport of solutes. User's guide. ETSCCPB-UPC and ICTJA-CSIC.

Schouez R A, Lorrain R D (1991) Ice composition and glacier dynamics, Springer Verlag, Amsterdam.

Sherman D (1998) Mineral-filuid interactions at molecular scale. ERC Geochmistry of crustal fluids, Crete, 22-27 May (abstract).

SKI SITE-94 (1996) SKI Site 94 Deep Repository performance assessment projects. SKI Report 96:36.

Stauffer B, Neftel A, Oeschger H, Schwander J (1985) CO2 concentration in air extracted from Greenland ice samples. In: Langway, C. et al. (eds) Greenland ice core: geophysics, geochemistry and the environment. Geophysical Monograph 33, pp 85-89, AGU, Washington.

Steefel C I, Mc Quarrie K T B (1996) Approaches to modelling of reactive transport in porous media. In Lichtner et al. (eds) Reactive transport in porous media. Rev. In Mineralogy. Vol. 34 series ed. P.H.Ribbe. Min. Soc. Am. P. 83-130.

Stumm and Morgar (1981) Aquatic Chemistry, John Wiley and sons, N.Y.

Svensson U (1996) Regional groundwater flow due to an advancing and retreating glacier - scoping calculations. SKB PR U-96-35.

Svensson U (1997) A regional analysis of groundwater flow and salinity distribution in the Äspö area. SKB TR-97-09, Stockholm, Sweden.

Tóth J (1963) A theoretical analysis of groundwater flow in small drainage basins. J. of Geophys. Res., 68 (10) 4795-4812.

Tóth J, Sheng G (1996) Enhancing safety of nuclear waste disposal by exploiting regional groundwater flow: the recharge area concept. Hydrogeology J., v. 4 (4)4-25.

Trudell M R, Gillham R W, Cherry J S A (1986) An in situ study of the occurrence and rate of denitrification in a shallow unconfined aquifer. J. Hydrol., 83:251-268.

Tsang Y W, Witherspoon P A (1985) Effects of fracture roughness on fluid flow through a single deformable fracture. Hydrogeology of rocks of low permeability, IAH mem. Vol XVII (I) 683-694.

Waber N, Schorscher H D, Peters T (1990) Mineralogy, petrology and geochemistry of the Poços de Caldas analogue study site, Minas Gerais, Brazil. Osamu Utsumu uranium mine. Nagra NTB 90-20, Wettingen, Switzerland, 485 pp.

Weertman J (1968) Comparison between measured and theoretical temperature profiles of the Camp Century boreholes, Greenland. J. of Geophys. Res. 73(8):2691-2700.

White A F, Yee A (1985) Aqueous oxidation-reduction kinetics associated with coupled electron-cation transfer from iron-containing silicates at 25ºC. Geochim. et Cosmochim. Acta, 49, 1263-1275.

Yang Q, Mayewski P A, Linder E, Whitlow S, Twickler M (1996) Chemical species spatial distribution and relationship to elevation and snow accumulation rate over the Greenland Ice Sheet. J. of Geophys. Res. 101 (D13):18629-18637.

ISSN 1404-0344
CM Gruppen AB, Bromma, 1999